

November 2021

## **Microencapsulation of Thermo-chromic Materials for Thermal Storage and Energy Efficiency of Buildings**

Abdullatif Hakami  
*University of South Florida*

Follow this and additional works at: <https://digitalcommons.usf.edu/etd>

 Part of the [Electrical and Computer Engineering Commons](#)

---

### **Scholar Commons Citation**

Hakami, Abdullatif, "Microencapsulation of Thermo-chromic Materials for Thermal Storage and Energy Efficiency of Buildings" (2021). *USF Tampa Graduate Theses and Dissertations*.  
<https://digitalcommons.usf.edu/etd/9678>

This Dissertation is brought to you for free and open access by the USF Graduate Theses and Dissertations at Digital Commons @ University of South Florida. It has been accepted for inclusion in USF Tampa Graduate Theses and Dissertations by an authorized administrator of Digital Commons @ University of South Florida. For more information, please contact [scholarcommons@usf.edu](mailto:scholarcommons@usf.edu).

Microencapsulation of Thermochromic Materials for Thermal Storage  
and Energy Efficiency of Buildings

by

Abdullatif Hakami

A dissertation submitted in partial fulfillment  
of the requirements for the degree of  
Doctor of Philosophy  
Department of Electrical Engineering  
College of Engineering  
University of South Florida

Co-Major Professor: Elias K. Stefanakos, Ph.D.  
Co-Major Professor: Sesa S. Srinivasan, Ph.D.  
Arash Takshi, Ph.D.  
Venkat Bhethanabotla, Ph.D.  
Ryan Toomey, Ph.D.

Date of Approval:  
November 2, 2021

Keywords: Phase Change, Building Applications

Copyright © 2021, Abdullatif Hakami

## **Dedication**

To my father, whom I have never seen.

## **Acknowledgments**

I would like to thank my advisor Dr. Elias. Stefanakos for believing and helping me to pursue my Ph.D. degree. I am also thankful to Dr. Sesa Srinivasan for all the support he has provided and for making available the research facilities at Florida Polytechnic University. Speacial thanks to the Ph.D. committee members Dr. Arash Takshi, Dr. Venkat Bhethanabotla, and Dr. Ryan Toomey for their valuable suggestions. Gratefully acknowledging the technical support received from Dr. Scott Wallen, from Florida Polytechnic University, and Dr. Prasanta K Biswas from University of South Florida for all the support, comments, advice, and help.

I would like to also thank my wife, Dr. Babaeer, for her support and patience, in the past 12 years while in the USA, during the completion of this dissertation. Also, to my beloved daughters, I wish to see them soon.

## Table of Contents

List of Tables .....	iv
List of Figures .....	v
Abstract .....	x
Chapter 1: Introduction .....	1
1.1 Motivation for the Work .....	5
1.2 Research Objective .....	5
1.3 Scope of the Dissertation .....	6
Chapter 2: Background / Review of Thermochemical Materials: Development, Characterization and Applications .....	8
2.1 Introduction .....	8
2.2 Thermochemicalism .....	11
2.2.1 Crystal Field Effect on the <i>d-d</i> Orbital Transition of Transition Metal Ions .....	11
2.2.2 Band Gap Energy Change of a Semiconductor .....	12
2.2.3 Phase Transitions of Solid Electrolytes .....	13
2.2.4 Change in Coordination Geometry of Metal-Complex Species .....	13
2.2.5 Change in Coordination Number of Metal Complex Species .....	13
2.2.6 Interconversion of Stereoisomeric Forms with Conformational Inversion .....	13
2.2.7 Change in Molecular Structure .....	14
2.2.8 Change in Crystal Structure .....	14
2.3 Classifications of TCMs .....	15
2.3.1 Inorganic Thermochemical Materials (ITCM) .....	15
2.3.2 Organic Thermochemical Materials (OTCMs) .....	17
2.3.3 Organic-Inorganic Hybrid Thermochemical Materials (OIHTCMs) .....	18
2.3.4 Polymeric Thermochemical Materials (PTCMs) .....	18
2.3.5 Polymers with Inherent Thermochemicalism .....	18
2.3.6 Polymers Embedding the Thermochemical Pigments .....	19
2.3.7 Polymers with Thermo Responsive Additives .....	20
2.3.8 Polymers with Protic, Thermo Responsive Dyes .....	20
2.3.9 Potentiality on the Classification of Thermochemical Materials .....	21
2.4 Synthesis and Characterization of TCMs .....	21
2.4.1 Microemulsion Technique .....	22
2.4.2 Solvothermal Technique .....	25

2.4.3 Sol-Gel Technique .....	25
2.4.4 Chemical and Electrochemical Polymerization Technique .....	26
2.4.5 Mechanical Grinding Technique.....	27
2.4.6 UV Irradiation Technique .....	28
2.4.7 Schiff Base Synthesis Technique.....	28
2.4.8 Microwave Irradiation Technique.....	29
2.5 Microencapsulation of TCMs .....	29
2.5.1 Overview of Different Techniques of Microencapsulation .....	32
2.5.2 Physical Methods .....	32
2.5.3 Spray Drying.....	32
2.5.4 Solvent Evaporation.....	33
2.5.5 Chemical Methods .....	34
2.5.6 <i>In situ</i> Polymerization .....	34
2.5.7 Interfacial Polymerization.....	35
2.5.8 Suspension Polymerization .....	35
2.5.9 Emulsion Polymerization.....	36
2.5.10 Physicochemical Method.....	37
2.5.11 Supercritical Emulsion Extraction .....	37
2.5.12 Sol-Gel Processing.....	37
2.5.13 Coacervation Method.....	38
2.5.14 Melt Coaxial Electrospinning Method.....	39
2.6 Thermochromic Coating .....	40
2.6.1 Physical Vapor Deposition (PVD).....	40
2.6.2 Pulsed Laser Deposition (PLD) .....	41
2.6.3 Sol-gel Depositions.....	42
2.6.4 Chemical Vapor Deposition (CVD).....	43
2.6.5 Advantages and Disadvantages of the Coating Methods.....	43
2.7 Photodegradation and Thermal Degradation of TCMs.....	45
2.8 Applications of TCMs.....	47
Chapter 3: Microencapsulation and Characterization of TCM and PCM Materials .....	50
3.1 Introduction.....	50
3.2 Characterization .....	50
3.2.1 Scanning Electron Microscopy .....	51
3.2.2 Transmission Electron Microscopy .....	52
3.2.3 Differential Scanning Calorimetry (DSC) .....	52
3.2.4 UV-Visible Spectrophotometry .....	53
3.2.5 Fourier Transform Infrared (FTIR) Spectroscopy .....	54
3.2.6 X-ray Diffraction (XRD) .....	55
3.2.7 CIE Lab Color Meter .....	55
3.3 Encapsulation of Thermochromic Material with a Polymer Shell.....	56
3.3.1 Materials .....	57
3.3.2 Preparation of a Blue Dye Three-Component System, as the Core Ts.....	57
3.3.3 Preparation of a Three Component TCM Encapsulated with a Polymer and a Metal Oxide.....	58

3.3.4 Results and Discussion .....	59
3.3.4.1 Fourier Transform Infrared (FTIR) Spectroscopy .....	59
3.3.4.2 Differential Scanning Calorimetry (DSC) .....	62
3.3.4.3 Scanning Electron Microscopy (SEM) .....	65
3.4 Encapsulation of Phase Change Materials with Metal Oxide Shell Structures .....	67
3.4.1 Materials .....	69
3.4.2 Encapsulation of <i>n</i> -eicosane with a TiO <sub>2</sub> Shell.....	70
3.4.3 Results and Discussion .....	71
3.4.3.1 Fourier Transform Infrared (FTIR) Spectroscopy .....	71
3.4.3.2 X-ray Diffraction (XRD) .....	73
3.4.3.3 Differential Scanning Calorimetry (DSC) .....	74
3.4.3.4 Scanning Electron Microscopy (SEM) .....	76
3.5 Effect of Surfactant on the TiO <sub>2</sub> Microencapsulation of Thermochromic .....	77
3.5.1 Preparation of TiO <sub>2</sub> Precursor Solution, Encapsulation and Filtration.....	80
3.5.2 Results and Discussion .....	81
3.5.2.1 SEM, HRTEM, EDS.....	81
3.5.2.2 DSC - Thermal Heat Flow .....	85
3.5.2.3 CIE LAB Color Simulation .....	87
3.5.2.4 UV-Visible Spectrophotometer Absorption and Reflectance.....	89
3.5.2.5 XRD Phase Analysis.....	90
3.5.2.6 FTIR Spectral Data Analysis .....	91
 Chapter 4: Effects of Multilayer Thin Film Coatings on Different Thermochromic Materials for Thermal Energy Storage Applications .....	 94
4.1 Introduction.....	94
4.2 Experimental.....	95
4.3 Results and Discussion .....	97
 Chapter 5: Conclusions and Recommendations for Future Work .....	 107
5.1 Conclusions.....	107
5.2 Recommendations for Future Work.....	108
5.3 Abbreviation .....	109
 References.....	 110
 Appendix A: Permissions, Copyright and Acceptance Letter .....	 129
 About the Author .....	 End Page

## List of Tables

Table 1: Synthesis of Six Batches of a Three-Component System with Different Weight Ratios .....	56
Table 2: DSC Raw Data of a TCM and an Encapsulated TCM .....	64
Table 3: Nomenclature.....	79
Table 4: The Compositions of the TTIP* and Surfactant Types .....	80
Table 5: Peak Temperatures and Enthalpy Values for the Plain and Encapsulated CDTCM for Surfactants, CTAB and SDBS .....	86
Table 6: C.I.E. L*a*b* Data Sets for the Samples at Room Temperature (Standard) and at 50 °C (Sample).....	88
Table 7: Compositions of All Components with a Binder.....	96
Table 8: C.I.E. L*a*b* Data Sets for the Samples Treated at Room Temperature (Standard) and at 40 °C (Sample).....	102

## List of Figures

Figure 1: Energy Consumption in North America in Residential and Commercial Buildings (2010) [3] .....	1
Figure 2: Diagram of Different Electricity Sources by 2040 [4] .....	2
Figure 3: Graphical Abstract: Enhanced Energy Efficiency of Buildings with Smart Coatings of Microencapsulated TCMs .....	9
Figure 4: Reversible Color Changes of a TCM Dye Encapsulated by SiO <sub>2</sub> at Different Temperatures [41] .....	10
Figure 5: Various Mechanisms Responsible Types and Salient Examples for Thermochromism .....	12
Figure 6: Classification of TCMs .....	17
Figure 7: Synthetic Approaches to Prepare TCMs .....	22
Figure 8: A Schematic of Various Techniques Used for the Characterization of Thermochromic Materials .....	23
Figure 9: XRD of a Microencapsulated Phase Change Material (A) and Photocatalytic Degradation of Methyl Orange (MO) .....	24
Figure 10: Microstructure of Microencapsulated Phase Change Material of Different Geometries [41] .....	24
Figure 11: Optical Glass Images of the Black and Blue Thermochromic Materials .....	24
Figure 12: Transmission (A) and Spectral Reflectance (B) of TiO <sub>2</sub> Encapsulated Black Dye and Blue Dye .....	25
Figure 13: DSC (A) and TGA (B) Profiles of TCM and TCM Encapsulated with SiO <sub>2</sub> [41] .....	27
Figure 14: FTIR of TCM Encapsulated with SiO <sub>2</sub> [41].....	28
Figure 15: TCM Microencapsulation Process .....	30
Figure 16: HRTEM Images of Core TCM Microencapsulated with SiO <sub>2</sub> Shell [41].....	32

Figure 17: Common Methods of Microencapsulation Along with Their Basic Principle of Deposition and Properties .....	33
Figure 18: Microencapsulation Mechanism Showing Tiny Particles (Droplets) of Active Ingredients are Surrounded by a Coated Shell (Multilayer Liquid Crystalline Microsphere) .....	36
Figure 19: Electrospinning Apparatus (A) [168] and Optical/SEM Microscopic (B) Images of Electrospun Thermochromic Fibers Encapsulated with TCM [169] .....	39
Figure 20: Optical Coatings of (a) Plain TCM , (b) TiO <sub>2</sub> Coating and (c) TCM with TiO <sub>2</sub> [170] .....	40
Figure 21: Classification of the Electromagnetic Radiation Spectral Wavelength Range .....	46
Figure 22: Schematic of a Building with Different Layers of Roof Insulation [202].....	48
Figure 23: Different Applications of TCMs .....	49
Figure 24: Scanning Electron Microscope (Hitachi SU3500) at Florida Polytechnic University .....	51
Figure 25: Picture of the Transmission Electron Microscopy (Tecnai TF-20) at the USF NREC .....	52
Figure 26: TGA / Differential Scanning Calorimetry (METTLER TOLEDO) TGA/DSC 2 TGA 1 at Florida Polytechnic University .....	53
Figure 27: UV-Vis Spectrophotometer (Cary 5000 UV-Vis-NIR) at Florida Polytechnic University .....	54
Figure 28: CIE Lab Color Meter at Florida Polytechnic University .....	55
Figure 29: Encapsulation Process of a Thermochromic Material.....	56
Figure 30: Preparation of the Three Component TCM.....	58
Figure 31: Preparation of the Three Component TCM Encapsulated with a Polymer.....	59
Figure 32: FTIR Spectral Profiles of Polymer Encapsulated and Plain TCM.....	61
Figure 33: DSC Thermograms of Cooling and Heating Transitions of the Plain TCM Phase Change Material.....	62
Figure 34: DSC Profiles of the Plain and Polymer Encapsulated TCM Melting Transitions.....	63

Figure 35: Heating DSC Profiles of the Polymer Encapsulated TCM for Many Consecutive Cycles .....	63
Figure 36: Ramping Rate vs Heat Flow (at Peak Melting Transition) of the Plain and PMMA Encapsulated TCM (A) .....	65
Figure 37: Changes in Heat Flow and Peak Temperature of Melting Between PMMA Encapsulated and Plain TCM (B) .....	65
Figure 38: SEM Images of the Microcapsules Encapsulated by the Polymer Shell Layer at Different Magnifications .....	66
Figure 39: SEM Images of the Microcapsule's Smooth Surface Morphologies of PMMA Encapsulated TCMs .....	67
Figure 40: Preparation of Microencapsulation of TiO <sub>2</sub> Shell with <i>n</i> -eicosane as Core .....	70
Figure 41: Schematic Diagram of the PCM Encapsulation Process Using a TiO <sub>2</sub> Shell .....	71
Figure 42: FTIR Spectra of the Pure and TiO <sub>2</sub> Microencapsulated PCM <i>n</i> -Eicosane .....	72
Figure 43: XRD of TiO <sub>2</sub> Microencapsulated <i>n</i> -eicosane and Plain <i>n</i> -Eicosane .....	74
Figure 44: Heating DSC Curves of the Microencapsulated <i>n</i> -Eicosane and Plain <i>n</i> -Eicosane .....	75
Figure 45: Heating and Cooling Cycling Behavior from DSC Profiles of Encapsulated and Plain PCM .....	75
Figure 46: SEM Micrographs of the Plain <i>n</i> -Eicosane at Different Magnifications (a) to (f) .....	76
Figure 47: EDS Map Sum Image and Spectrum of the Microencapsulated <i>n</i> -Eicosane (A) .....	77
Figure 48: EDS Elemental Mapping of TiO <sub>2</sub> Encapsulated <i>n</i> -Eicosane Wt% Inserted in the Images (B) .....	77
Figure 49: Microencapsulation Process of CDTCM@TiO <sub>2</sub> Using Different Surfactants .....	78
Figure 50: A Surfactant Micelle in Water: Three Different Regions of a Micelle are Identified as the Outer Region, the Palisade Region, and the Core .....	79
Figure 51: Preparation of TiO <sub>2</sub> Encapsulated Black Dye .....	81
Figure 52: SEM-HRTEM Micrographs of CDTCM@TiO <sub>2</sub> by Using CTAB Surfactant .....	83

Figure 53: SEM-HRTEM Micrographs of CDTCM@TiO <sub>2</sub> by Using a SDBS Surfactant.....	84
Figure 54: EDS Spectrum of the Microencapsulated CDTCM with a Crystalline TiO <sub>2</sub> Shell CTAB.....	85
Figure 55: EDS Spectrum of the Microencapsulated CDTCM with a Crystalline TiO <sub>2</sub> .....	85
Figure 56: DSC Profiles of CDTCM & CDTCM@TiO <sub>2</sub> Encapsulated.....	87
Figure 57: CIE LAB Color Simulation of the Samples at Room Temp & at 50 °C.....	88
Figure 58: Absorbance (A) and Reflectance (B) Spectra of CDTCM and CDTCM@TiO <sub>2</sub> Room Temp and 50 °C.....	90
Figure 59: The XRD Patterns of CDTCM, CDTCM@TiO <sub>2</sub> -CTAB and SDBS.....	91
Figure 60: The FTIR Spectra CDTCM, CDTCM@TiO <sub>2</sub> -CTAB and SDBS.....	92
Figure 61: Schematic Showing Thick and Thin Glass with Layers (A) and UV-VIS Spectrophotometer Wavelength Range (B).....	96
Figure 62: Absorbance Spectra of Plain Black Dye, Plain Blue Dye, SiO <sub>2</sub> /Blue Dye, TiO <sub>2</sub> /Black Dye, and TiO <sub>2</sub> /Blue Dye at (A) Room Temperature and at (B) 40 °C.....	100
Figure 63: Transmission Spectra of Plain Black Dye, Plain Blue Dye, SiO <sub>2</sub> /Blue Dye TiO <sub>2</sub> /Black Dye, and TiO <sub>2</sub> /Blue Dye at (C) Room Temperature and at (D) 40 °C.....	100
Figure 64: Reflection Spectra of Plain Black Dye, Plain Blue Dye, SiO <sub>2</sub> /Blue Dye, TiO <sub>2</sub> /Black Dye, and TiO <sub>2</sub> /Blue Dye at (E) Room Temperature and at (F) 40 °C.....	101
Figure 65: SEM Micrographs of Black Dye with Sodium Silicate Binder Coated on a Thick Glass Substrate at (A) Lower Magnification and (B) Higher Magnification.....	101
Figure 66: SEM Micrographs of Blue Dye with Sodium Silicate Binder Coated on a Thick Glass Substrate at (C) Lower Magnification and (D) Higher Magnification.....	102
Figure 67: Photographic Images of the Coated Samples at Room Temperature (Left) and 40 °C (Right) CIE LAB Color Simulation of the Samples.....	104
Figure 68: DSC Profiles of Plain Blue Dye and SiO <sub>2</sub> Encapsulated Blue Dye in Both Heating and Cooling Cycles Exhibit Thermal Storage Characteristics While Changing Its Color from Blue to White and Vice-Versa.....	105

Figure 69: Different Surfactants Beside TCM@TiO<sub>2</sub> ..... 108

## **Abstract**

Thermochromism and thermochromic materials research and development are of great interest in various applications such as energy efficient building structures, textile industries, thermal or heat storage, antique maintenance processing, and sensors, etc. In general, thermochromic materials have been classified into four categories, including inorganic, organic, polymeric, and hybrid systems, based on their unique material properties and operating conditions. Thermochromic materials have been prepared via different physico-chemical techniques with some of them combined to maximize the yield, stability, and efficiency of the prepared TCMs. Pristine TCMs often undergo severe degradation when exposed to various external stimuli including UV irradiation from sunlight and ambient environmental conditions such as temperature, pressure, and humidity variations. Such degradation causes property and physical behavioral changes in TCMs. Various microencapsulation procedures and coating techniques are utilized to enhance the thermochromic performance of the materials and to protect the core TCMs from degradation. Many desirable candidate materials have been developed and extensive metrological tools have been deployed to understand the structural, morphological, microstructural, thermal, chemical, surface, and interfacial characteristics of these TCMs and their microencapsulated variants. The potential applications of the microencapsulated TCMs in industrial, commercial, and residential sectors are briefly discussed in this dissertation. The future looks bright for the development of novel microencapsulated TCMs possessing nano-

structural derived properties that can be effectively used in inks, paints and coating agents for sustainable energy efficiency and many other applications.

This dissertation focuses on different types of microencapsulated materials for thermal energy storage such as a three-component thermochromic core material microencapsulated by a stable PMMA shell formed by the polymerization of a monomer, polymethyl methacrylate (MMA), a synthesized *n*-eicosane phase change material (PCM) encapsulated by a crystalline sol-gel titania, TiO<sub>2</sub>, shell, and the design of a commercial dye thermochromic powder as a core with a structured TiO<sub>2</sub> shell for reversible and durable thermal energy storage. These three types of encapsulated materials were successfully encapsulated by different methods. Moreover, various thermochromic coatings on glass slides were used to investigate the potential of titanium dioxide (TiO<sub>2</sub>) to protect thermochromic particles (such as a three-component blue dye, prepared in the lab, or a commercially available black dye) from UV radiation.

## Chapter 1: Introduction

The fast rise of industries, population, and production in the past few years has increased the use of natural resources. It is projected that the world population will increase from 7 billion currently to be over 9.9 billion by 2050 [1], requiring an increase in the energy consumption in buildings of 7-40% [2]. Figure 1 shows the energy use in different sectors, with the highest amount consumed by commercial and residential buildings [3]. Renewable energy sources are becoming a principal portion of electricity generation worldwide, with an expected increase of 42% from 2021 to 2040 (Figure 2).

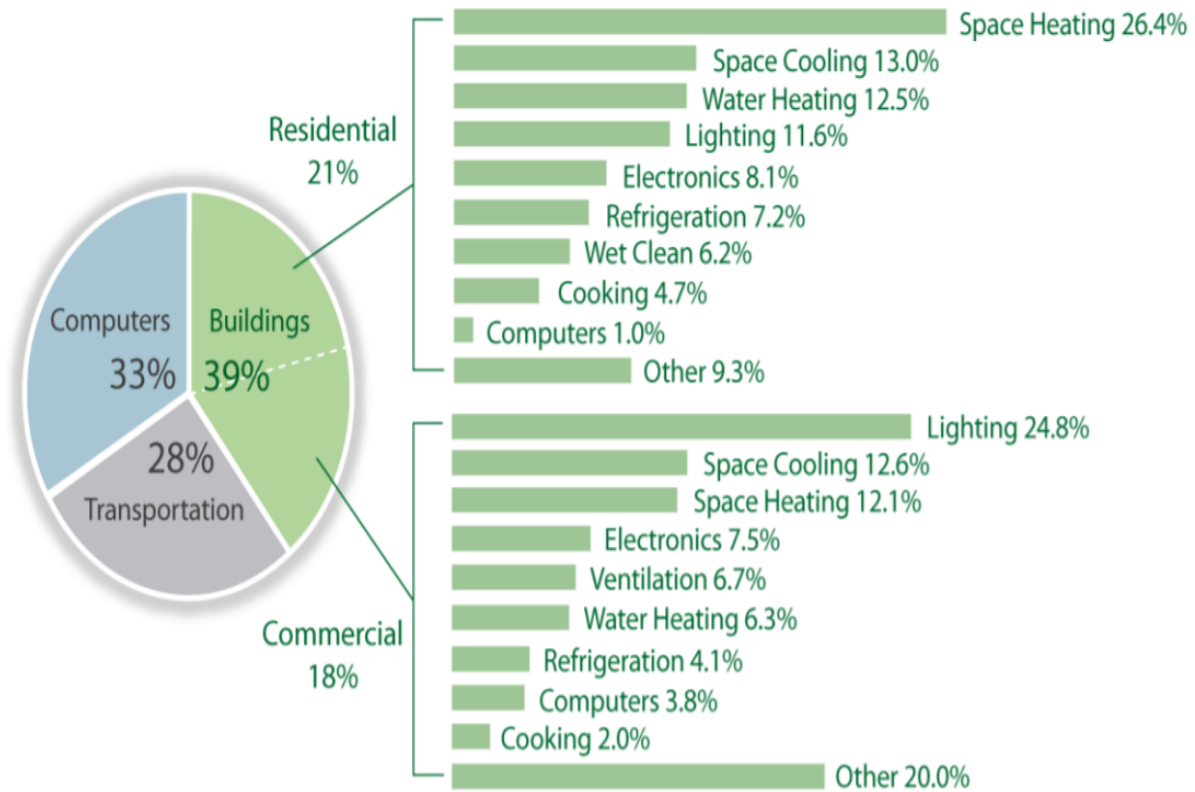


Figure 1: Energy Consumption in North America of Residential and Commercial Buildings (2010) [3].

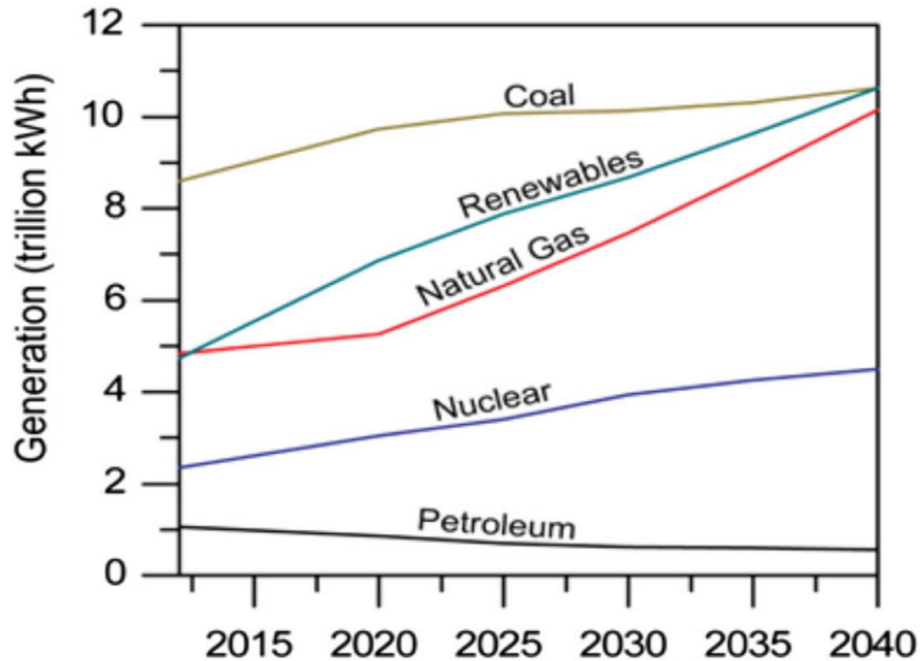


Figure 2: Diagram of Different Electricity Sources by 2040 [4].

A considerable amount of energy can be saved by the use of thermochromic materials (TCMs) and energy storing phase change materials (PCMs). The reversible color change of microencapsulated TCMs, as the temperature changes, and the ability of PCMs to store significant amounts of thermal energy, can be used to increase the energy efficiency of buildings, especially in hot and cold climates [5]. For example, TCMs can change color from black (when it is cold) to white (when it is hot), thus reflecting sunlight in the summer and absorbing sunlight in the winter. TCMs can also be used as coatings on glass surfaces, to produce smart windows, or on roofs of buildings. However, there are still some challenges that need to be addressed, for example, photodegradation and chemical reactions of TCMs with surrounding materials [6]. TCMs can also be used in other applications such as safety warning signs, security sensors, consumer packaging, product labels, toys, medical thermography, and renewable energy systems (e.g., thermal storage and energy efficiency) [7]. There are different types of thermochromic materials, such as liquid crystals, leuco dyes, and a nontoxic chlorophenol (CPR) - water

system[8] for promising applications including 3D printing and screen-printing inks. Liquid crystals exhibit a continuously changeable spectrum of specific colors during the temperature change which is a significant part of the color-display. The leuco dye systems having different ratios of leuco dye with respect to co-solvent can produce different reversible color changes with changes in temperature [9]. In the case of the three-component thermochromic system, there is a unique solvent, like an intermediate material synthesis during the change of temperature, which is responsible for its phase change behavior. For the case of CPR-water thermochromic systems, the change in color due to temperature changes is primarily governed by the melting/crystallization of the solvent without a need for a developer [8].

In general, thermochromic materials change color because the application of heat changes the chromophoric nature of the material and this changes its absorption behavior giving rise to different colors. But practically the materials may have different functional groups which may have ability to change color by the interaction of suitable reacting species. For example, a three-component system possesses a suitable dye, a color developer and a solvent where the dye carries the color former by adjustment of its concentration, which is pH-sensitive, while the color developer forms a complex [10] with the dye by a proton or electron transfer process to produce a stable color, and, finally, the solvent possesses hydrophobic interactions. Hence, this kind of thermochromic system may be designated by a specific name, such as composite pigment (Ts) which changes color at a specific temperature. In many cases, the components of thermochromic materials are not suitable for heat sensitivity, but the system may possess pH sensitivity that can change with temperature [11]. The primary role of protons in the color former is to allow the material to turn from color to colorless, using the color developer as a proton reservoir. To make sure of the amount of color developer added, it is necessary to systematically adjust this until one

obtains the desired color. Most importantly, the solvent environment must be a suitable medium for interaction between the dye and the color provider. The solvent has a liquid state when the temperature is less than that at the color change due to the increase of temperature and the interaction between the color developer and the dye results in the colorful system. During the melting process, the dye is solvated due to the interaction between the color developer and the dye upon which the main color in the system will change [12, 13]. In some cases, the temperature in a specific transition can change the color in the system that depends on the type of solvent transition temperature which brings an advantage to the thermochromic system.

According to the literature, many researchers have covered different types of dyes, especially regarding crystal violet lactone (CVL), and different types of developers with their corresponding behaviors. For instance, studies show that bisphenol A (BPA) [14-18] has been used extensively as a color developer. For solvent purposes, as a part of a Ts, the 1-tetradecanol [18-22], 1-dodecanol [23], 1-hexadecanol [19, 20, 22], 1-octadecanol [22, 24], 1-octanoic acid methyl ester [16], myristic acid [9], and stearic acid [14] have been used. However, color formers having furan activating groups have been omitted in many cases in the synthesis of thermochromic materials. Furthermore, to develop and improve thermochromic benzofluoran [25], a series of hydroxyaryls has been used to synthesize the three-component system without bisphenol A. A different research group investigated a new technique by using reductive alkylation in aminofluorene to create a wide range of hydroxybenzaldehydes, leading to a new and novel thermochromic material that uses methyl stearate without any color developer [26]. Attempts have also been made to synthesize thermochromic materials by using BPA as a developer, benzofluoran as a dye, and octadecanol or tetradecanol as solvent. Thermal analyses

of the developed materials obtained by using different molar ratios of the dye, developer, and solvent have been performed and the results reported [25].

### **1.1 Motivation for the Work**

The increased demand for improved energy efficiency and better thermal energy storage has encouraged research in thermochromic encapsulation technologies, with emphasis on material selection and methodology optimization [27]. In addition to the normal benefits derived from the use of TC materials, the heat of melting, during the TCM phase change, can be used for thermal storage [21] and utilized on the roof of buildings to reduce heat transfer to the building [28]. TiO<sub>2</sub> microencapsulation of polymer encapsulated TC particles or plain organic three-component systems has been investigated to obtain TCMs that can be used for thermal storage and energy efficiency of buildings [29, 30]. Thermochromic microcapsules that can be used by the energy industries in outdoor applications is indeed an important research area. The problem with outdoor use is the degradation of organic materials when exposed to sunlight (photodegradation). Since TC materials that change color at low temperatures are mainly organic, inorganic metal oxides could be used to prevent photodegradation. In addition to photodegradation, issues such as cost, selection of materials and safety, must be addressed. Similar concerns exist with the use of thermochromic textiles in outdoor applications.

### **1.2 Research Objective**

The overall objective of this research is to develop microencapsulated, phase change, thermochromic particles that can be used in outdoor applications. Several strategies can be applied in the effort to achieve the above objective.

The first part of this research focuses on the fabrication and characterization of polymer encapsulated, thermochromic, three-component blue dyes. The thermochromic system includes

crystal violet lactone (CVL), a leuco dye, bisphenol A (BPA), a color developer, and 1-tetradecanol (TD) as the solvent. An emulsion polymerization technique was employed by using polymeric and co-polymeric materials such as polymethyl methacrylate (PMMA) and polymethyl methacrylate-co-methacrylic acid PMMA-co-MA for the microencapsulation of the thermochromic system.

The second part of this research pursues the fabrication and characterization of inorganic metal oxide ( $\text{TiO}_2$ ) encapsulated n-eicosane (PCM) and a blue TC dye, in the form of a core-shell structure. In this objective, the role of  $\text{TiO}_2$  encapsulation is to protect the thermochromic, phase change particles from degradation due to solar radiation. Anionic surfactants, such as sodium dodecyl sulfate (SDS), have been used to synthesize the  $\text{TiO}_2$  microencapsulated, phase change, thermochromic particles with tetrabutyl titanate (TBT) as the precursor to  $\text{TiO}_2$ .

In the third part, we investigate the effects of different surfactants and their concentrations on the  $\text{TiO}_2$  microencapsulation of commercially procured, thermochromic black dyes. These off-the-shelf phase change materials involve Leuco dye particles that have demonstrated color change (black to white) behavior at the low transition temperature of about 31 °C. The role of  $\text{TiO}_2$  encapsulation is to protect these thermochromic particles from solar photodegradation. Various surfactants such as CTAB, SDBS, hexadecanol and tetradecanol at different concentrations have been used to synthesize the  $\text{TiO}_2$  microencapsulated, phase change, thermochromic particles.

### **1.3 Scope of the Dissertation**

The primary purpose of this research is to focus on thermochromic microencapsulation by using different types of thermochromic materials, such as commercial black dyes and three-component system prepared blue dyes and synthesized n-eicosane phase change material (PCM),

encapsulated by a crystalline, sol-gel titania,  $\text{TiO}_2$ , shell. The outline of the dissertation is as follows.

As a brief introduction, thermochromic microencapsulation and a review of thermochromic materials, including development, characterization, and applications are presented in Chapter 2. Chapter 3 discusses thermochromic material characterization techniques, preparation of thermochromic materials, and microencapsulation methods. In Chapter 4, the behavior of multilayer thin film coatings on different thermochromic materials and the effect of non-toxic titanium dioxide ( $\text{TiO}_2$ ) coatings are investigated. Conclusions and recommendations for future work are presented in Chapter 5.

## Chapter 2: Background / Review of Thermochromic Materials: Development, Characterization and Applications<sup>1</sup>

### 2.1 Introduction

Thermochromic materials reversibly change color when their temperature changes (Figure 4). This thermal effect may cause changes in the material's molecular structure [5] which is accompanied by changes in its crystalline phase. Many industries involved in manufacturing chemical-based materials would benefit from color responsive, thermochromic materials-based temperature indicators because the temperature of the system due to the loss or gain of heat in chemical reactions kinetically controls the reaction steps resulting in better yields of industrial products. In the case of chemical storage [31], maintenance of the storage temperature can be critically important and any thermochromic material used in this application must involve a rapid, robust color responsive temperature indicator. Common examples of extensively used thermochromic materials are inorganic oxides such as VO<sub>2</sub>, TiO<sub>2</sub>, ZnO mixed with organic leuco dye systems [32] and less common thermochromic materials such as NbO<sub>2</sub>, FeSi<sub>2</sub> and Ti<sub>2</sub>O<sub>3</sub> [33].

Thermochromic materials (TCMs) have wide applications in the manufacturing of inks [34], smart materials coating of window glass surfaces to produce smart windows, textiles [35], cements, color indicators [36], and luminescent thermosensors. As TCM change color with temperature,

---

<sup>1</sup>This chapter was accepted in *Journal of Coatings Technology and Research* and moved on to production (*in press*) (Hakami, A., Srinivasan S. S., Biswas, P. K., Krishnegowda, A. S., Wallen S. L., and Stefanakos E. K., "Review of Thermochromic Materials: Development, Characterization and Applications." Acceptance information is included in Appendix A.

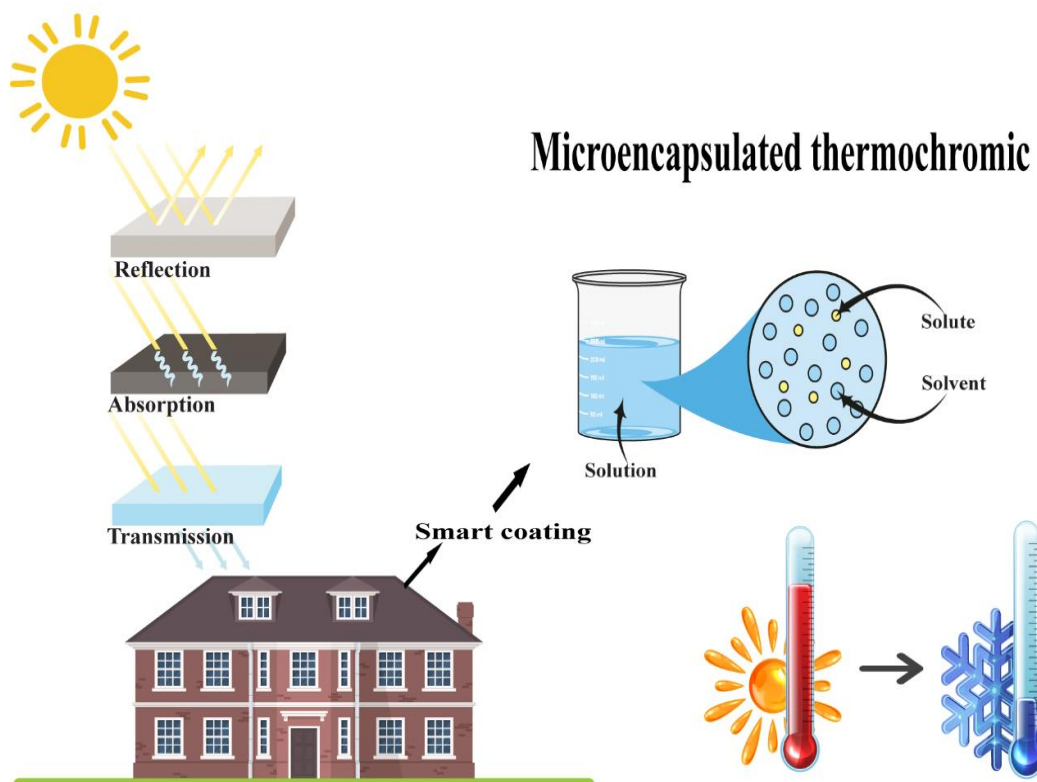


Figure 3: Graphical Abstract: Enhanced Energy Efficiency of Buildings with Smart Coatings of Microencapsulated TCMs.

One example of naturally occurring TCMs is ruby, it appears red in color but on heating above certain temperature turns into shiny green and returns to red on cooling[37] due to the change in energy levels of  $d-d$  transition of the chromium impurity, giving rise to different absorbance behavior. During heating, the crystal field energy is relatively high while for cooling it is relatively low which occurs by the change in crystal symmetry at the phase transition. As the photon energy of green is relatively high with respect to that of red, the material behaves as a TCM. Thermochromism has been known since antiquity [13]. Since 1963 the reversible and irreversible thermochromism phenomena in single component based inorganic or organic compounds as well as in organic-inorganic hybrid materials have been investigated by different workers [38-40]. In the past decade, significant development has been made in the field of thermochromism due to the advancement of nanotechnologies applied to the area. These

developments have contributed immensely to the synthesis and modification of thermochromic materials with desired functional properties in several application areas. This has considerably enlightened the synthesis of organic and inorganic TCM semiconductor nanoparticles, nanofibers, and other nanoarchitectures with the ability to abruptly change the materials' physical properties. With the advancement of nanotechnology, there is great potential for the development of TCMs that can be used in many applications, by enhancing their properties and aid in the adoption of these materials in real energy efficient systems.

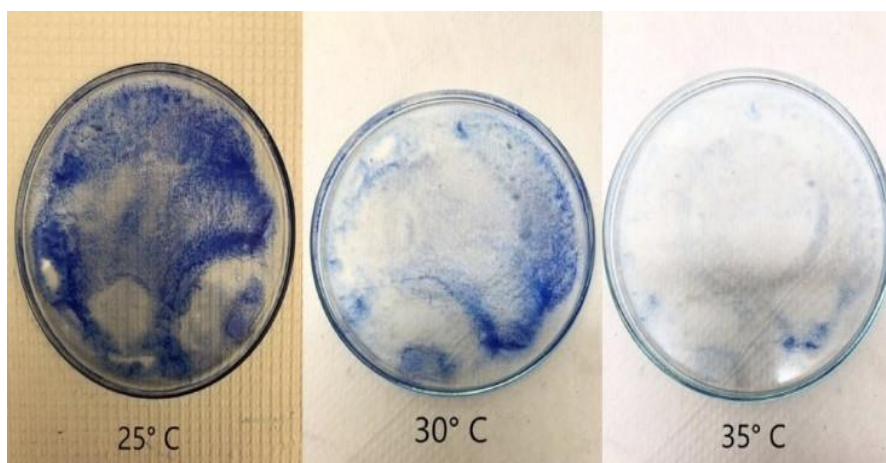


Figure 4: Reversible Color Changes of a TCM Dye Encapsulated by SiO<sub>2</sub> at Different Temperatures [41].

The origin of thermochromism in TCMs, their classification, synthesis, encapsulation, and their structural and physical characterization, along with their applications as bulk materials and as coatings are reviewed and reported in this paper. The thrust is on the discussion of microencapsulation of TCMs and its ability to make them highly stable and durable materials. The application of encapsulated materials as an overlayer (referred to as a shell) on top of the TCM substrate (the core) is also an important part of the discussion. The photodegradation and thermal degradation behavior of TCMs and their protective mechanisms are highlighted with potential applications of these unique materials.

## 2.2 Thermochromism

Thermochromic materials have the property of thermochromism which generally involves a reversible color change due to heating and cooling cycles. In the case of inorganic thermochromic compounds, not often reversible color changes are due to the thermoresponsive variation of crystal symmetry, which occurs due to the corresponding reversible phase transitions upon heating and cooling. The basic mechanism is the change in the ligand geometry and / or change in coordination number brought about by changes in temperature that cause variation in the crystal field energy lying in the photon energy range of visible electromagnetic radiation. In the case of the organic and polymeric thermochromic materials, changes in molecular structure give rise to variation in the highest occupied molecular orbital (HOMO) and the lowest unoccupied molecular orbital (LUMO) energy levels. The interconversion of stereoisomeric forms in organic molecules can also be a factor for causing thermochromism. There are several mechanisms responsible for thermochromism and some are briefly described below (Figure 5).

### 2.2.1 Crystal Field Effect on the *d-d* Orbital Transition of Transition Metal Ions

Temperature-dependent changes in crystal symmetry may occur in the case of transition metal ions which cause variation of ligand field energy levels. This phenomenon may result in change in the color of thermochromic materials. For example, ruby, naturally occurring corundum ( $\text{Al}_2\text{O}_3$ ) with the transition metal ion,  $\text{Cr}^{3+}$ , impurity replacing about 1% of the  $\text{Al}^{3+}$  ions that gives rise to the red color of the *d-d* transition of the crystal field splitting which corresponds to photon energy resulting in red color. Ruby changes color since upon heating [42] it changes crystal symmetry giving rise to relatively high crystal field energy where the *d-d* transition corresponds to green color of relatively high photon energy. Other examples are provided by dye in a previous review[43].

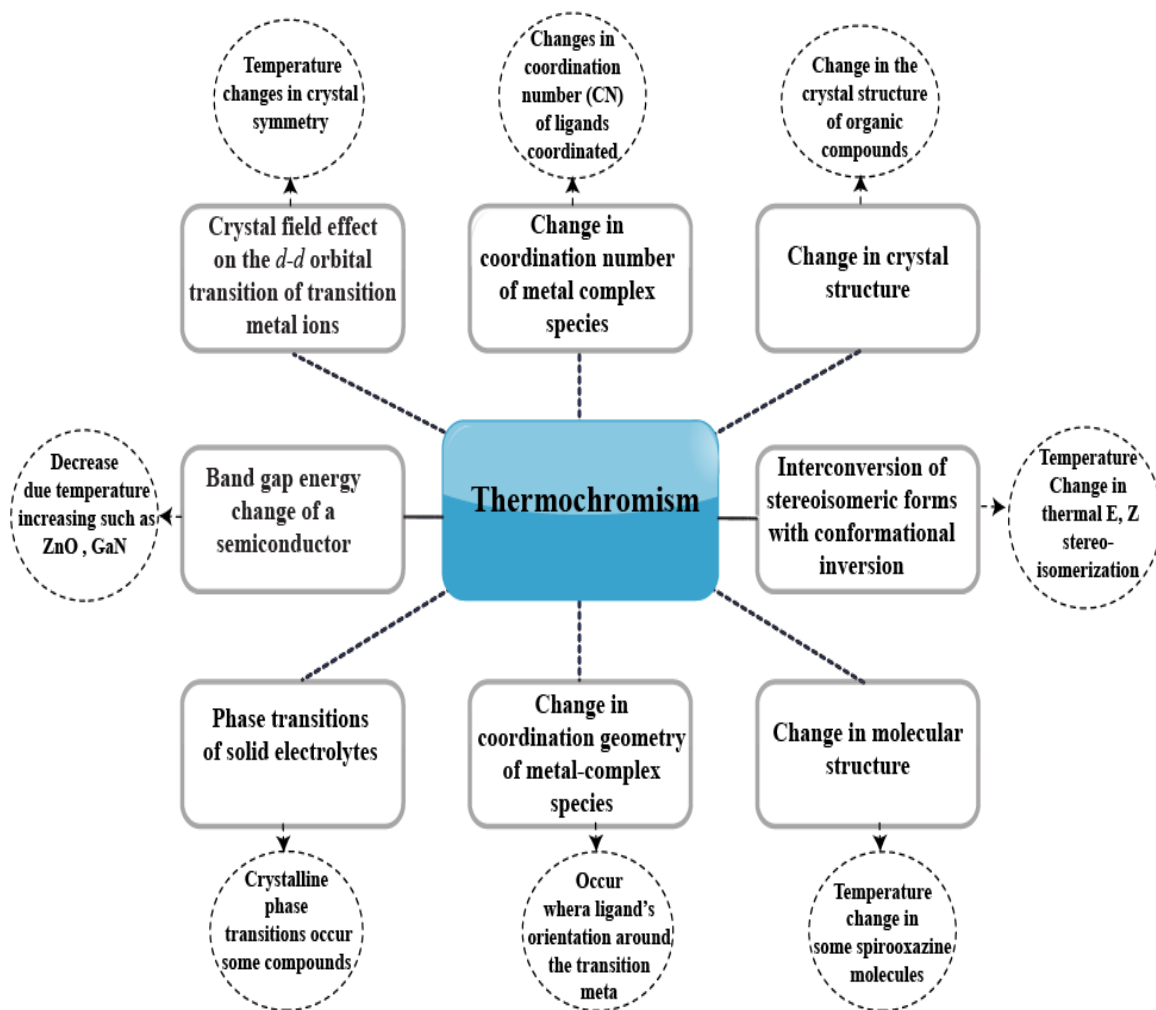


Figure 5: Various Mechanisms Responsible Types and Salient Examples for Thermochromism.

### 2.2.2 Band Gap Energy Change of a Semiconductor

The band gap energies of semiconductors decrease with increasing temperature. Hence, changes in the temperature of a semiconductor alters its band gap energy. For example, ZnO is white and changes to a yellow color upon heating due to a change in the band gap. The different band gaps exhibit different absorption behavior leading to the development of different colors. This occurs due to the creation of defect centers in ZnO. The heating removes a minor quantity of oxygen from the system leaving free electrons at interstitial sites. Accordingly, the band gap of the heated ZnO differs significantly from that at room temperature [44].

### 2.2.3 Phase Transitions of Solid Electrolytes

Temperature-driven crystalline phase transitions may occur in some typical compounds resulting in color change. For example, cuprous mercuric iodide,  $\text{Cu}_2\text{HgI}_4$ , is red at  $20^\circ\text{C}$  in the ordered tetragonal phase and is maroon / black [40] at  $70^\circ\text{C}$  in the disordered, pseudo-cubic phase, possibly from transformation to a solid solution where the ionic conductivity is relatively high [45].

### 2.2.4 Change in Coordination Geometry of Metal-Complex Species

Temperature-driven changes in the coordination geometry of complexed species may also occur where a ligand's orientation around the transition metal ion can be developed, causing color changes. For example, at  $20^\circ\text{C}$ , bis(diethylammonium)tetrachloridocuprate(II) complex,  $(\text{Et}_2\text{NH}_2)_2\text{CuCl}_4$ , has a square planar geometry and it appears green, while at  $43^\circ\text{C}$ , a transition to tetrahedral geometry causes it to appear yellow [46].

### 2.2.5 Change in Coordination Number of Metal Complex Species

Temperature-driven changes in the coordination geometry of complexed species may also occur where a ligand's orientation around the transition metal ion can be developed, causing color changes. For example, at  $20^\circ\text{C}$ , bis(diethylammonium)tetrachloridocuprate(II) complex,  $(\text{Et}_2\text{NH}_2)_2\text{CuCl}_4$ , has a square planar geometry and it appears green, while at  $43^\circ\text{C}$ , a transition to tetrahedral geometry causes it to appear yellow[46].

### 2.2.6 Interconversion of Stereoisomeric Forms with Conformational Inversion

Interconversion of stereoisomeric forms of a compound on change in temperature also results in color changes. For example, thermal E, Z stereo-isomerization with conformational inversion was found to occur in the bianthrone series. The yellow-colored 2,2'-disubstituted

bianthrone, with carbonyl ( $>C=O$ ) groups at the 10,10'- positions, turns green upon melting with an increase in temperature [47]. In this case, a twisted conformation is formed with an accompanying conformational inversion which is responsible for the observed thermochromism.

### 2.2.7 Change in Molecular Structure

A change in temperature causes structural change in some spirooxazine molecules where ring opening usually occurs. This may result in changes in absorption behavior due to the different structures of the existing chromophore. The ring opening isomerization of the  $C_{\text{spiro}} - O$  chromophore occurs by both thermal and/or UV irradiation effects which generate different colors during heating and cooling as the molecular structure changes [48]. This type of molecule in a suitable medium may also change color with change in concentration. Thermal equilibrium exists between the parent molecule and the structurally changed molecule [49]. For example, some spirooxazines show strong color changes upon melting. In addition, a colorless very dilute solution of the order,  $10^{-6}$  mol/L in ethanol turns blue with increase in concentration.

### 2.2.8 Change in Crystal Structure

Variation in temperature may lead to a change in the crystal structure of organic compounds, causing color change. For example, liquid crystals may change their color due to a change in temperature. Rod-shaped liquid crystals are basically calamitic molecules which possess orientational order and these are aligned in the spiral position of a helical axis. The optical properties are symmetric about this axis and depend on this chiral nematic phase. If the temperature is changed, a phase transition occurs. The cholesterol derivatives exhibit color changes with temperature due to the existence of a nematic phase where the cholesteric type, liquid crystals are characterized by the helix pitch depending on the crystal's rotation with respect to the helical axis. The pitch length range of the helical structure is from 100 nm to

infinite. If the pitch length is in the visible region, then the reflection color becomes visible. Change in the pitch length of the helical structure of cholesteric liquid crystals may occur at different temperatures which results in different reflecting colors in the visible wavelength region [50].

In general, thermochromism in inorganic thermochromic compounds are due to a phase change of the entity to a different crystal structure and ligand geometry-based isomerization effects. For the organic and polymeric thermochromic materials, changes in molecular structures give rise to variations in the energy levels of the LCAO (linear combination of atomic orbitals) as well as interconversion of stereoisomeric forms which are the main factors responsible for thermochromism.

### **2.3 Classifications of TCMs**

On the basis of the chemical composition, thermochromic materials (TCMs) belong to four major categories. These include inorganic, organic, organic-inorganic hybrid, and polymeric TCMs [51-55] (Figure 6).

#### **2.3.1 Inorganic Thermochromic Materials (ITCM)**

The inorganic thermochromic materials exhibit thermochromic behavior at temperatures ranging from 70°C - 500°C. The ITCMs with a color change near 70°C have attracted much research interest for their prospective applications in building construction and energy efficiency[40]. The ITCMs are thermally stable above 200°C and maintain stable chromaticity, mechanical durability, and shelf-life stability for their stable crystal symmetry, as required for their reversible thermochromic effect. But these materials have some disadvantages for showing an irreversible and reversible thermochromic effect [56] at relatively high and fixed transition temperatures. Major ITCMs are toxic in nature, hence, suitable sealing to prevent environmental

release is required for their use. Examples of inorganic thermochromic materials are  $\text{Cu}_2\text{HgI}_4$  [57],  $\text{ZnO}$  [46],  $\text{Cr}_2\text{O}_3\text{-Al}_2\text{O}_3$  [58],  $\text{VO}_2$  and  $\text{TiO}_2$ [59]. In the  $\text{VO}_2$  and  $\text{TiO}_2$  system, the thermochromic effect is obtained from  $\text{VO}_2$  while  $\text{TiO}_2$  is responsible for only the photocatalytic effect. This work is focused on the multifunctional properties. Among these,  $\text{VO}_2$  is the most suitable inorganic thermochromic compound with its characteristic optical and electrical properties at transition temperatures around  $68^\circ\text{C}$   $\text{VO}_2$  [60] which exhibits a crystal phase transition [37a] with an accompanying thermochromic effect when the monoclinic (M) insulating phase [37b] transforms to the tetragonal, rutile (R), metallic form of the material. In this case, the vanadium atoms occupy the lattice point of the body-centered cubic structure and are located at the centers of the tilted  $\text{VO}_6$  octahedra. During the cooling phase transition from  $\text{VO}_2(\text{R})$  to  $\text{VO}_2(\text{M})$ , the vanadium atoms move along the V-V direction, resulting in the pairing and tilting of  $\text{VO}_6$  octahedra. The number of atoms in one  $\text{VO}_2(\text{M})$  unit cell is 12 which is doubled compared to the 6 atoms in one  $\text{VO}_2(\text{R})$  unit cell. Hence, dramatic changes occur in the optical properties in the near-infrared region during heating due to the metallic phase character at the transition temperature which is highly reflective with the ability to regulate solar heat flux by the automatic response to environmental temperature. The phase transition temperature can be decreased by incorporating a suitable dopant.[35, 61]. Although the rutile phase is apparently in a metallic domain, it is of anomalously low conductivity with other unusual properties due to strong electron-electron correlations according to the Mott model [38a]. However, thrust has been given to dope suitable metal oxides into the  $\text{VO}_2$  system to lower the transition temperature [62] for their smart and potential use to reflect solar heat flux. Presently work on localized surface plasmonic resonance (LSPR) of metallic character of  $\text{VO}_2$  system is being utilized by making composite with metamaterial, elastomer. The plasmonic effect due to the metallic

character of VO<sub>2</sub> has been followed in this case [39 b] to have relatively high absorption in the near IR region. One disadvantage is the toxicity of the VO<sub>2</sub> compound [63, 64].

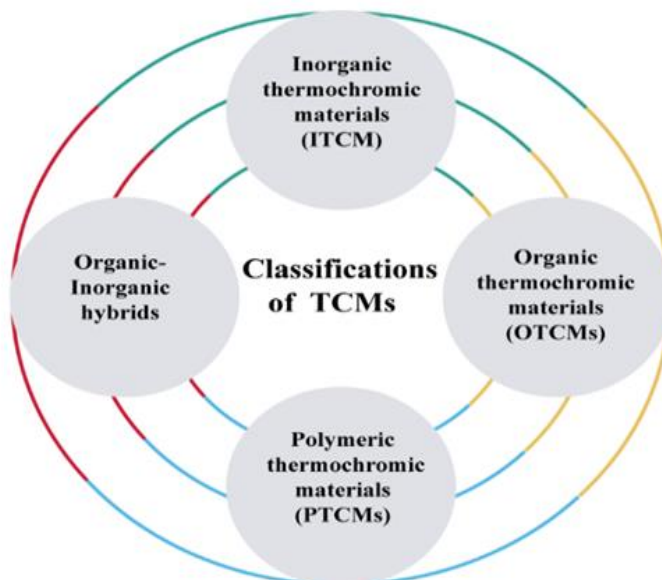


Figure 6: Classification of TCMs.

### 2.3.2 Organic Thermochromic Materials (OTCMs)

An organic, lactone ring-based dye, called a leuco dye, is a common organic thermochromic material (OTCM) due to its ability to switch between two reversible color forms. Structural changes (opening or closing of the lactone ring) occur by heat, light, or pH changes which cause a reversible change of color of the dye. Therefore, some leuco dyes are heat sensitive. Practically the color generating system of this type of organic dye consists of three components which include a lactone-based dye, a selected developer, and a selected solvent [65, 66]. Examples of leuco dyes are crystal violet lactone (CVL) [66, 67], spirolactones [68], fluorans [69], spirooxazine [70], and spiropyran [65, 71] leuco dyes. Crystal violet lactone is a mixture of the lactone derivative of crystal violet 10B and a triarylmethane organic dye. It changes color through heat treatment causing absorption at longer wavelengths. CVL possesses a high absorption coefficient, high chromaticity, and excellent oil solubility [67, 72]. Additionally,

the cost of this material is relatively low. On the other hand, spiropyrans change their colors through a ring opening reaction caused by UV irradiation and this occurs through the interconversion of the two species. These types of organic dyes have some advantages as isomerization occurs efficiently by simple irradiation with UV light. Moreover, the isomeric open and closed forms are thermally stable with very high photo-fatigue resistance [73-76].

### 2.3.3 Organic-Inorganic Hybrid Thermochromic Materials (OIHTCMs)

Organic-inorganic hybrid thermochromic materials usually involve a structural phase transition due to heat treatment which results in color change. Other factors such as changes in interatomic distance, intermolecular charge transfer, or strong  $\pi$ - $\pi$  interactions in the organic parts may also cause thermochromism [77, 78] in hybrid materials. For example,  $[(\text{PyCH}_2\text{NH}_3)_6][\text{Pb}_5\text{I}_{22}]\cdot 3\text{H}_2\text{O}$  is an OIHTCM in which a 2D inorganic layer is produced in between two organic layers through heat treatment. Reversible color change is observed turning from orange at room temperature to red at  $80^\circ\text{C}$  [79-82].

### 2.3.4 Polymeric Thermochromic Materials (PTCMs)

Polymeric thermochromic materials are of four types: (a) A polymer is itself thermo responsive with an inherent thermochromic property; (b) the polymer embeds thermochromic pigments; (c) the polymer possesses thermo responsive additives; and (d) the polymer contains a thermo-responsive dye having protic properties.

### 2.3.5 Polymers with Inherent Thermochromism

Liquid crystalline and conjugated polymers belong to this category [37]. If the liquid crystal polymers have a chiral molecular structure, they form helical superstructures and show a Bragg's reflection type of thermo-responsive effect on exposure to visible light [83]. The most common liquid crystalline phase is cholesteric liquid crystalline polymers [84]. The pitch length

of this type of liquid crystalline polymer changes with temperature which results in color changes for thermochromism. Examples of liquid crystalline polymers are cholesteric liquid crystalline polymers[84], polymer gels[85, 86], and thermochromic pigments which are microencapsulated cholesteric liquid crystals of relatively low molecular weight [50]. Among these, the most studied and commercially available are cholesteric liquid crystalline polymers [37]. The conjugated polymers also have inherent thermochromic properties [37]. They possess conjugated  $\pi$ -electron system, i.e. a backbone chain of alternate double and single bonds [37]. These polymers are colored as they absorb in the visible and there is variation of color with any change in their conjugation state with temperature which results in thermochromism [87]. Even a small change in their conformation such as a change in the stereoisomeric form results in significant color change which occurs during a phase transition [87]. Generally, conjugated polymers show reversible thermochromic effects. However, if the thermal treatment is kinetically controlled, then irreversible thermochromism will be observed [37]. Some examples of conjugated polymers are polyacetylenes [88, 89], polydiacetylenes(PDA) [90, 91], polysilanes [92, 93], polythiophenes [94, 95], and poly-(phenylenevinylene) [96, 97]. Another type of inherent thermochromic effect is observed in polymers having overcrowded partial stems of polycyclic aromatic groups. The thermochromism is observed for the increased thermal atomic oscillations [98] of the distorted molecules present in the overcrowded partial stems of the polymers.

#### 2.3.6 Polymers Embedding the Thermochromic Pigments

The most widely used thermochromic pigments are polymer microencapsulated leuco dye-developer-solvent systems. Usually, a polymer shell separates the core of thermochromic components which is basically a mixture of leuco dye, a developer, and a solvent. In the solid

state, they are generally colored but turns to a colorless liquid when heated [37]. There are also a few examples of a color change occurring in the phase transition from a liquid to a solid[99]. One example of leuco dye-developer-solvent is crystal violet lactone (CVL) – lauryl gallate (LG) -long chain alcohol (LCA) system. The system consists of the three components combined in the molar ratio of 1:6:40 [50]. LG and the LCA react strongly and form a colorless compound (LG)<sub>2</sub>-LCA. In the molten state, LG interacts weakly with LCA and strongly with CVL, resulting in the formation of colored complexes of the formula, (LG)<sub>x</sub>-CVL, where x can range from 3 to 9. Solidification with slow cooling causes expulsion of CVL from the (LG)<sub>x</sub>-CVL and results in the formation of the colorless (LG)<sub>2</sub>-LCA compound. Here, LCA also acts as a decolorizer by deactivating the CVL by complexation [55, 100]. Cholesteric liquid crystals of low molecular weight may also be used as a component of composite thermochromic pigments. In the case of using thermochromic pigments, microencapsulation of the pigments by a suitable polymer is the common art for technological development [50].

### 2.3.7 Polymers with Thermo Responsive Additives

Organic liquid crystalline materials possess helical superstructures, and these encompass a cholesteric type liquid crystal of chiral nature. Reversible phase transitions occur during heat  $\approx$  cool treatment. If this type of material is used as an additive with a non-thermochromic polymer matrix, then the overall polymer matrix shows thermochromism [83, 101].

### 2.3.8 Polymers with Protic, Thermo Responsive Dyes

A temperature dependent interaction occurs between the pH indicator dyes and hydrogel like polymers. For example, cross linking of polyvinyl alcohol (PVA) and borax yield a hydrogel polymer network. A temperature dependent phenol-phenolate equilibrium was observed in the PVA based hydrogel system of Reichardt betaine dye, 2,6-diphenyl-4-2,4,6-(triphenyl-1-

pyridinio)-phenolate (DTTP) and cresol red. The dye changes its color by protonation and deprotonation in aqueous media which allows it to function as a pH indicator [37].

### 2.3.9 Potentiality on the Classification of ThermoChromic Materials

Out of the different types of thermoChromic materials, the inorganic and organic hybrid materials possess unique physical, mechanical, and thermal properties due to the interfacial interactions between the organic polymer and inorganic species. These new hybrid materials possess tuneable, combined properties of both the organic polymer and inorganic glass. As there are thermoChromic materials of inorganic compounds as well as of organic polymers, combination of organic and inorganic thermoChromic materials with different physicochemical properties results in a multifunctional hybrid system with unique functional properties [102]. Examples of these hybrids are polydiacetylene (PDA)/ZnO [103], PDA/SiO<sub>2</sub> [104], cobalt(II)-chloro complexes [105], Ag/PDA [106], [C<sub>2</sub>-Apy][PbI<sub>3</sub>] C<sub>2</sub>-Apy<sup>+</sup> = 1-ethyl-4-aminopyridinium) [102], (2-aminobenzothiazolium)<sub>2</sub>CuCl<sub>4</sub> [107], [BMIP][Pb<sub>2</sub>C<sub>16</sub>] and [BMIP][Pb<sub>1.5</sub>Cl<sub>5</sub>]·H<sub>2</sub>O (BMIP<sup>2+</sup>=1,3-bis(1methylimidazolium)propane) [108].

### 2.4 Synthesis and Characterization of TCMs

The efficiency of thermoChromic materials can be upgraded by increasing the surface area of the material's particles. For better performance of thermoChromism it is important to increase the crystalline quality of the material striving for a low density of crystal defects [109]. If a nanoparticle synthesis route is exploited for the preparation of TCMs, then increases in surface area and crystalline quality can be achieved. There are a number of techniques to synthesize these materials as shown in Figure 7. However, the most commonly used techniques include microemulsion [110-112], sonochemical [113, 114], sol-gel, [115, 116], hydrothermal [117, 118], solvothermal [119], and gas pyro-hydrolysis [120]. Various characterization

techniques such as X-ray diffraction (XRD), Scanning Electron Microscopy (SEM), Energy Dispersive Spectroscopy (EDS), UV-Vis spectroscopy [6], shown in Figure 7.

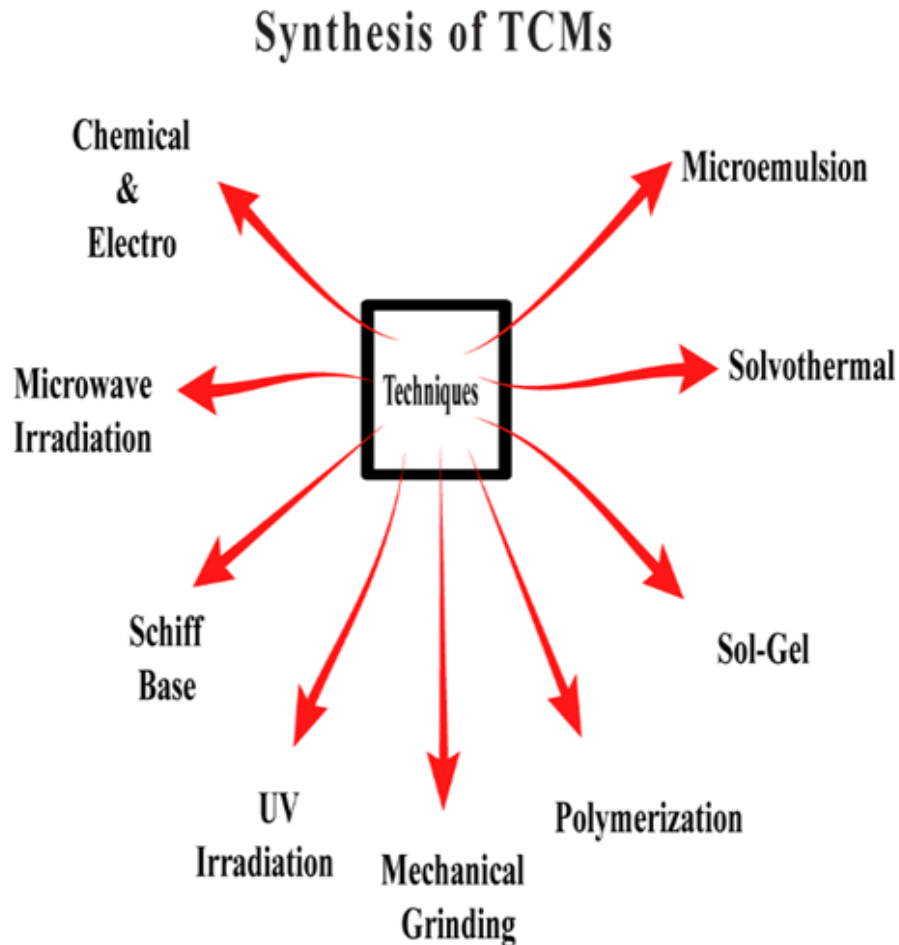


Figure 7: Synthetic Approaches to Prepare TCMs.

#### 2.4.1 Microemulsion Technique

The most frequently used technique for microemulsion first involves the synthesis of the material (possessing properties such as phase change, thermochromic, etc.), followed by in-situ encapsulation of the material. In the case of a phase change material that can be used for thermal storage, a surfactant-assisted microemulsion technique was used to synthesize  $\text{TiO}_2$  with an anatase rich phase and spherical shape (Figure 9A) [121, 122], where surfactant micelles act as a template for particle growth.

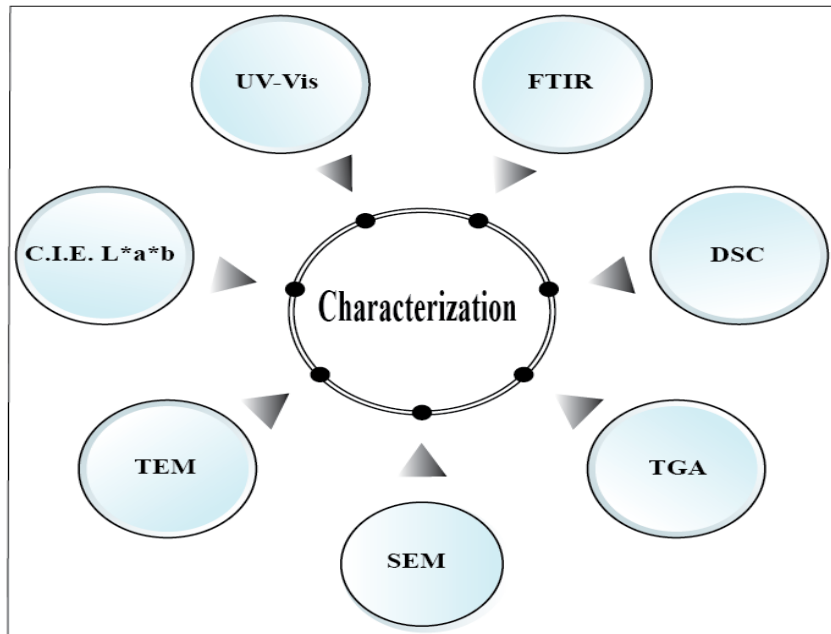


Figure 8: A Schematic of Various Techniques Used for the Characterization of Thermo-chromic Materials.

Increase in the acidity, by using the anionic surfactant sodium dodecyl sulfate (SDS), increased the nanocrystallinity [110]. Different shapes of TiO<sub>2</sub> such as rice, flower and star shapes (Figure 9 B) were obtained using tetramethyl ammonium hydroxide (TMAH) as a surfactant template in a hydrothermal route [123]. The hydrothermal process also helped develop high rutile, active site facets with photocatalytic activity three times that of a normal rutile site [124]. Cationic, anionic, and neutral surfactants (CTAB, SDS, and Triton X-100) were used to understand the effects of the surfactant and its charge on the phase-controlled synthesis of TiO<sub>2</sub> via pH and temperature dependent hydrothermal and microemulsion processes [125]. The synthesized TiO<sub>2</sub> phase was characterized using x-ray diffraction (XRD) (Figure 10 A) and scanning electron microscopy (SEM). The methyl orange degradation method (Figure 10 B) showed excellent photocatalytic activity which depends on several factors, especially the particle size and phase crystallinity. The control of particle size also depends on the stability, size, and shape of the surfactant micelles used for their synthesis [125]. The optical properties have been

determined by coating glass slides with different thermochromic materials with specific thickness around 300 μm (Figures 11 and 12).

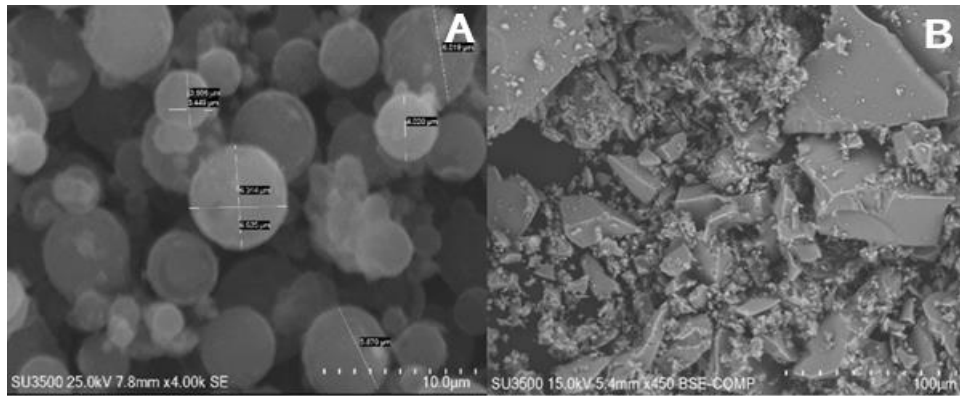


Figure 9: XRD of a Microencapsulated Phase Change Material (A) and Photocatalytic Degradation of Methyl Orange (MO) [41].

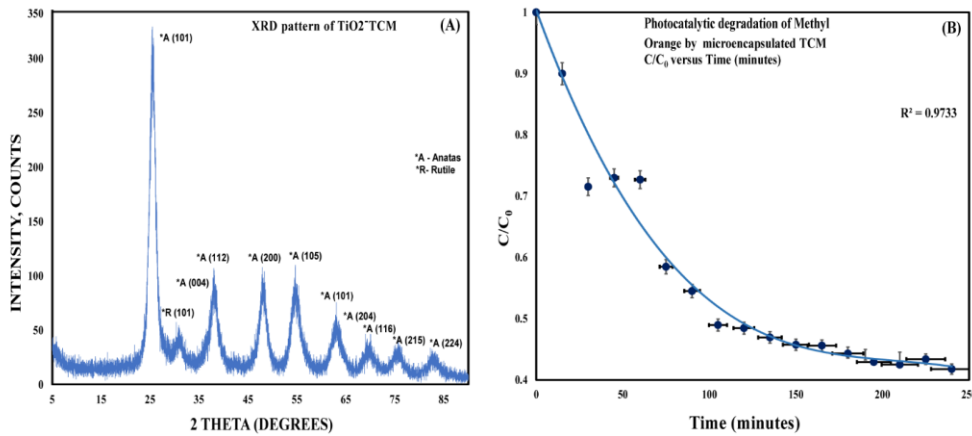


Figure 10: Microstructure of Microencapsulated Phase Change Material of Different Geometries [41].

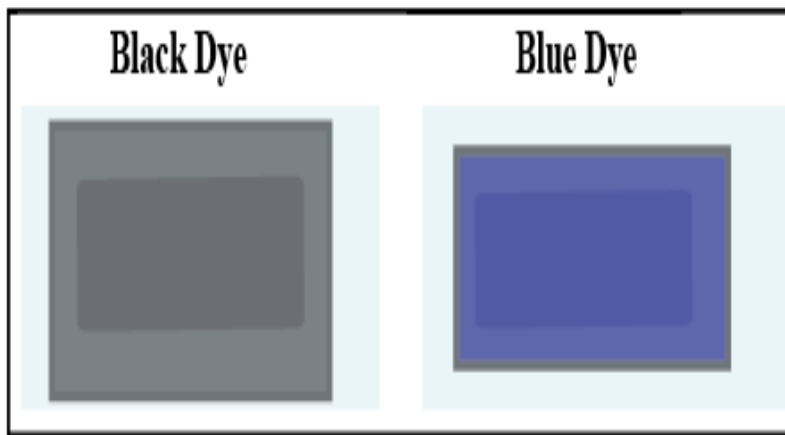


Figure 11: Optical Glass Images of the Black and Blue Thermochromic Materials.

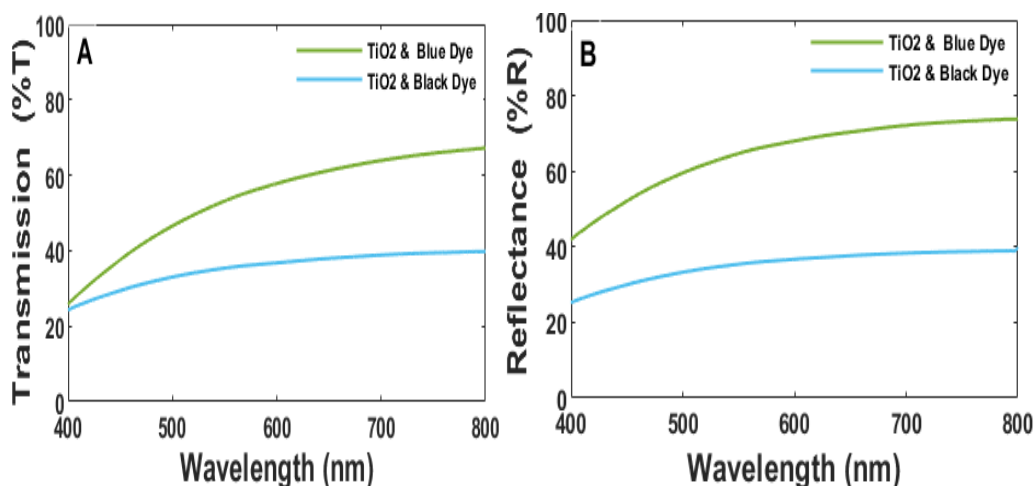


Figure 12: Transmission (A) and Spectral Reflectance (B) of TiO<sub>2</sub> Encapsulated Black Dye and Blue Dye.

#### 2.4.2 Solvothermal Technique

Slag wool fibers (SWF) can be modified by the deposition of cetyl trimethyl ammonium bromide (CTAB) to produce CTAB modified slag wool fibers (CMSWF). The SWF and the CMSWF were coated with anatase TiO<sub>2</sub> using a solvothermal method where the solvent was pure ethanol and the anatase TiO<sub>2</sub> precursor was titanium isopropoxide [119]. It was observed that TiO<sub>2</sub> coated CMSWF were stable upon UV irradiation and have a higher photocatalytic activity than the TiO<sub>2</sub> coated SWF [119]. A surfactant-free, solvothermal method was used to synthesize a rutile TiO<sub>2</sub> microsphere/graphene oxide (TiO<sub>2</sub>/GO) composite [126]. As the GO imparts excess charge transport routes to the system, the TiO<sub>2</sub>/GO composite showed an accelerated dye degradation performance compared to that of the TiO<sub>2</sub> microspheres alone [126].

#### 2.4.3 Sol-Gel Technique

Iodine-doped, nanovoid-structured TiO<sub>2</sub> was developed by sol-gel processing using titanium isopropoxide as a TiO<sub>2</sub> precursor diluted in a suitable solvent. Characterization by Fourier Transform Infrared (FTIR) and Raman spectroscopy, TEM, XRD, and the methylene blue degradation method revealed the surface-specific efficiency of photocatalytic activity which

is approximately 10 times higher than that of the commercial, P25 TiO<sub>2</sub> photocatalyst of smaller surface area [109]. Both ionic and non-ionic templating agents resulted in porous nanostructured TiO<sub>2</sub> coating of polyvinylidene fluoride membrane with a hierarchical structure and improved hydrophobicity [127] through sol-gel processing. The structure, wettability and desalination performance of the coating were dependent on the physical and chemical properties of the templating agents [127]. Simple sol-gel process has been followed to prepare spin coated VO<sub>2</sub> thin films on pure silica glass. Vanadium(V) oxide was dissolved in 30% hydrogen peroxide to make gel precursor. The VO<sub>2</sub> film was done by annealing the film at higher temperature (~750°C) in vacuum. These were characterized by XRD, microstructure, UV-Visible-NIR spectral studies, etc. The film exhibited very good thermochromic properties near 65 °C due to reversible metal-~insulator phase transition. The characteristic spectral behaviour (250 – 2500 nm) and the hysteresis loop (temperature versus % transmittance) due to heating and cooling in the temperature range (20 - 100 °C) were studied by N. Wang et al.

#### 2.4.4 Chemical and Electrochemical Polymerization Technique

The derivatives of the conductive polymer polythiophene exhibit good thermal and environmental stability and can be synthesized by introducing different groups at the 3- and/or 4-positions of the thiophene rings followed by polymerization through oxidation with iron (III) chloride (FeCl<sub>3</sub>) [128]. A copolymer of an alkylthiophene and azothiophene was synthesized which possessed improved solubility, optical, and chromic properties. The copolymer was characterized by high-performance size exclusion chromatography (HPSEC), thermal analysis, and UV-Vis spectroscopy. These systems exhibited thermochromic and solvo thermochromic properties [129]. Polythiophene-derived copolymers containing varying content of pyrene units were successfully synthesized using FeCl<sub>3</sub> as an oxidizing agent, and characterized by FTIR

spectroscopy, proton nuclear magnetic resonance spectroscopy ( $^1\text{H-NMR}$ ), and thermal gravimetric analysis (TGA) [130, 131]. Both copolymers exhibited good thermal stability and their transmittance spectra showed temperature dependent behavior [130, 131]. Figures 13,14 shows representative DSC ,TGA and FTIR profiles of pristine and microencapsulated TCM with  $\text{SiO}_2$  [132].

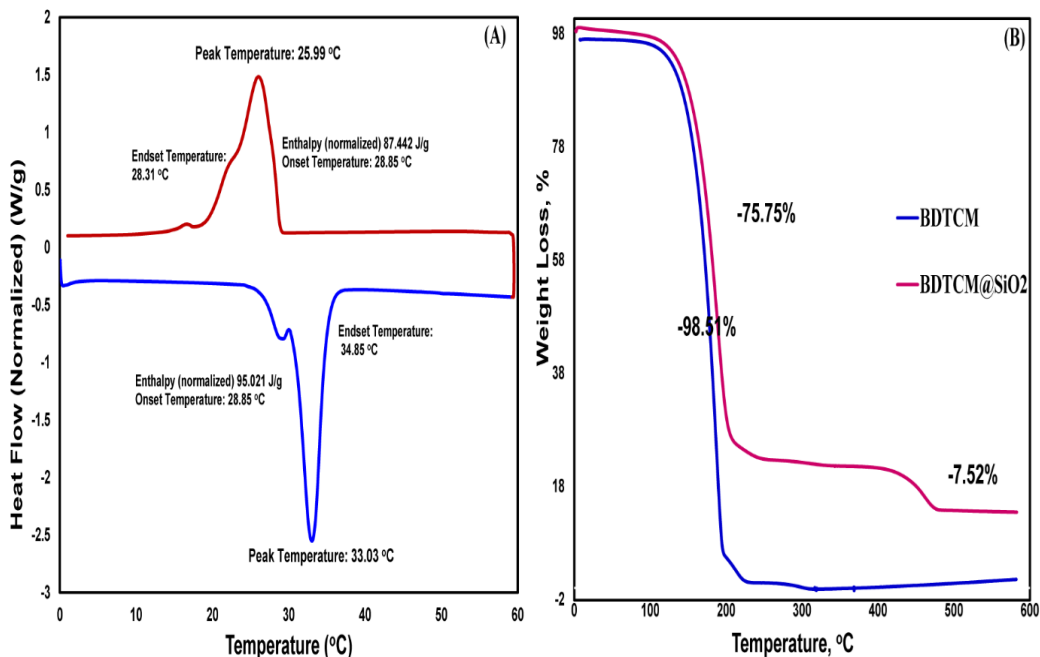


Figure 13: DSC (A) and TGA (B) Profiles of TCM and TCM Encapsulated with  $\text{SiO}_2$  [41].

#### 2.4.5 Mechanical Grinding Technique

A thermochromic Ni(II) complex, synthesized by grinding Ni(II) chloride with dilute HCl in an agar mortar pellet, exhibited a stable and significant thermochromic property as characterized by elemental analysis, FTIR spectroscopy, diffuse reflectance spectroscopy (DRS), SEM, thermal analysis including TGA, differential thermal gravimetry (DTG) and differential scanning calorimetry (DSC), XRD, and magnetic susceptibility studies [133]. The complex changed color from green to yellow / spring green by heating from room temperature to 100°C. Increasing the temperature to 120°C, it turns to dark blue. This color change was confirmed by

visual observation as well as by spectral measurements. This change in color with temperature is due to a change in the structural geometry of the complex's symmetry [133].

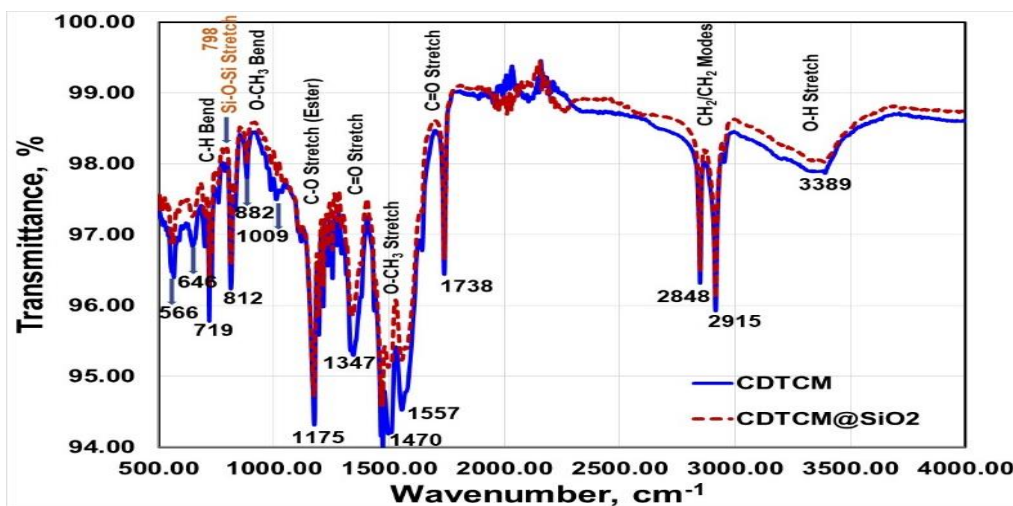


Figure 14: FTIR of TCM Encapsulated with SiO<sub>2</sub> [41].

#### 2.4.6 UV Irradiation Technique

Polydiacetylene (PDA) can be modified using carbamide like small compounds that can form hydrogen bonds and results in a polydiacetylene-based compound with improved properties which exhibits high temperature reversible thermochromism with a relatively high melting point. Mapazi et al. synthesized deep blue colored poly-pcd-urea by the irradiation of UV light (254 nm) onto the fine mixed powders of the starting components. The radiation introduced urea to the head group of 10, 12-pentacosadiynoic acid. The compound was characterized by UV-Vis spectroscopy, XRD, TGA and differential scanning calorimetry (DSC) analyses. The characterization of the compound revealed that poly-pcd-urea turned back into its original blue color on heating up to 150°C and the resultant polymer was thermally stable up to 315°C [134].

#### 2.4.7 Schiff Base Synthesis Technique

Zhu et al. synthesized three Schiff base compounds that are naphthaldehyde hydrazone derivatives, viz., N-(5-phenylthiazole-2-yl)-2-hydroxynaphthaldehydehydrazone (1), N-(4'-

chloro-5-phenylthiazole-2-yl)-2-hydroxynaphthaldehydehydrazone (2), N-(4'-nitro-5-phenylthiazole-2-yl)hydroxynaphthaldehydehydrazone (3) [129]. They characterized their thermochromic properties by temperature-variable IR, UV-Vis spectroscopic studies, TGA, and DSC analyses [135]. It was found that only compound 2 is thermochromic resulting from the original enol-imine tautomer switching to a keto-amine tautomeric form on heating [135]. Since all of the compounds had similar structures with the only difference being the substituted functional groups on the phenyl ring, it was expected that the ring substitutions made an important contribution to the thermochromism [135].

#### 2.4.8 Microwave Irradiation Technique

Mehta et al. used a polycondensation reaction to synthesize thermochromic material with bisphenol-A-based, benzoxazine monomer by microwave irradiation without using any solvent or catalyst. They characterized the product by FTIR and DSC analyses [136]. These results help in understanding and developing a smart thermochromic system based on polybenzoxazine.

### 2.5 Microencapsulation of TCMs

To increase the durability, versatility, and provide protection from the external environment, thermochromic materials are encapsulated with suitable film-forming materials to form microcapsules. Microencapsulation also protects TCMs from contamination as well as avoiding melting or sublimation of thermochromic components. If the thermochromic materials are organic and polymers, there is large possibility of photodegradation by UV radiation. Hence suitable encapsulation is essentially required to protect the TCM from photodegradation (vide supra). *In-situ*, chemical, polymerization-based deposition of a shell layer may be accomplished with a nanostructured shell component which is incorporated during the synthesis of leuco dye based TCMs by the microemulsion technique (vide supra). Moreover, the shell materials can also

be deposited onto the TCMs surface by different physical deposition techniques such as spraying, wetting / dipping, etc. As an example, Figure 15 shows how spraying technique develops homogeneous coating step by step. Solidification of all the components of TCM and shell material may also yield an encapsulated final product. Overall, the shell materials can be classified into three categories depending on their chemical nature: organic shells, inorganic shells, and organic-inorganic hybrid shells [137]. Organic shell materials include the natural and synthetic polymers which have sealing properties, structural flexibility, and are resistant to volume changes associated with the repeated transformations of thermochromic materials. Some examples of organic shells used in microencapsulation are poly (methyl methacrylate) [21, 138], urea-formaldehyde resin[139], polyurethane [140], polylactic acid [141] and melamine formaldehyde resin [142]. However, the applications of organic shells are restricted due to several limitations. Disadvantages include flammability, low thermal conductivity, and poor mechanical properties [143].

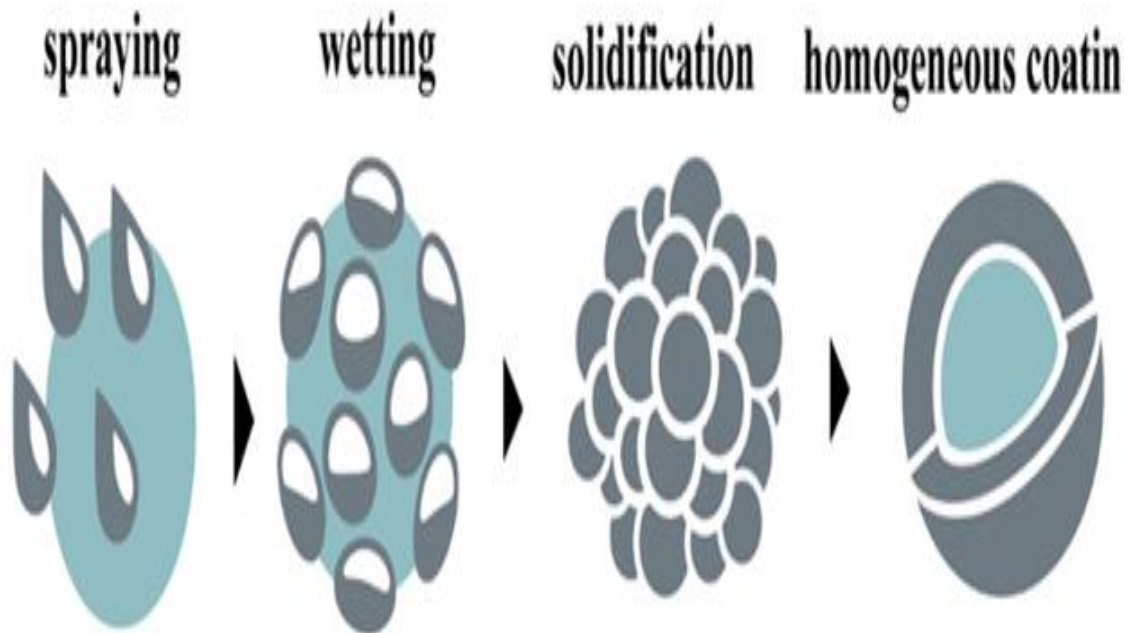


Figure 15: TCM Microencapsulation Process.

Recently, inorganic shells have been widely used for the encapsulation of thermochromic materials owing to their higher rigidity, mechanical strength, and better thermal conductivity as compared to organic shells [137]. Inorganic shell materials that are generally used for microencapsulation are SiO<sub>2</sub> [35, 144, 145], ZrO<sub>2</sub> [146], HfO<sub>2</sub>[147], and TiO<sub>2</sub> [145]. As the organic thermochromic materials (OTCMs) are usually degraded by UV radiation, these materials are protected by the development of core-shell structures (Figure 16) where the shell material is usually nanostructured, photocatalytic TiO<sub>2</sub> and SiO<sub>2</sub> mixed TiO<sub>2</sub>, and the core is the OTCM. To stabilize this shell structure, SiO<sub>2</sub> may be added to the TiO<sub>2</sub> system [148]. In addition, the shell material should possess a nanostructured form with a relatively high surface area possessing appreciable amounts of active sites for the formation of a chemically bonded, stable shell layer. A lot of work has been performed to develop nanostructured crystalline titania (vide supra) and silica-titania [148-150] systems which make the TiO<sub>2</sub> or TiO<sub>2</sub>-SiO<sub>2</sub> microencapsulated shell structure as desirable.

In order to take advantage of the individual properties of both organic and inorganic shells in a single material such as an organic-inorganic hybrid, hybrid shells have been developed and used intensely in the microencapsulation of thermochromic materials. To illustrate the individual properties, it may be stated that high rigidity, mechanical strength, and thermal conductivity are prevailing in the inorganic shells while good structural flexibility and sealing properties are present in the organic shells to complete entire desirable function of microencapsulation. Some examples of organic-inorganic hybrid shells are poly(methyl methacrylate)-SiO<sub>2</sub> [151], poly(methyl methacrylate)-TiO<sub>2</sub>[152], polyurethane-SiO<sub>2</sub>[153], and polyurea-SiO<sub>2</sub> [153]. Both organic and inorganic shells in a single material such as an organic-inorganic hybrid, hybrid shells are most focuses in this section.

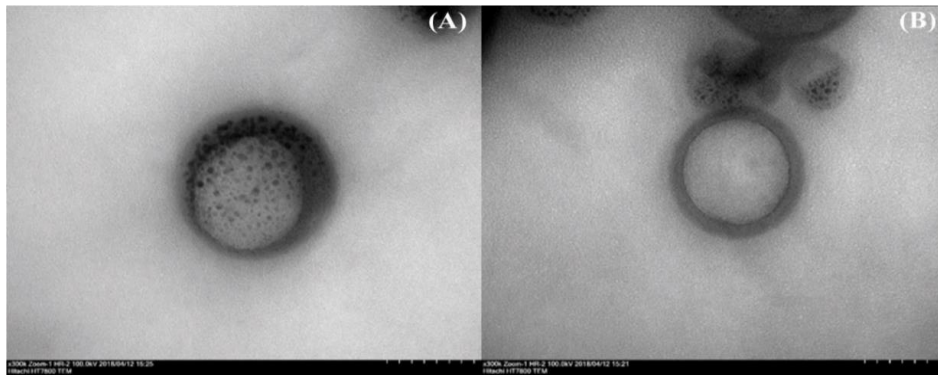


Figure 16: HRTEM Images of Core TCM Microencapsulated with a SiO<sub>2</sub> Shell [41].

### 2.5.1 Overview of Different Techniques of Microencapsulation

Several processes have been reported for the microencapsulation of thermochromic materials. Based on the deposition techniques, there are three types which can be defined as physical methods, chemical methods, and physicochemical methods. Each method has its own advantages and disadvantages which are depicted pictorially in (Figure 17).

### 2.5.2 Physical Methods

Thermochromic materials can be encapsulated by physical processes like drying, dehydration, and adhesion using processes such as spray-drying and solvent evaporation [137].

### 2.5.3 Spray Drying

In the spray drying method, an oil-water emulsion containing the thermochromic and shell materials is prepared, and then the emulsified material is sprayed in a drying chamber using an atomizer. The sprayed droplets are dried by passing a drying, gas stream at an optimum temperature, and then solid particles are separated by a cyclone and filtered [154]. Hawlader et al. microencapsulated paraffin particles with gelatin and gum arabic using the spray drying method, which was shown to have a thermal energy storage / release capacity of about 145-240 J/g. Therefore, the method is very promising and the product can be a potential storage material for solar energy [155]. Microencapsulation of paraffin Rubither®RT27 with carbon nanotubes

by the spray-drying method resulted in an enhanced thermal conductivity of paraffin which was found to be stable and reversible on microencapsulation [156].

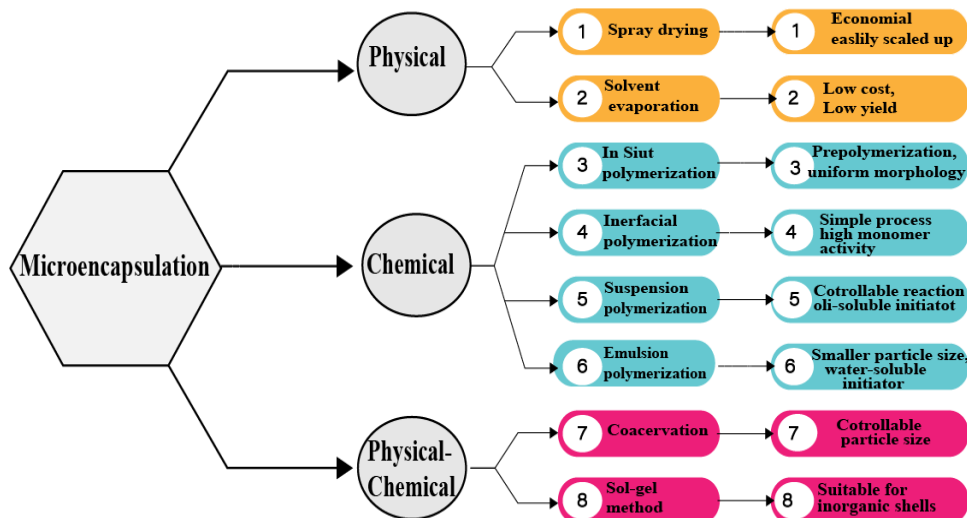


Figure 17: Common Methods of Microencapsulation Along with Their Basic Principle of Deposition and Properties.

#### 2.5.4 Solvent Evaporation

Solvent evaporation is another method of encapsulation which involves the preparation of polymer solution precursor first by dissolving the shell materials in a volatile solvent, then followed by addition of thermochromic materials to the solution to form an oil-water emulsion. On solvent evaporation, shells are formed on the droplets of the thermochromic material, resulting in microcapsules after filtration and drying [137]. For example, microencapsulation of sodium phosphate dodecahydrate (DSP) with poly(methylmethacrylate) (PMMA) by the solvent evaporation method resulted in microcapsules which possess an interesting energy capacity of 142.9 J/g at 51.51°C and can be used for several applications [157]. Microencapsulation of myristic acid with ethyl cellulose using the solvent evaporation method prevented the leakage of melted myristic acid with consequent storage and release of latent heat through a solid-liquid phase transition [158]. Microencapsulation also prevented its contact with the external

environment [158]. Physical methods of microencapsulation offer several advantages which include low processing cost, production of a wide variety of potential coating materials with good encapsulation efficiency, and good stability of the microcapsules. These methods can be scaled-up in a continuous process mode [159]. Aside from these advantages, the physical methods have the disadvantage of possible temperature-degradation of temperature-sensitive materials. These methods also have limitations with respect to controlling particle size and the yields are relatively low in small batches [159].

#### 2.5.5 Chemical Methods

In chemical microencapsulation, shells are formed around the core by the polymerization or condensation of monomers, oligomers, or prepolymers at an oil-water interface [137]. The chemical methods of microencapsulation include *in situ* polymerization, interfacial polymerization, suspension polymerization, and emulsion polymerization [137].

#### 2.5.6 *In situ* Polymerization

In *in situ* polymerization, prepolymerized monomers are further polymerized on the surface of an emulsion droplet [137]. In this process, thermochromic material was added to the solution of surfactant to prepare the oil-in-water emulsion, and a separate prepolymer solution was formed from the monomers. Then, at optimum reaction conditions, the prepolymer solution was added to the oil-in-water emulsion to form the microcapsules [137]. Zhang et al. prepared microcapsules containing an n-eicosane core and ZrO<sub>2</sub> shell by *in situ* polymerization [146]. The microcapsules prepared had dual functionality which included latent-heat storage / release capability and photoluminescence. Thermochromic microcapsules containing thermochromic compounds as a core material and urea-formaldehyde as a shell material were prepared by *in situ* polymerization. It was observed that the surface morphology and the particle size of the

microcapsules were affected by the emulsifying agents preconditioning. Zhu et al. [139] proposed that the properties of the microcapsules are dependent on the stirring rate and core-to-shell ratio.

#### 2.5.7 Interfacial Polymerization

In interfacial polymerization, the polymerization takes place at the oil-water interface where two reactive monomers are dissolved separately under the action of an initiator [137]. Chang et al. reported the encapsulation of VO<sub>2</sub> films within hafnium dioxide (HfO<sub>2</sub>) layers.[147], as HfO<sub>2</sub> has a suitable refractive index (1.85 – 2.1) with low absorption in the range, UV to the mid IR [160]. Moreover, it has natural hydrophobicity, a relatively low vapor pressure transmission rate, and excellent mechanical properties which result in enhancing the thermochromic performance of VO<sub>2</sub>. Hence, HfO<sub>2</sub> provides an excellent protective layer as an overcoat of VO<sub>2</sub> films [147].

#### 2.5.8 Suspension Polymerization

The suspension polymerization method involves the suspension of dispersed droplets containing thermochromic materials, monomers and initiators in a continuous aqueous phase with the help of surfactants and mechanical stirring [137]. Here, the initiator free radicals are released into the suspension to initiate monomer polymerization at an optimum temperature and stirring rate [146]. Novel and low, supercooling spherical microcapsules containing a n-octadecane core with n-octadecyl methacrylate-methacrylic acid (MMA) copolymer as a shell were prepared by suspension polymerization [161]. The n-octadecane was microencapsulated in the thermochromic pigment / PMMA shells using a suspension polymerization method with five different pigment-to-MMA ratios. The highest melting and crystallization enthalpies were achieved for the microcapsules without pigment [162].

# Microencapsulation

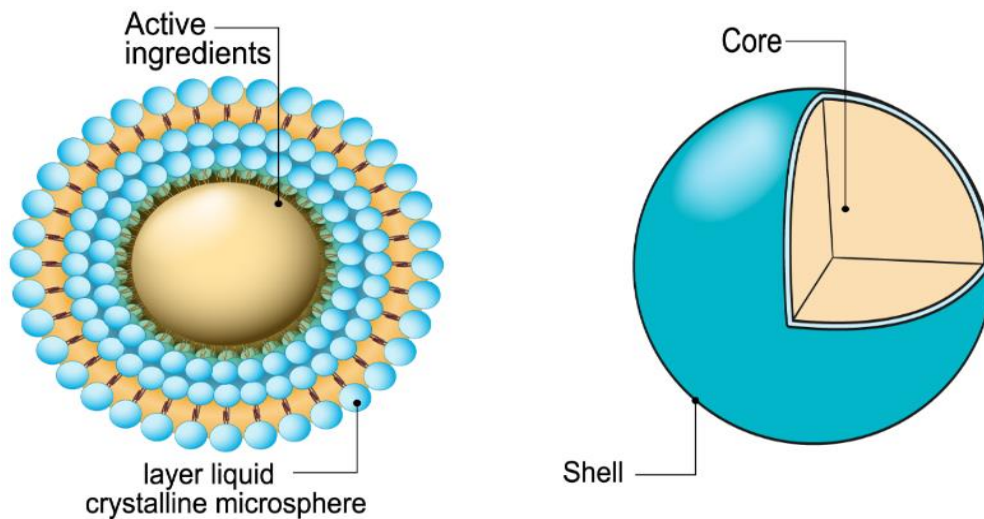


Figure 18: Microencapsulation Mechanism Showing Tiny Particles (Droplets) of Active Ingredients are Surrounded by a Coating Shell (Multilayer Liquid Crystalline Microsphere).

## 2.5.9 Emulsion Polymerization

Emulsion polymerization (Figure 18) involves suspension of a dispersed phase consisting of thermochromic materials and monomers in a continuous phase as discrete droplets with the help of surfactant and vigorous agitation. Here, the initiator present in water and solution media triggers the polymerization [163]. Ma et al. demonstrated the microencapsulation of thermochromic dyes with water-soluble monomers or polymers using an emulsion polymerization process in which thermochromic dyes were emulsified in water followed by polymerization on the surface of microbeads of the thermochromic dyes. The microcapsules formed protected the sensitive thermochromic dyes from building coating components [164]. Encapsulation of  $\text{TiO}_2$  nanoparticles with a highly uniform shell of carbon ( $\text{TiO}_2@\text{C}$  nanoparticles) by emulsion polymerization alleviated the problem of moderate photocatalytic activity displayed by  $\text{TiO}_2$  semiconducting nanoparticles due to their relatively high band gap and high rate of electron-hole recombination [165].

#### 2.5.10 Physicochemical Method

In the physicochemical method, physical processes such as phase separation, heating, and cooling are combined with the chemical processes such as hydrolysis, cross-linking, and condensation to achieve efficient microencapsulation. Examples of physicochemical methods are supercritical emulsion extraction, sol-gel method, coacervation, and melt-coaxial electrospinning.

#### 2.5.11 Supercritical Emulsion Extraction

In the continuous supercritical emulsion extraction (SEE-C) method, organic solvents are continuously extracted from emulsions using a counter current packed tower [161]. This results in microsphere formation which are recovered from the bottom of the tower in the form of a water suspension [166]. Campardelli et al. produced photoactive and biodegradable polylactic acid/TiO<sub>2</sub> (PLA/TiO<sub>2</sub>) nanostructured particles [141]. exploiting the supercritical emulsion extraction technique. TiO<sub>2</sub> particles were encapsulated with PLA microspheres by the continuous supercritical emulsion extraction technique retaining the photocatalytic and bactericidal activity of TiO<sub>2</sub> [141].

#### 2.5.12 Sol-Gel Processing

The sol-gel method is the most commonly and widely used method for the core microencapsulation. It involves the uniform dispersion of the constituents such as thermochromic materials, precursor, solvent, and emulsifier, in a continuous phase to form a colloidal suspension / solution by the hydrolysis reaction of the components, followed by formation of a polymeric gel system through polycondensation / polymerization of monomers, which results in microcapsules after drying, sintering, and curing processes. In this method, inorganic materials like SiO<sub>2</sub> and TiO<sub>2</sub> can be generally used to form the shells [145]. Yi et al. prepared composite

thermochromic and phase-change materials (CTPCM) containing bromocresol purple, boric acid, and tetradecyl alcohol. They encapsulated it in the three-dimensional network of the SiO<sub>2</sub> gel using the sol-gel method. These CTPCM exhibited good thermochromic behavior and thermal properties with a good appearance on treated textiles [144]. Zhang et al. prepared silica encapsulated thermochromic leuco dye nanocapsules (TLD@SiO<sub>2</sub>) by a sol-gel method to generate dye polyester fabrics [35]. For encapsulation, they hydrolyzed tetraethyl orthosilicate and condensed it onto the surface of the emulsified thermochromic leuco dye nano-droplets [35]. Dyeing of fabrics with TLD@SiO<sub>2</sub> provided durable, reversible color changing fabrics with excellent color response fastness [35].

#### 2.5.13 Coacervation Method

Depending on the number of shell materials used in the coacervation, it is categorized into simple coacervation and complex coacervation. The simple process involves only one type of shell material while the complex one requires two types of shell materials of opposite charge. Complex coacervation results in microcapsules with better morphology, uniform size, and better stability than in simple coacervation. Complex coacervation involves the dispersion of thermochromic materials in an aqueous polymer solution to form an emulsion, followed by the addition of a second aqueous polymer solution of opposite charge, resulting in the deposition of shell material on the surface of droplets by electrostatic interactions. Then stable microcapsules are formed by cross linking, desolvation, or thermal treatment [145]. Wu et al. microencapsulated reversible thermochromic phase change material containing a spironolactone derivative as color former, a phenolic hydroxyl compound as color developer, and 1-hexadecanol as the phase change material and co-solvent. This was followed by complex coacervation of modified gelatin containing vinyl groups and gum Arabic. The stability of microcapsules and

encapsulation efficiency were further improved by the cross-linking between vinyl groups on modified gelatin, a divinyl crosslinker and subsequent glutaraldehyde cross-linking [142].

#### 2.5.14 Melt Coaxial Electrospinning Method

The melt coaxial electrospinning method allows microencapsulation of non-polar solids by combination of melt electrospinning and a coaxial spinneret [167]. A phase-transformation thermochromic material, consisting of CVL (crystal violet lactone), bisphenol A, and 1-tetradecanol core, was encapsulated in a poly(methyl-methacrylate) nanofiber shell Figure 19A by the melt coaxial electrospinning technique. Figure 19 B shows SEM microscopic images of electrospun thermochromic fibers encapsulated with TCM. The fabricated core-shell nanofibers have good thermal energy management, fluorescent thermochromism, and reversibility. Hence this method has good potentiality in the preparation of temperature sensors with good fluorescent signals and body-temperature co-reactive materials to give rise to intelligent thermal energy absorption, retention, and release [21].

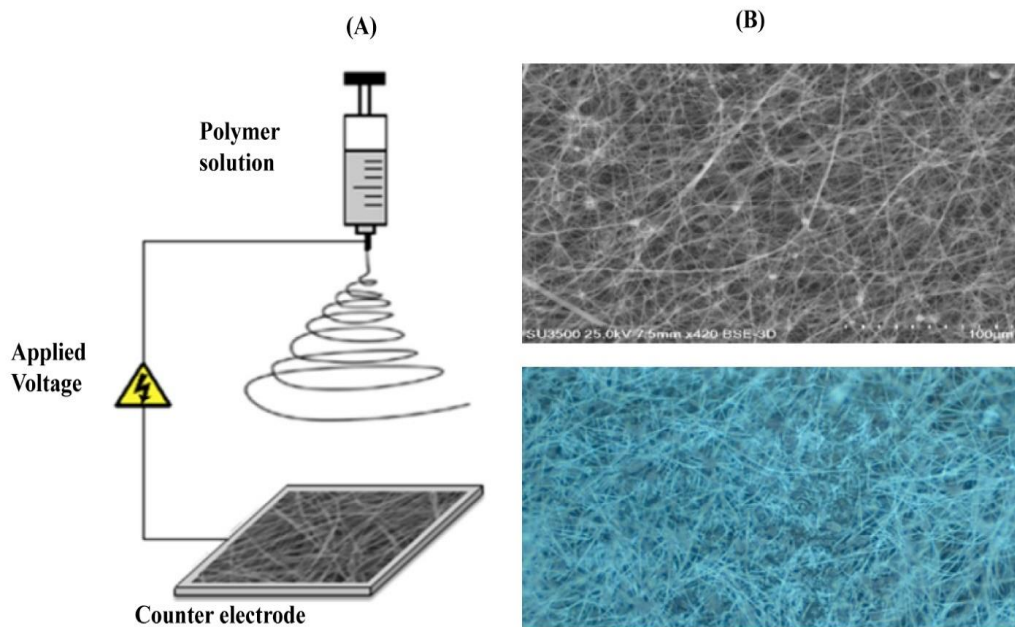


Figure 19: Electrospinning Apparatus (A) [168] and Optical/SEM Microscopic (B) Images of Electrospun Thermochromic Fibers Encapsulated with TCM [169].

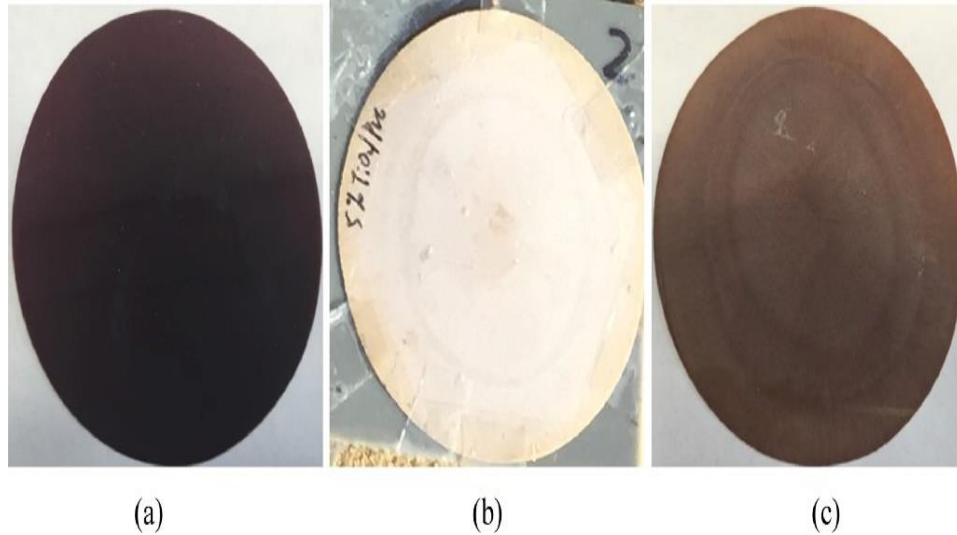


Figure 20: Optical Coatings of (a) Plan TCM , (b)  $\text{TiO}_2$  Coating and (c) TCM with  $\text{TiO}_2$  [170].

## 2.6 Thermochromic Coating

The properties and functionality of thermochromic coatings (Figure 20) can be enhanced by making the precursor wettable to a substrate by mixing with an appropriate surfactant. The precursor materials are of different forms as required for the deposition technique used. Coating also provides protection from the external environment like exposure to UV radiation, weather conditions, oxidation, and other elements susceptible to react. There are different methods available for thermochromic coatings that include physical vapor deposition, pulsed laser deposition, sol-gel deposition, and chemical vapor deposition methods [171].

### 2.6.1 Physical Vapor Deposition (PVD)

In this method, thermochromic materials to be coated are chosen as target which is bombarded using high energy beam of electrons or ions under reduced pressure. This results in displacement and vaporization of the atoms from the surface of the thermochromic materials[171] that targets the substrate surface through the created flux path. Thus, this method mainly involves evaporation of the thermochromic materials. Sputtering method is a PVD

technique. There are several types of sputtering methods that are used for the deposition of thermochromic materials. As for example, radio frequency magnetron sputtering[172], direct current magnetron sputtering[173] and ion beam sputtering[174] are suitable sputtering systems for these materials. Using the PVD technique, suitable doping can also be accomplished by incorporating the doped material into the main target TCM. However, in this case, preparation of a doped target is a critical job as doping is dependent on target size of homogeneous mixed components. The simple mixing would generate inhomogeneous film product. However, the doped target is placed in the vacuum deposition chamber for the coating [175].

### 2.6.2 Pulsed Laser Deposition (PLD)

Recently, laser ablation has been used for the coating of thermochromic materials. It is also a type of PVD technique. This was initially used to deposit the superconductor oxides and it is very suitable for metal oxide film growth. In PLD, the thermochromic material to be deposited is placed in a vacuum chamber and targeted with a high energy pulsed laser beam in order to withdraw atoms / molecules from the target. The deposition can be done either in ultra-high vacuum or in the presence of background gas, which is selected according to the desired product. For example, oxygen is used for the deposition of oxides. The vaporized thermochromic materials are deposited as thin films on the substrate [171]. This technique was first used by Borek et al. in 1993 for the deposition of VO<sub>2</sub> film. They used a krypton fluoride (KrF) pulsed excimer laser (248 nm) to withdraw the atoms from the metallic vanadium target placed in the deposition chamber filled with argon and 10% oxygen (100-200 mTorr). Deposition of pure VO<sub>2</sub> on the substrate was maintained at approximately 500°C.[176] The same method was also applied to deposit a thin film of VO<sub>2</sub> on sapphire substrates at 630°C using the KrF pulsed excimer laser (193 nm) to withdraw / expel atoms from 99% pure pressed V<sub>2</sub>O<sub>3</sub>[177].

### 2.6.3 Sol-gel Depositions

This method is widely used for thermochromic coatings [178]. In this method, a colloidal sol of thermochromic material is prepared in a suitable solvent / solvent mixer medium by controlled hydrolysis and polycondensation reactions [179]. Maintenance of wettability, viscosity, and concentration control is very important for the deposition of layers on suitable substrates by the dipping or spinning technique. Wettability depends on the surface tension of the medium and adherence of the precursor with the substrate depends on the wettability. The resulting physical thickness of the coatings / films depends on the viscosity of the precursor. Relatively high thickness films have been developed from the precursors of relatively high viscosity. Physical thickness also depends on the concentration of the precursor. The higher concentration would generate relatively high thickness. The colloidal precursor sol thus prepared was subjected to physical treatment like drying, heating or aging for the attainment of suitable concentration, viscosity, porosity and crystallinity. This results in the formation of a metal oxide network by connection of metal (M) and oxygen (O) as -M-O-M- or -M(OH)-M- polymers in a gel of the precursor, by following condensation reaction. The hydroxo containing polymer is partially condensation polymer. This precursor is used to deposit films onto a substrate either by the dipping or spin coating method. Takahashi et al. used three types of precursor sols containing (i) polyvanadate with W and V, (ii) polymolybdate with W and Mo, and (iii) polytitanate with W and Ti to prepare thermochromic materials. These were used to deposit materials onto suitable substrates by the spin coating technique for the successful development of thermochromic coatings using sol-gel processing [171]. Moreover, physical thickness of the coatings / films depends on the viscosity of the precursor in this case of method.

#### 2.6.4 Chemical Vapor Deposition (CVD)

This method is widely used in the industry to make the thermochromic thin films with high functionality and premium quality. In CVD, thermochromic thin films are deposited via chemical reactions in the gaseous phase using suitable precursor chemicals such as hydrides, halides, and organometallics. In addition, materials including metals, carbides, nitrides, oxides, and sulfides, are utilized as precursors [171]. Deposition of pure VO<sub>2</sub> films by the CVD technique usually exploits organometallic vanadium compound-based precursors. However, some researchers refer to this technique as metal-organic CVD or organometallic CVD. Coating using CVD techniques can be atmospheric pressure-assisted or aerosol-assisted. Greenberg successfully deposited pure VO<sub>2</sub> thin films onto glass substrate using vanadyl tri-isopropoxide as a precursor in an open atmosphere, with and without post-annealing [180]. Takahashi et al. also deposited pure VO<sub>2</sub> thin films onto glass substrate; however, they used vanadyl tri(isobutoxide) as a precursor [181]. Barreca et al. prepared VO<sub>2</sub> and V<sub>2</sub>O<sub>5</sub> thin films using vanadyl precursors VO(L)<sub>2</sub>(H), where L is a β-diketonate ligand at 380°C in different atmospheres such as O<sub>2</sub>, N<sub>2</sub> and a mixture of N<sub>2</sub> and H<sub>2</sub>O [182]. In the case of VO<sub>2</sub> films, the precursors used in CVD require post-reduction to form the desired vanadium (IV) oxide thin films.

#### 2.6.5 Advantages and Disadvantages of the Coating Methods

There are several advantages and disadvantages associated with the different techniques adopted for thermochromic coatings. As the PVD technique has a slow film growth rate, it can produce homogeneous ultra-thin TCM coatings and is a relatively easy and efficient way of utilizing precursors, if no dopant is used. In the case of formation of doped TCM coatings, fabrication of a suitable target requires a lot of effort [183]. Its feasibility at low temperatures makes it a compatible technique with different substrates. However, maintenance of requisite

vacuum at reduced pressure, in the case of physical vapor deposition (PVD) sputtering systems, takes considerable time and overall, the equipment is expensive. Accordingly, the cost of production is relatively high for the slow rate of production. Thus, the application of PVD on a commercial scale is restricted as it is not economical[184]. The PLD technique has the advantage of maintaining the target stoichiometry in the coated films which is due to the high ablation rate that allows the target metal to evaporate simultaneously. It is a clean, versatile, and economic coating technique [185]. However, it has the disadvantage of a limited sample size. Inhomogeneity in film / coating quality occurs, if the substrate / sample size is increased. This results in thermal surface defects due to particulate splashing of the film[185]. Moreover, the equipment is of relatively high maintenance cost. Sol-gel techniques / processing is very simple and cost effective as simple mixing of requisite components including the dopant system can be accomplished homogeneously in a suitable solvent medium to prepare a precursor. Its shelf life can be increased by using chemical stabilizer. And the equipment for deposition is of very low cost as a simple dipping operation followed by withdrawal is enough for the deposition of a homogeneous layer onto the substrates in the sizes ranging from 2.0 cm x 2.0 cm to 100.0 cm x 100.0 cm. The spin coating technique can also be used for the deposition, but the substrate size range is limited to ensure homogeneous coatings. But the main drawback of this processing is that it is a slow and a multi-step process may be required for deposition of relatively high thickness. It also requires considerable time for sol establishment, maintenance of uniform viscosity and surface tension. However, using this technique, the substrate is fully coated with a uniform thickness throughout its surface at low temperature by using readily available precursors [186]. CVD is an effective technique that offers high coating rates at low temperatures, and it can also produce pure, dense, and uniform thin films / coatings with good adhesion properties. It

requires inexpensive precursors which are readily available and thus is a very economical technique on the industrial scale. It does not require a vacuum or reduced pressure and has a moderately high film growth rate [187]. But for large scale production, the cost of equipment for a large scale manufacturing unit is quite high and it is not possible to perform multiple layer coatings with defined stoichiometry using this technique [188].

## **2.7 Photodegradation and Thermal Degradation of TCMs**

The lifespan of the TCMs is affected by the external environment including solar radiation, high temperature, aerial oxygen, and atmospheric pollutants [189]. Photodegradation and thermal degradation are the two main problems hindering the successful application of the TCMs. Deterioration occurs when the TCM is exposed to solar radiation and higher temperatures, leading to the loss of the reversible thermochromic effect. These phenomena are known as photodegradation and thermal degradation. Exposure to solar radiation either breaks the polymer chains of TCMs or cross-links them, resulting in changed mechanical and chemical properties that eventually lead to the loss of a reversible thermochromic effect [190, 191]. Several TCMs have exceptional thermal stability, however, exposure to higher temperature may result in an irreversible color change. In some TCMs, made of phosphates, carbonates and hydroxides groups such type of behavior is observed due to their decomposition. The resultant color of the irreversible TCMs depends on the environmental temperature and the time of exposure in that environment. The solar radiation that reaches the Earth's atmosphere is in the wavelength range from 295 to 2500 nm. These radiation wavelengths are classified as UV-B (280-315 nm), UV-A (315-400 nm), visible (400-780 nm) and near-infrared (780-2500 nm). (Figure 21) [192]. The UV-B radiation has the highest photon energy and quickly degrades TCMs through the direct photolysis of the covalent bonds of the organic / polymeric TCM components. Fortunately,

because of the stratospheric layer, a very small amount of UV-B reaches the Earth's surface. Solar radiation contains about 4-5% UV-B and UV-A and this can greatly damage organic TCMs. Visible light may also cause damage to the TCMs due to the presence of photosensitizing chromophores in the materials that accelerate polymer degradation, but this damage is very very low. Finally, infrared radiation can also cause thermal degradation of TCMs, resulting in a transformation to a darker pigmentation [193].

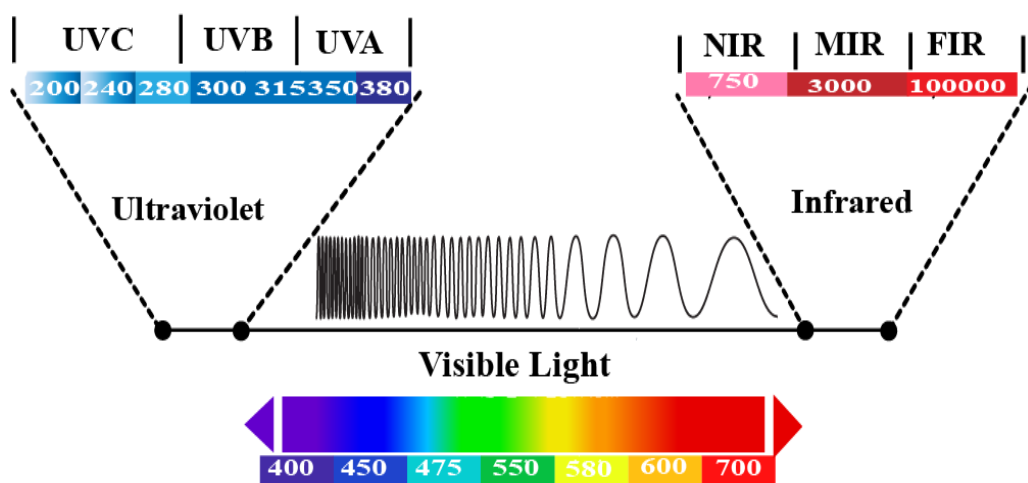


Figure 21: Classification of the Electromagnetic Radiation Spectral Wavelength Range.

TCMs often undergo photooxidation in the presence of aerial oxygen and thereby solar radiation generates peroxidic species that initiate a free radical chain reaction to accelerate photodegradation. Use of photo-antioxidants and quenchers during fabrication of TCMs helps in inhibiting photooxidation. Photo-antioxidants deactivate generated peroxidic species and quenchers deactivate the excited species of the chromophore present in the polymer. As for example, the chromophore, carbonyl groups in the polymer dissipate energy in the form of heat or fluorescent and phosphorescent radiations. As most of the quenchers are salts or chelates of nickel that turn the TCMs green, compatibility and environmental contamination issues restrict the application of these quenchers [189].

Photodegradation can be inhibited or reduced using photostabilizers, like UV-absorbers or light screening pigments, that prevent the effects of exposure to solar radiation on the TCM polymer matrices [189]. Light screening pigments minimize the penetration of harmful solar radiation by selectively absorbing the incident radiation, and to some extent, also deactivating the photoactivated species [194]. UV-absorbers are colorless compounds that possess high absorption coefficients in the UV region of the solar spectrum. They absorb harmful actinic solar radiations preventing the generation of excited chromophoric impurities, thereby, protecting the TCMs from photo induced damages [195, 196].

Thermal degradation of TCMs is an auto-oxidation process and this occurs due to overheating. Higher temperatures or longer exposure to near infrared radiation may cause breaking of the TCM backbone, the fragments of which on reacting with each other change the physical and chemical properties of the parent TCM [197]. Thermal stabilizers including polypropylene and polyethylene can be used to prevent the thermal degradation of TCMs by keeping the polymer chains and the original molecular structure intact, thereby retaining the thermochromic properties of TCMs over a longer period of time [198].

## **2.8 Applications of TCMs**

TCMs can play an important role in the development of energy-efficient buildings as shown in Figure 22 and demonstrated through modelling using Energy Plus [170], to reduce energy consumption and greenhouse gas emissions. Due to lighting, air-conditioning, and heating, buildings consume 40% of the energy and emit almost 30% of the anthropogenic greenhouse gases [199, 200]. TCM coatings on building fenestrations is a feasible approach to reduce the building energy consumption. TCM coatings are reflective in the summer due to the temperature-based transition to a white colored phase and can reduce the air-conditioning energy

consumption. In the winter they are absorptive due to their low temperature colored state (black), thereby reducing the energy needed to heat a building [201].

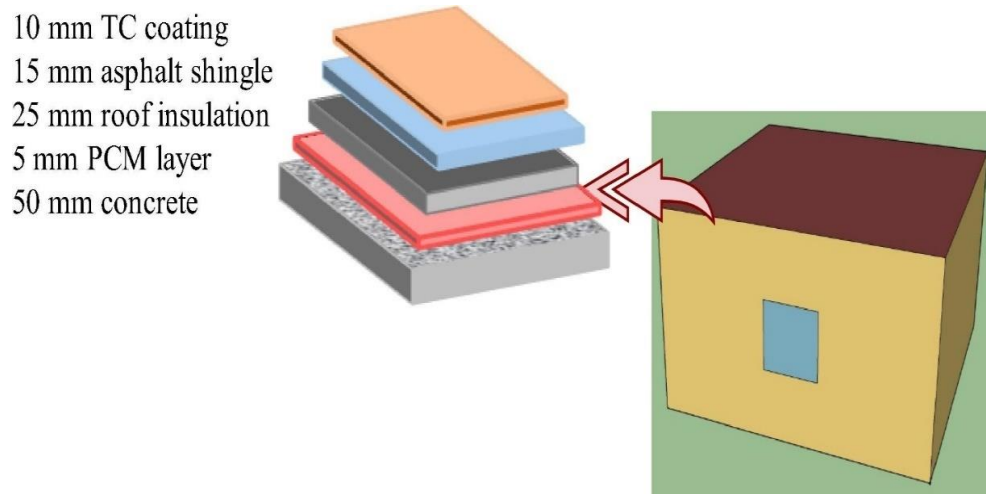


Figure 22: Schematic of a Building with Different Layers of Roof Insulation [202].

In addition, TCMs have applications in the biomedical field. With the recent advances in technology, several devices have been developed based on the properties of thermochromic and liquid crystal materials. As for example, optical display systems, imaging, microscopy, spectroscopy, and optically probing biological systems [203] are outcomes based on the properties of liquid crystals. TCMs have applications (Figure 23) as the active component of sensors owing to their color changing property on exposure to different temperatures. A simple thermochromic polydiacetylene (PDA) sensor has been developed by introduction of urea to the head group of 10,12-pentacosadiynoic acid that exhibited reversible thermochromism up to 150°C [134]. Biosensors based on TCMs have also been developed that allow observation of biological phenomenon with the naked eye[204]. TCMs have been used to develop a temperature monitor “ThermoSpot”, which is basically a skin sticker that changes color from green to black when an organism suffers from hypothermia (core temperature of < 35°C) [205, 206]. The photocatalytic property of TiO<sub>2</sub> encapsulated TCMs makes them effective in the mineralization

of organic pollutants in water and air. For example, the TiO<sub>2</sub> nanofibers have practical application in photocatalytic waste-water treatment and air purification processes[207, 208]. Sakthivel compared the solar photocatalytic degradation of azo dye by ZnO and TiO<sub>2</sub> and observed that ZnO absorbs a larger fraction of the solar spectrum and more light quanta than TiO<sub>2</sub>. The complete mineralization of azo dye was determined by total organic carbon analysis, COD measurement, and estimation of the formation of inorganic ions such as NH<sub>4</sub><sup>+</sup>, NO<sub>3</sub><sup>-</sup>, Cl<sup>-</sup>, and SO<sub>4</sub><sup>2-</sup> [31, 209].

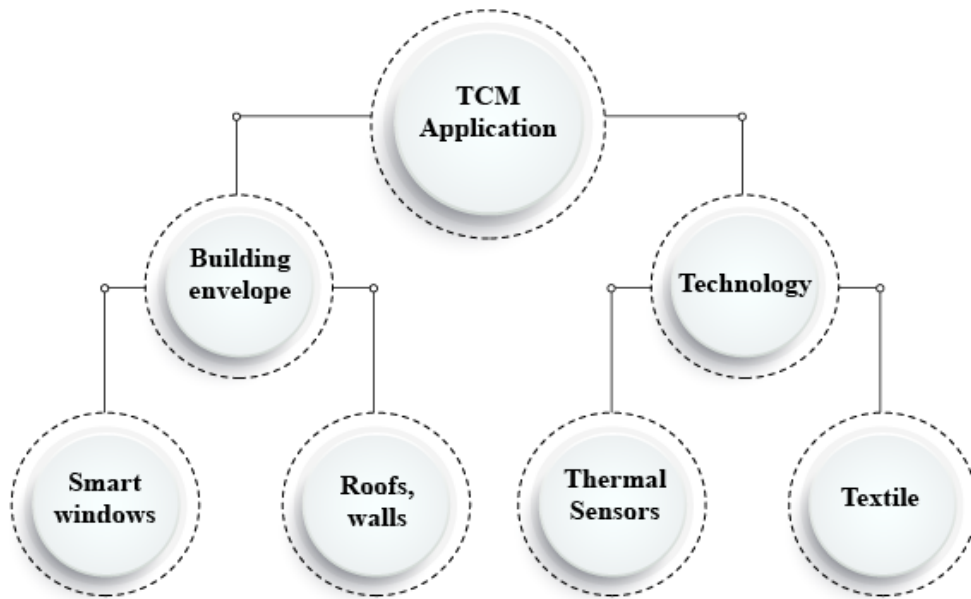


Figure 23: Different Applications of TCMs.

## Chapter 3: Microencapsulation and Characterization of TCM and PCM Materials<sup>2</sup>

### 3.1 Introduction

This chapter focuses on three types of microencapsulated materials: (1) a three-component thermochromic core material microencapsulated by a stable PMMA shell, formed by the polymerization of a monomer, in the presence of a cross linker and methacrylic acid (MA); (2) a synthesized *n*-eicosane phase change material (PCM), encapsulated by a crystalline, sol-gel titania, TiO<sub>2</sub>, shell; and (3) a thermochromic, 3-component system composed of a leuco dye containing crystal violet lactone, bisphenol-A, and myristyl alcohol, and a commercial dye, thermochromic powder used as the core material encapsulated by TiO<sub>2</sub>. Two types of surfactants, CTAB and SDBS, were used for obtaining the best performance and behavior in the microemulsion process leading to the formation of the TiO<sub>2</sub> shell. A single surfactant was finally used successfully to encapsulate the commercial dye, thermochromic material powder (CDTCM) by TiO<sub>2</sub>. We first describe the encapsulation of a blue dye, as a three-component system, with a PMMA; second, the encapsulation of *n*-eicosane by a crystalline TiO<sub>2</sub> shell; and third, investigate the effects of different surfactants and their concentrations in the fabrication of microencapsulation with TiO<sub>2</sub> phase change, thermochromic materials. Different physicochemical characterization techniques, such as XRD, FTIR, DSC, SEM, TEM. CIE Lab Color Meter, and EDS were used to determine their successful synthesis.

---

<sup>2</sup>This chapter has been submitted at Elsa – Elsevier as a book chapter (Hakami, A., Biswas, P. K., Srinivasan, S. S., and Stefanakos, E. K. "Thermochromic and color switching phase change materials." ISBN: 603879. Submission is included in Appendix A.

## 3.2 Characterization

### 3.2.1 Scanning Electron Microscopy

Scanning electron microscopy was carried out with a Hitachi SU3500 with EDS capability to obtain the chemical composition of the materials. The SEM was operated at 25 kV as shown in Figure 24. The SEM is capable of working not only under vacuum but also at increased pressures inside the chamber of up to 600 PSI. This enables the study of surface morphology and microstructure, which are very reactive, and sensitive to moisture. The SEM images revealed a variety of sizes in both the polymeric shell and the TCM core structures. The SEM image results show that the polymers possess a smooth surface and uniform encapsulation. Most of the samples were tested at both higher SEM magnification (100-500 microns) and at lower magnification (30-40 microns).



Figure 24: Scanning Electron Microscope (Hitachi SU3500) at Florida Polytechnic University.

### 3.2.2 Transmission Electron Microscopy

A transmission electron microscope (TEM), Tecnai TF-20, with a maximum accelerating voltage of 200 kV was used for the characterization of the materials (Figure 25). The powder sample thermochromic material was prepared with DI water and then dried for the TEM analysis that took around three hours. The sample thickness must be less than 200 nm to allow electrons to transmit through it. For encapsulated TCMS or PCMS, the TEM can identify the shell and core thicknesses. [210].



Figure 25: Picture of the Transmission Electron Microscope (Tecnai TF-20) at the USF NREC.

### 3.2.3 Differential Scanning Calorimetry (DSC)

The instrument used for testing the thermochromic powder samples was a TGA/DSC 1 thermogravimetric analyzer manufactured by Mettler-Toledo GmbH (Figure 26). The DSC was used to analyze the material's thermal behavior and the effect of microencapsulation of thermochromic materials on the melting point and enthalpy changes. It was also used for the

thermal characterization of the samples (<15 mg sample), such as heat flow, weight loss or gain, transition temperature before melting (sensible heat) or phase change (latent heat), purity, and stability. It is a good technique for powders, thin films, liquids, and fibers. The TGA/DSC is highly sensitive as a micro balance scale allows analysis of the heat flow of the microencapsulated TCM. For each experiment, the plain thermochromic sample was ran at the same time as the encapsulated thermochromic material [211, 212]. Moreover, DSC shows the transition state of the solid-liquid or liquid-solid phase change of the material corresponding to the color change when temperature changes.

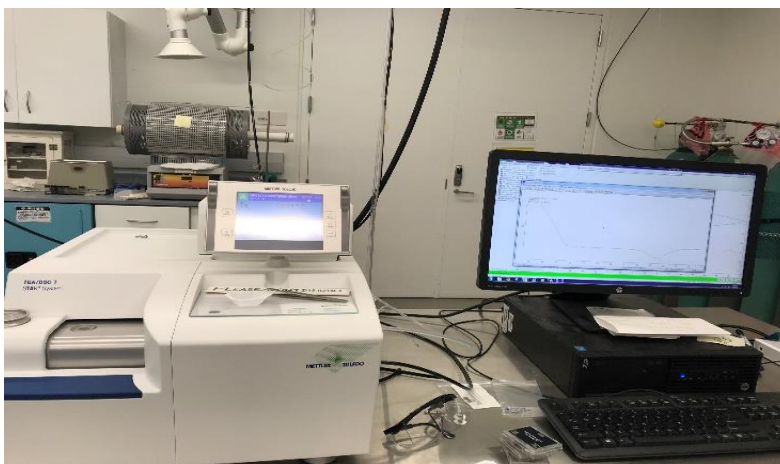


Figure 26: TGA / Differential Scanning Calorimetry (METTLER TOLEDO) TGA/DSC 2 TGA 1 at Florida Polytechnic University.

### 3.2.4 UV-Visible Spectrophotometry

A series of the samples' optical spectra were obtained using a UV-Visible spectrophotometer (Cary 5000 UV-Vis-NIR) shown in Figure 27. The main objective was to measure and analyze the UV-Vis spectra of thin film samples of microencapsulated thermochromic materials to study the absorption, transmission, and spectral reflectance behavior of the blue dye, black dye and also of the CVL [213] upon encapsulation. In this work different samples were prepared on glass substrates using a film applicator (doctor blade) to apply a

uniform 300  $\mu\text{m}$  coating. The samples were dried at room temperature (20  $^{\circ}\text{C}$ ) for at least 6 hours. All samples were protected by a suitable parafilm cover. The main purpose of this work was to study the performance of different types of glass-coated dyes.



Figure 27: UV-Vis Spectrophotometer (Cary 5000 UV-Vis-NIR) at Florida Polytechnic University.

### 3.2.5 Fourier Transform Infrared (FTIR) Spectroscopy

The Fourier Transform Infrared Spectroscopic analysis of the plain dyes (black and blue) and polymer encapsulated TCMs was carried out to understand the bonding characteristics of the polymer used for encapsulation. The FTIR spectra for plain and polymer encapsulated TCMs were recorded [214]. The broad peaks range from 500-4000  $\text{cm}^{-1}$ , each broad peak representing a different functional group vibration, such as the hydrogen-bonded hydroxyl of the color developer BPA used in the blue dye [215]. Moreover, the developed TCM undergoes a phase transition at  $T_s$  when the solid TCM transforms to liquid. Usually both intramolecular and intermolecular hydrogen bonding persists in both solid and liquid form which can be distinguished by the FTIR spectra. The most important reason for using the FTIR spectra of the core TCM and that of the  $\text{TiO}_2$  encapsulated TCM is to obtain a better understanding of the encapsulation behavior of  $\text{TiO}_2$ . All of the thermochromic samples were in powder form. The FTIR can help to obtain the bands and compared with plain materials were used.

### 3.2.6 X-ray Diffraction (XRD)

The XRD uses a powder sample to identify unknown crystalline materials through determination of their crystal structure. The x-ray diffraction patterns of the plain and encapsulated samples were used to analyze the thermochromic materials, by matching different peaks with the JCPDS database to identify magnetite crystal diffractions for  $2\theta$  taken with the XRD system [216, 217]. Also, it allowed identification of nanostructural crystallites when compared to the highly crystalline plain PCM phase.

### 3.2.7 CIE Lab Color Meter

The CIE LAB color apparatus is a color measurement instrument established by the International Commission on Illumination in 1976 is shown in Figure 28. The CIE Lab represents a standard color by three numerical values, the lightness,  $L^*$ , the green–red,  $a^*$ , and the blue–yellow color,  $b^*$  [218]. The thermochromic color change can be identified by obtaining the CIE LAB coordinates [219]. The CIE LAB color instrument was used to analyze the microencapsulated thermochromic samples at room temperature and at higher temperature, around  $40^\circ\text{C}$ , after the sample changed color.



Figure 28: CIE Lab Color Meter at Florida Polytechnic University.

### 3.3 Encapsulation of Thermochromic Material with a Polymer Shell

One of the main objectives of this research is to microencapsulate polymeric TC and PC materials in order to protect them from environmental effects, especially chemical reactions and photodegradation. Additionally, microencapsulation of thermochromic materials is treated as the end product for delivery in industry and this is a critical issue in many industrial applications. The three-component thermochromic and phase change material (Figure 29) was prepared by using different ratios (Table 1) of CVL (as a dye), BPA (as the color developer), and 1-tetradecanol (as the solvent). The three-component based blue dye was then used as the central core while the polymethyl methacrylate, methyl methacrylate-co methacrylic acid was used as the polymeric shell material (Figure 1).

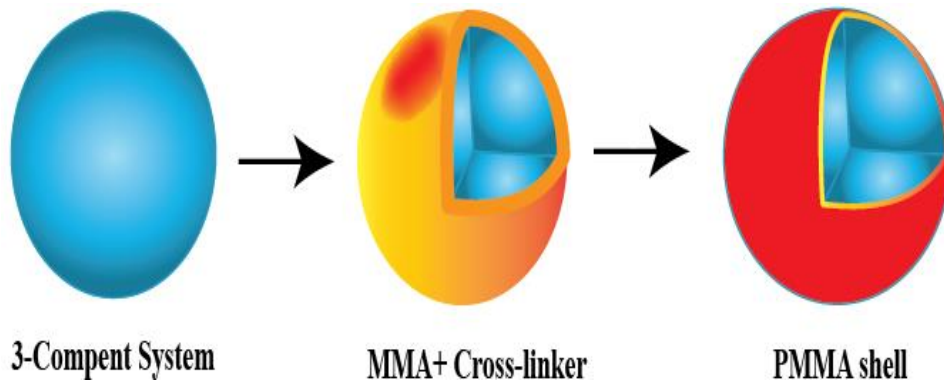


Figure 29: Encapsulation Process of a Thermochromic Material.

Table 1: Synthesis of Six Batches of a Three-Component System with Different Weight Ratios.

Batch#	Ratio			Crystal violet lactone(g)	BPA (g)	1-tetradecanol (g)
	CVL	BPA	TD			
1	1	4	70	0.4	1.1	20
2	1	4	60	0.4	1.1	17.14
3	1	4	50	0.4	1.1	17.3
4	1	6	70	0.4	1.65	20
5	1	6	60	0.4	1.65	17.14
6	1	6	50	0.4	1.65	14.3

### 3.3.1 Materials

The components of the three-component TC were leuco dye CVL (purity: > 99.1 %, Millipore Sigma), BPA (purity: > 99.5-99.1 %, Millipore Sigma) and 1-tetradecanol TD (purity: > 99.1 %, Sigma-Aldrich). All the chemicals had the same purity and were used for the preparation of the main core solution. Methyl ester of methacrylate (MMA) and methacrylic acid (MM) were used as monomer and cross linker, respectively. Ethylene glycol dimethylacrylate (EGDMA) was used as the main connector for cross-linking. These were procured from Alfa Aesar Company with high purity (>99%) and used to synthesize the microencapsulated shell material. Polyethylene glycol (PEG) (Sigma-Aldrich, purity  $\geq 95\%$ ) was used as a surfactant. Ferrous sulfate heptahydrate ( $\text{FeSO}_4 \cdot 7\text{H}_2\text{O}$ ) (Alibaba Company, purity 99%), tert-butyl-hydroperoxide (Millipore Sigma, solution 70 %), ammonium persulfate (APS) ( $(\text{NH}_4)_2\text{S}_2\text{O}_8$ ) (Sigma Aldrich, purity 96%) and sodium thiosulfate (STS) ( $\text{Na}_2\text{S}_2\text{O}_7$ ) (Millipore Sigma, purity  $\geq 99\%$ ) were used as initiators for polymerization.

### 3.3.2 Preparation of a Blue Dye Three-Component System, as the Core Ts

The reported literature [26] helped to select the best ratio of the components of the three-component system (Batch # 2 of Table 1; CVL: BPA: TD = 1: 4: 60). Initially, the leuco dye, CVL, was heated at 80 °C for 1h and then mixed with bisphenol-A at the same temperature with stirring while 1-tetradecanol was added.; Stirring was then continued at 100-200 rpm for 2h to obtain a homogeneous mixture of the three-component system, a thermochromic phase change material (TPCM) at around 29°C as shown in Figure 30. Three-component thermochromic system: Crystal violet lactone (CVL, Dye) Bisphenol A (BPA, color developer)1-tetradecanol (solvent). Different weight ratio have been obtained and the weight ratio was as 20g of 1-tetradecanol ,0.4g CVL and 1.1g of BPA.

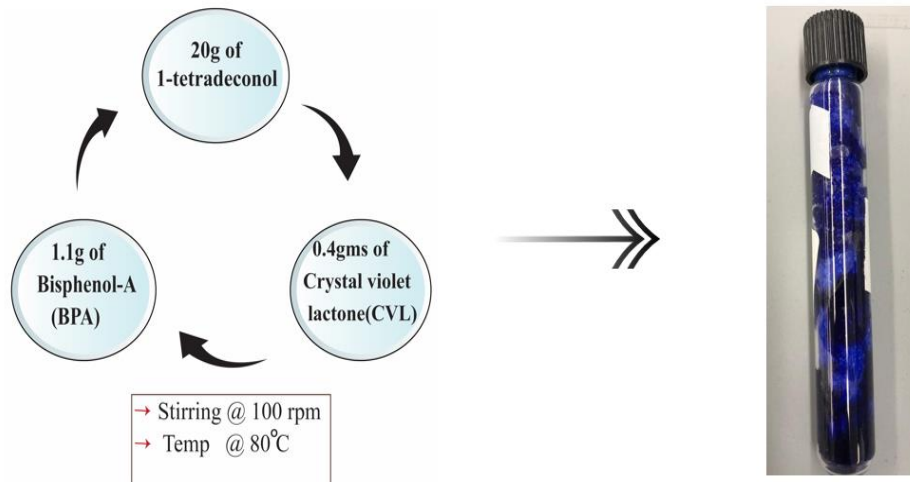


Figure 30: Preparation of the Three Component TCM.

### 3.3.3 Preparation of a Three Component TCM Encapsulated with a Polymer and a Metal Oxide

To study the encapsulation of the three-component TCM core with polymethyl methacrylate (PMMA) and methacrylic acid (MA) shells, multiple emulsion polymerization strategies [211] were followed. Initially 20.0 g of the 3-component system (blue dye) as the main core material and 0.8 g of PEG 1000 as surfactant were mixed in 64.0 mL DI water (labeled as solution A) at 50 °C while stirring was continued. The chosen temperature was above the melting point of the 3-component system (34 - 39 °C). The stirring was continued for an additional hour at a relatively high speed of ~10,000 rpm using a homogenizer (OMNI International, GLH 850) while the microemulsion was formed. Next, a 10.0 g mixture of MMA (monomer) and MA (cross linker) along with 1 mL of ethylene glycol dimethyl acrylate as additional cross-linker (labeled as solution B) was added dropwise to the emulsion (solution A) and stirred for more than one hour. Subsequently, 80.0 mL DI water was mixed with 0.12 g of ferrous sulfate heptahydrate,  $\text{FeSO}_4 \cdot 7\text{H}_2\text{O}$ , to prepare a stock solution (labeled as solution C) of an initiator. Approximately 0.4 mL from this stock solution was then mixed with the emulsion product developed from the solution mixture of A and B. Next 0.1 g of ammonium persulfate

((NH<sub>4</sub>)<sub>2</sub>S<sub>2</sub>O<sub>8</sub>), 0.1 g of sodium thiosulfate (Na<sub>2</sub>S<sub>2</sub>O<sub>7</sub>) and 5.0 g tert-butyl-hydroperoxide were added dropwise to the above final emulsion product for at least 1 h duration. At the last reaction step, the stirring speed was reduced from 10,000 to 1000 rpm while the temperature of the system was increased to ~90 °C. Finally, the stirring was continued for 4 h under a nitrogen atmosphere. The final emulsion was washed by DI water and dried at ~45 °C overnight. As per Table 1, a number of batches have been prepared. The most successful ratio of CVL: BPA: 1-tetradecanol was 1:4: 60 which is the same as that the chosen by Q. Feng et al [29]. The melting temperature of the thermochromic product was slightly above that of the TCM solvent as shown in Figure 31.

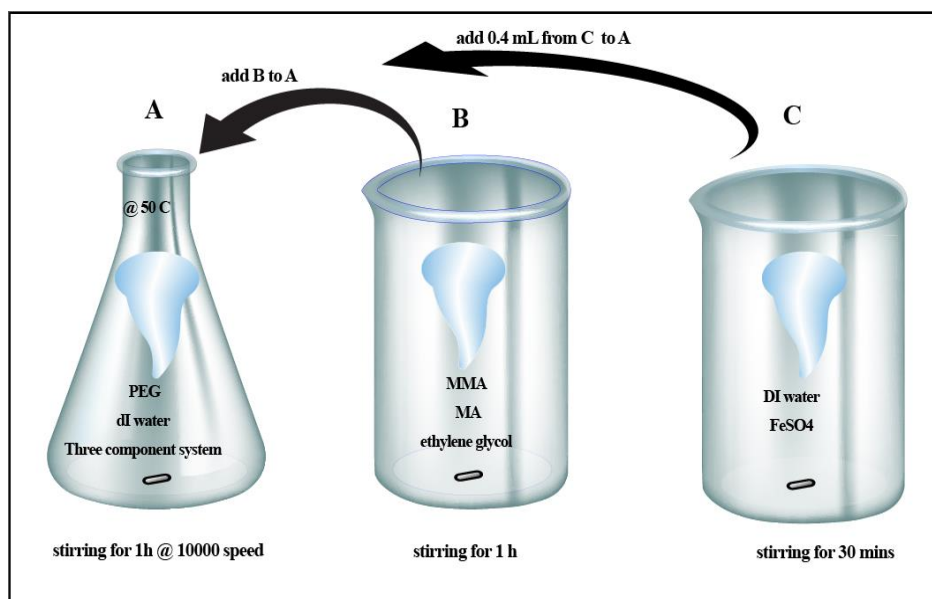


Figure 31: Preparation of the Three Component TCM Encapsulated with a Polymer.

### 3.3.4 Results and Discussion

#### 3.3.4.1 Fourier Transform Infrared (FTIR) Spectroscopy

The Fourier Transform Infrared Spectroscopic analysis of the plain and polymer encapsulated TC systems have been investigated to understand the bonding behavior of the polymer used for encapsulation. Figure 32 represents the FTIR of both plain and polymer

encapsulated, three component-based blue dye. The plain TCM is practically solid, and it is assumed it remains solid with the same molecular state after encapsulation by the polymer. Hence, it may be presumed that before the phase transition with respect to temperature, the FTIR spectra of the core TCM in the encapsulated product will be the same as that of the plain TCM. Therefore, we have recorded two FTIR spectra for the plain and polymer encapsulated TCMs as shown in Figure 32. The broad peaks in the range of  $3150 - 3500 \text{ cm}^{-1}$  are responsible for the free and hydrogen bonded hydroxyl groups. Both BPA and tetradecanol have -OH groups with hydrogen bonding. The color developer, BPA, forms a complex with CVL and gets linked. In addition, CVL may also link all components by hydrogen bonding. Hence, hydrogen bonding has a greater role in the system and, accordingly, this is reflected in the FTIR spectra. Moreover, the developed TCM undergoes a phase transition at  $T_s$  when the solid TCM transforms to liquid. Usually both intramolecular and intermolecular hydrogen bonding persists in both solid and liquid form which can be distinguished by the FTIR spectra. Usually, the stretching frequency due to the hydroxyl groups of intramolecular hydrogen bonding is red shifted with respect to that of the intermolecular hydrogen bonding. In addition, the absorption peak due to intramolecular hydrogen bonding is independent of concentration while that due to intermolecular hydrogen bonding is dependent on the concentration [214, 215, 220]. The plain TC system is well recognized at around  $3350 \text{ cm}^{-1}$ , while for the encapsulated product, the broad absorption in the range,  $3150 - 3500 \text{ cm}^{-1}$  signifies the presence of both inter- and intramolecular hydrogen bonding, assuming the well-defined shoulder at around  $3450 \text{ cm}^{-1}$  represents the intermolecular hydrogen bonding. Overall, the absorption in the broad region,  $3150 - 3500 \text{ cm}^{-1}$  cannot ignore the contribution due to the stretching frequency of the hydroxyl groups of BPA and tetradecanol. As the plain TCM is a solid product and it possesses intramolecular

hydrogen bonding as evident from its FTIR spectrum, it may be presumed that intramolecular hydrogen bonding prevails in the solid TCM. After encapsulation, shifting of the -C-H stretching frequency at around  $2900\text{ cm}^{-1}$  is possibly due to steric hindrance of the solvent (tetradecanol) upon encapsulation. Various strong absorption (at  $1490\text{ cm}^{-1}$  and  $1400\text{ cm}^{-1}$ ), and weak absorption (at  $750\text{ cm}^{-1}$  and  $760\text{ cm}^{-1}$ ) peaks, for the plain TCM, are possibly due to stretching of -C-H and -C-O in tetradecanol at the molten state. Bisphenol-A plays a good role in the thermochromic system when it reacts with crystal violet lactone (CVL) as the carboxylate forms a ring in the solid-state. According to the literature, there is a shift between the stretching frequency of carbonyl group of closed and open lactone rings to a relatively lower frequency, because of the H-bonded carbonyl's uniform behavior in the carboxylate group dealing with an open ring [221]. A maximum absorption occurs for the plain TCM due to the carbonyl group at  $1620\text{ cm}^{-1}$  where the CVL is in the closed ring configuration which diminishes in the case of plain TCM (Figure 32).

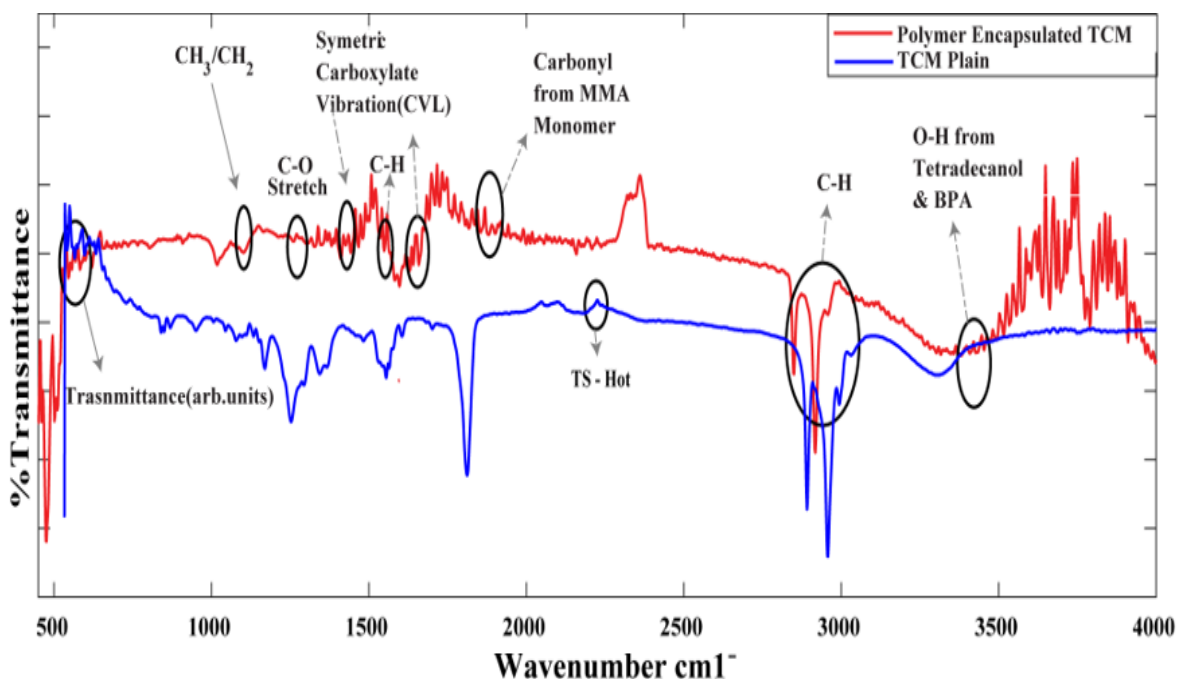


Figure 32: FTIR Spectral Profiles of Polymer Encapsulated and Plain TCM.

### 3.3.4.2 Differential Scanning Calorimetry (DSC)

Phase transitions of the polymer encapsulated TCM and the plain thermochromic system were determined by Differential Scanning Calorimetry (DSC). Both measurements of the cooling and heating cycle were carried out to estimate the reversibility and color changing characteristics. The DSC profiles of the polymer encapsulated and plain TC system are shown in (Figures 33-35). The graphs show that multiple transitions occur, as evident from the change in enthalpy and phase performance that depend on the temperature. An endothermic characteristic peak during the heating process was observed in all the DSC curves' cycles in both the polymer encapsulated TCM and the plain TC systems. Moreover, both solid and solid-liquid behaviors were observed during heating. A literature search verified the cooling curves regarding the liquid to solid transition, and the phase shift displayed as a colored vertical ellipse (Figure 33). Figure 34 shows the melting transition at around 37 °C for the plain, three-component thermochromic system, however, no melting was observed for the PMMA encapsulated TCM due to the effective encapsulation of polymer shell of the core TCM system compared with PMMA-TCM. The effect of crystal shape is not only dependent on the solid-to-solid transition but also on the increase of the solvent concentration in the plain TCM [9, 221, 222].

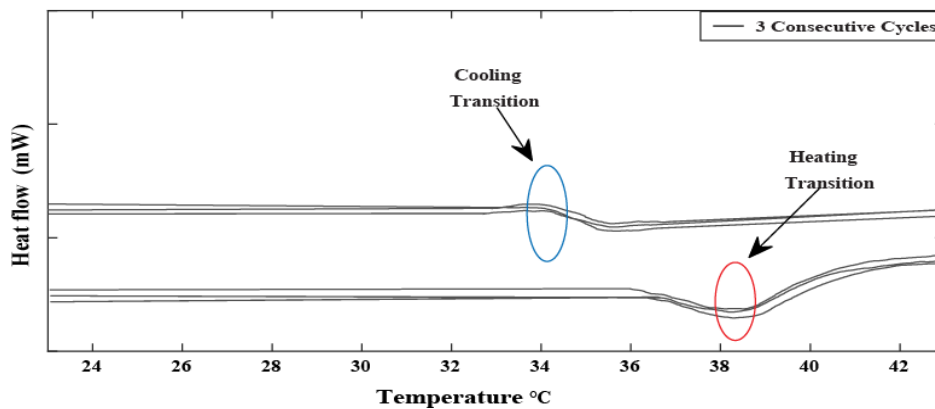


Figure 33: DSC Thermograms of Cooling and Heating Transitions of the Plain TCM Phase Change Material.

Figure 35 depicts the DSC profiles of the polymer encapsulated and plain TCMs with respect to temperature at a constant ramping rate. This exercise was carried out to understand the kinetics and heat flow enthalpies for these systems. Based on our analysis, it is very clear that the polymer encapsulated systems show the normalized (meaning same sample size for both plain TCM and PMMA encapsulated TCM) heat flow values which are at least 50 J/g lower than the heat flow required for the plain TCM samples. However, the accurate amounts of TCM in the PMMA encapsulated sample is obviously in fractional quantities, so the melting transition behavior was not as pronounced as the DSC endothermic peak of the plain TCM sample as shown in Figure 34. Based on the raw DSC data, Table 1 and Figures 36 and 37, the following analysis helps to understand the role of encapsulation of the core TCM by PMMA.

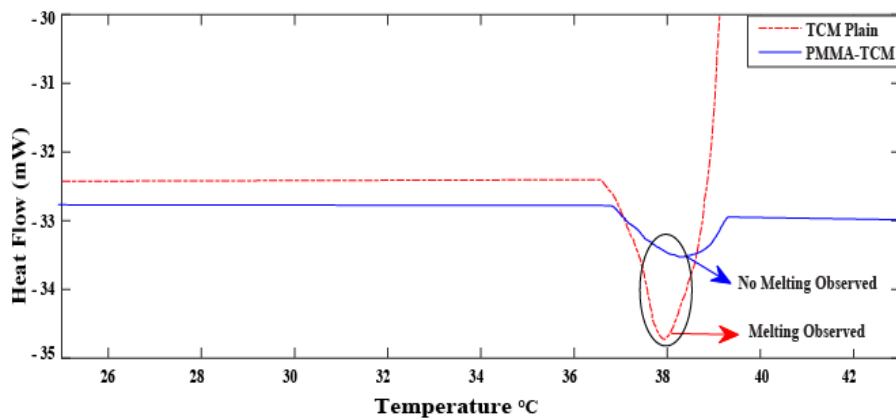


Figure 34: DSC Profiles of the Plain and Polymer Encapsulated TCM Melting Transitions.

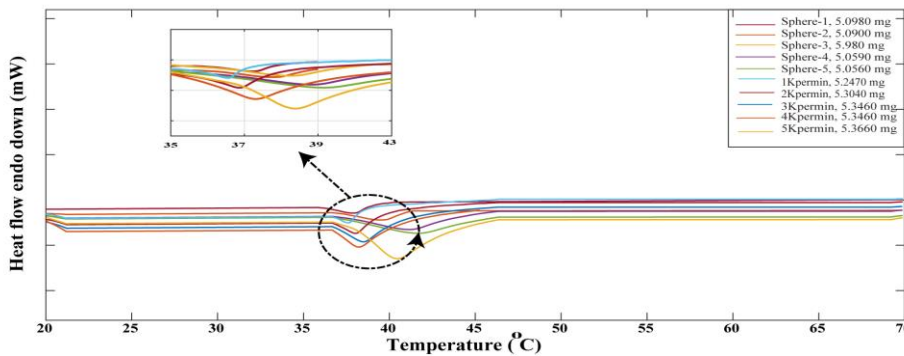


Figure 35: Heating DSC Profiles of the Polymer Encapsulated TCM for Many Consecutive Cycles.

Table 2: DSC Raw Data of a TCM and an Encapsulated TCM.

Plain TCM	Mass	Normalized	Onset	Peak
	mg	J/g <sup>-1</sup>	°C	°C
1°C/min	5.247	-130.46	35.15	37.14
2°C/min	5.304	-112.73	34.59	37.31
3°C/min	5.346	-133.92	33.98	37.51
4°C/min	5.366	-148.48	33.89	37.73
5°C/min	5.165	-142.75	33.69	37.62
Encapsulated TCM	Mass	Normalized	Onset	Peak
	mg	J/g <sup>-1</sup>	deg C	°C
1°C/min	5.098	-84.66	36.51	39.39
2°C/min	5.09	-63.38	36.32	40.23
3°C/min	5.097	-103.16	36.13	41.46
4°C/min	5.059	-96.93	36.19	42.65
5°C/min	5.065	-86.15	35.83	43.18

The heat flow characteristics of the PMMA encapsulated TCM for the endothermic phase transition are systematically higher than the plain TCM, however, the peak temperature of the melting phase transition is higher for the PMMA encapsulated TCM than the plain TCM. The results can be explained by the presence of the PMMA layer encapsulating the core TCM and the relative weights of the encapsulated and plain TCM materials. Depending on the PMMA layer thickness and the rate of change of temperature, delays in the melting of the core TCM are expected. Also, the relative weights of the core TCM and the encapsulating PMMA layer as well as the total weight (core + shell) of each sample will have a definite effect on the sensible and latent heat of the sample. The average difference of the heat flow values and the peak melting transition temperatures for the PMMA encapsulated TCM and those for the plain TCM, corresponds to ~46.8 J/g and ~4 °C, respectively. Depending on the PMMA layer thickness and the rate of change of temperature, delays in the melting of the core TCM are expected. Also, the relative weights of the core TCM and encapsulating PMMA layer as well as the total weight.

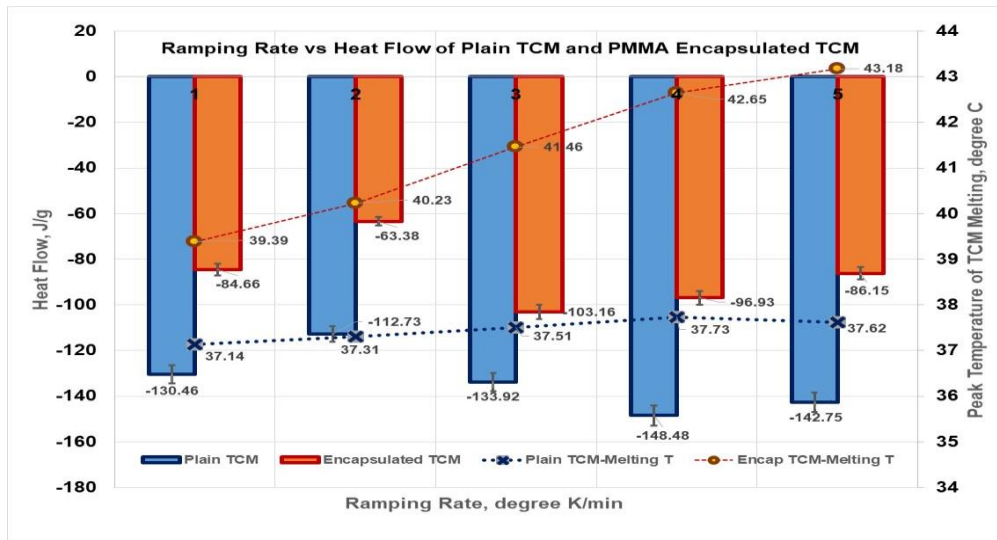


Figure 36: Ramping Rate vs Heat Flow (at Peak Melting Transition) of the Plain and PMMA Encapsulated TCM (A).

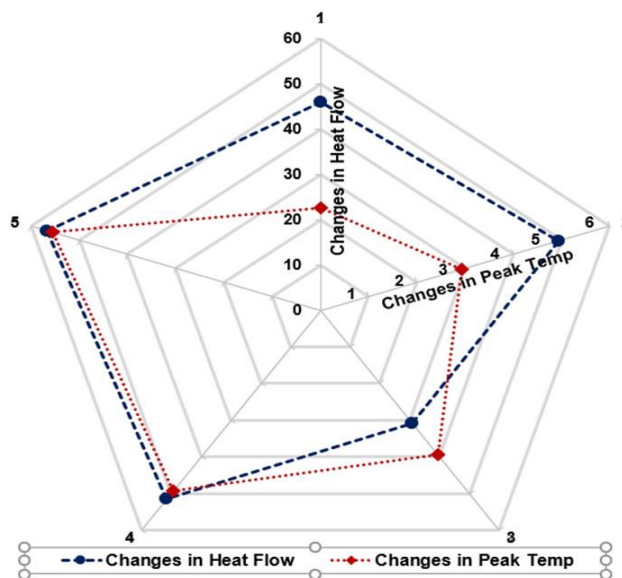


Figure 37: Changes in Heat Flow and Peak Temperature of Melting Between PMMA Encapsulated and Plain TCM (B).

### 3.3.4.3 Scanning Electron Microscopy (SEM)

Figures 38 and 39 show the Scanning Electron Microscopy (SEM) images of the (MMA-co-MA)/TS microcapsule layers and also their surface morphologies. Several images display spherical particles with a uniform surface feature. Moreover, the SEM images reveal that the particles are of different sizes as we deal with both polymeric shell and TCM core structures.

The SEM image results suggest that the polymers possess a smooth surface and provide uniform encapsulation [211, 212, 223]. The images of the encapsulated polymer shell (Figure 38) have been magnified and illustrate that the shells are netlike, and the unit length seems to be in the range of 300-500 nm. In addition, the magnified layered structure of the polymer shell also illustrates the placement of the cores in the overall moiety. It is interesting to comment that the core shell may have different forms, not just spherical. The cores are dispersed between the layers as shell-like flakes. On the other hand, a spherical core-shell structure may be present, but its fraction may be limited. This cannot be identified very clearly in this study. In Figure 39, the SEM images also demonstrate the agglomeration of PMMA encapsulated TCMs in smooth and porous morphologies.

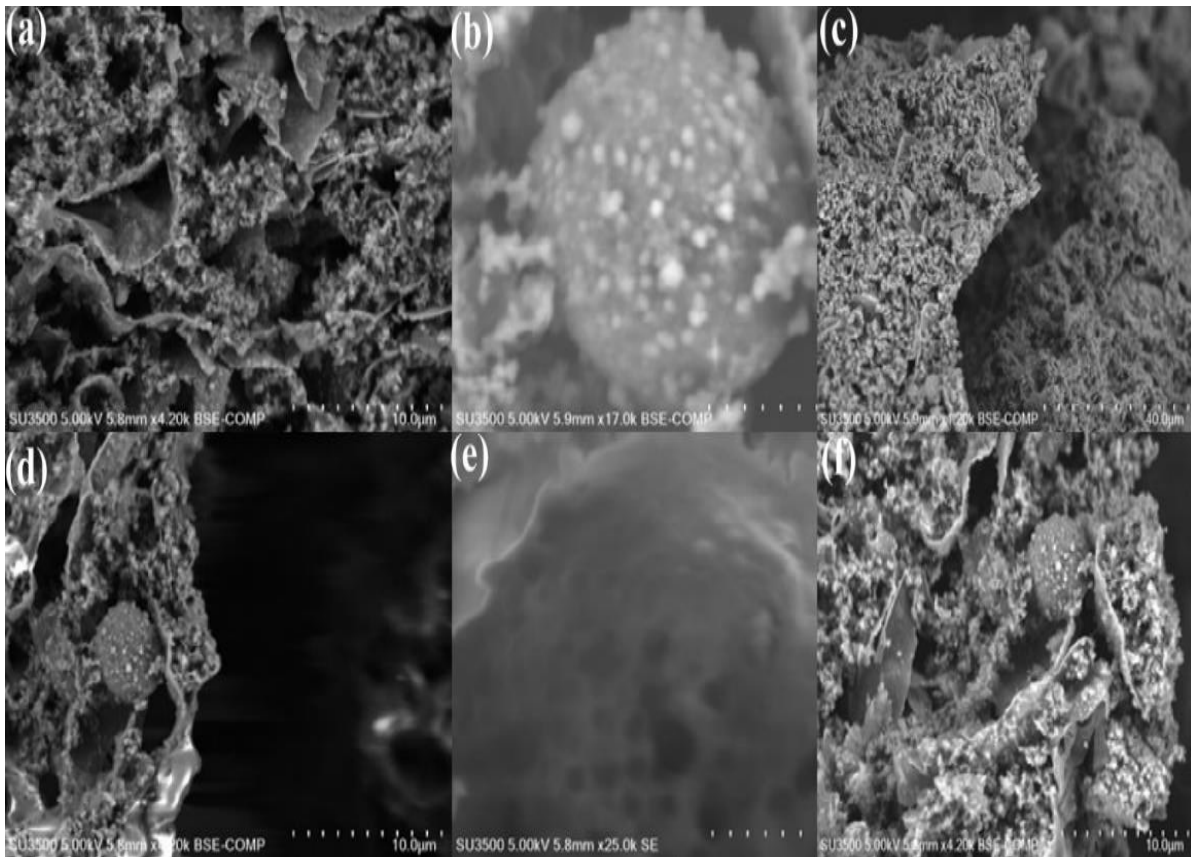


Figure 38: SEM Images of the Microcapsules Encapsulated by the Polymer Shell Layer at Different Magnifications.

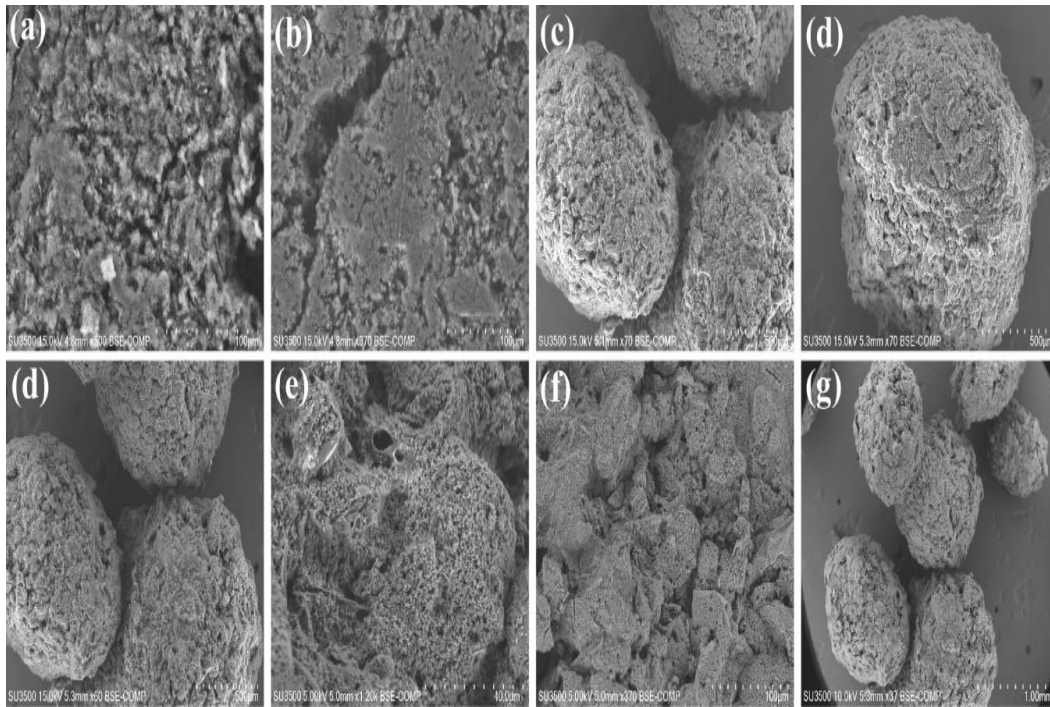


Figure 39: SEM Images of the Microcapsule's Smooth Surface Morphologies of PMMA Encapsulated TCMs.

### 3.4 Encapsulation of Phase Change Materials with Metal Oxide Shell Structures

There exists renewed interest in energy materials, focusing on materials exhibiting phase change (PCMs), that typically occurs during the melting-solidification transition at constant temperature (latent heat). The most effective use of phase change materials is to store and release a large amount of latent heat energy at the phase transition temperature. Increase of PCM use may contribute to a reduction of fossil fuel use and the corresponding generation of greenhouse gas. Hence, new areas of academic research and development in thermal energy storage are getting much attention. Many excellent and exciting results show the benefit of using high efficiency PCMs to reduce energy consumption [224, 225]. Phase change materials can also be used successfully to save energy in applications related to the energy efficiency of buildings, by absorbing or reflecting solar radiation, depending on the ambient temperature or thermal storage in hot water systems [226]. The most often used PCMs are organic paraffins, fatty alcohols and

acids, neopentyl glycol, eutectics, and some inorganic substances, such as salt-hydrates, that have good phase-change enthalpies in the range of 149-241 J/g [227].

However, there are some disadvantages of using PCMs in some applications. Some devices are of relatively high cost due to the need of containment of the PCM. In addition, the PCMs are not easy to handle when the phase transitions result in changes from solid to liquid. For applications in buildings, the thermal storage capability should be maintained [228, 229] by enhancing the salt hydrate proportion and crystal water stability of the composite PCMs. Additionally, some materials can interact quickly when mixed with other components, such as paraffin waxes, and evaporate into the air due to raising the amount of volatile organics [230]. In some applications, PCMs may require fast heat transfer, but occasionally exhibit very slow heat transfer. Hence, various methods are applied to increase thermal conductivity [231] and maintain stability with proper thermal management. Due to the above disadvantages, use of PCMs especially without encapsulation may not be feasible [229]. Different technologies and methods can be used to minimize the above problems and prevent chemical reactions with surrounding materials [232]. Encapsulation of PCMs can effectively minimize the above disadvantages and protect the PCM from environmental degradation.

The most effective method for encapsulating phase change materials is the formation of a shell-like cover around the PCM, by the interaction of the materials the TCM is made of. This technique can engulf liquid or solid particles as a strong wall with the benefit of stopping any leakage when the PCM is in the liquid state [233]. However, PCMs microencapsulated by polymeric shells possess poor and sometimes negative performance, especially when they are flammable and have poor thermal conductivity [234, 235]. Better thermal regulation transfer and energy storage can be achieved if the polymeric shell is replaced by a mechanically durable

inorganic shell material. Considerable research is now focused on the encapsulation of PCMs by different inorganic materials for better mechanical strength [231]. Thus, inorganic materials as a shell can be the best choice in the development of efficient and durable PCMs.

In the present study, for energy saving applications [236-238], PCMs were prepared utilizing an *n*-eicosane as the core, followed by encapsulation with a titania (TiO<sub>2</sub>) shell. The shell was synthesized by the hydrolysis and polycondensation of titanium alkoxide (tetrabutoxy-titanium) in liquid phase, a TiO<sub>2</sub> precursor of sol-gel route. The most essential purpose of using PCMs is for latent heat storage, absorption of considerable amount of thermal energy during the phase change. The interest is in the transfer of thermal energy at constant temperature for improving energy efficiency and heat regulations [239]. Microencapsulation of PCMs has been developed in recent times because of their wide number of applications in different areas such as solar heat conversion, thermal energy saving and other applications [240, 241]. Presently, the thermochromic application using the PCM as a core followed by TiO<sub>2</sub> encapsulation is utilized to increase mechanical durability. This study systematically considers the encapsulation and extensive characterization of the TiO<sub>2</sub> encapsulated PCM.

#### 3.4.1 Materials

Several chemicals were procured for the experimental work. Sodium dodecyl sulfate (SDS) was used as a surfactant and sodium fluoride (NaF) was used for the crystalline phase transformation of the TiO<sub>2</sub> layer. Both chemicals had a purity of 98% and were used directly as received. Both chemicals, *n*-eicosane and formamide, had the objective to serve as an emulsion of water phase and an oil phase. The tetrabutyl titanate (TBT) was the starting material of the sol-gel TiO<sub>2</sub> precursor, part of the chemical groups in this experiment. This precursor interacts with the outer surface of the emulsified drop through the hydroxyl group resulting in a titania.

### 3.4.2 Encapsulation of *n*-eicosane with a TiO<sub>2</sub> Shell

Microencapsulation the *n*-eicosane core by TiO<sub>2</sub> was synthesized by following the *in-situ* process of forming polymers in the nonaqueous system where the precursor components of the shell and core materials were chosen stoichiometrically. The essential items in the general synthesis procedure were: (i) a 500-mL one-neck round bottomed flask supplied with a heating mantle around it, (ii) a dropping system by a laboratory syringe, and (iii) a mechanical stirrer with high-speed (rpm) stirring capability. The mechanical system initially stirred a mixture of 83.3 mL of formamide, 8.3 g of *n*-eicosane, and 2.7 g of the surfactant SDS, with the mixture heated between 45 to 50 °C under continuous stirring at high speed. This resulted in an oil-water emulsion, a critical step of the process, with the development of the *n*-eicosane and formamide mixture as liquid water and oil phase change. Subsequently, 8.3 g of tetrabutyl titanate TBT was added to the emulsion with high-speed stirring (40 min) as shown in Figure 40.

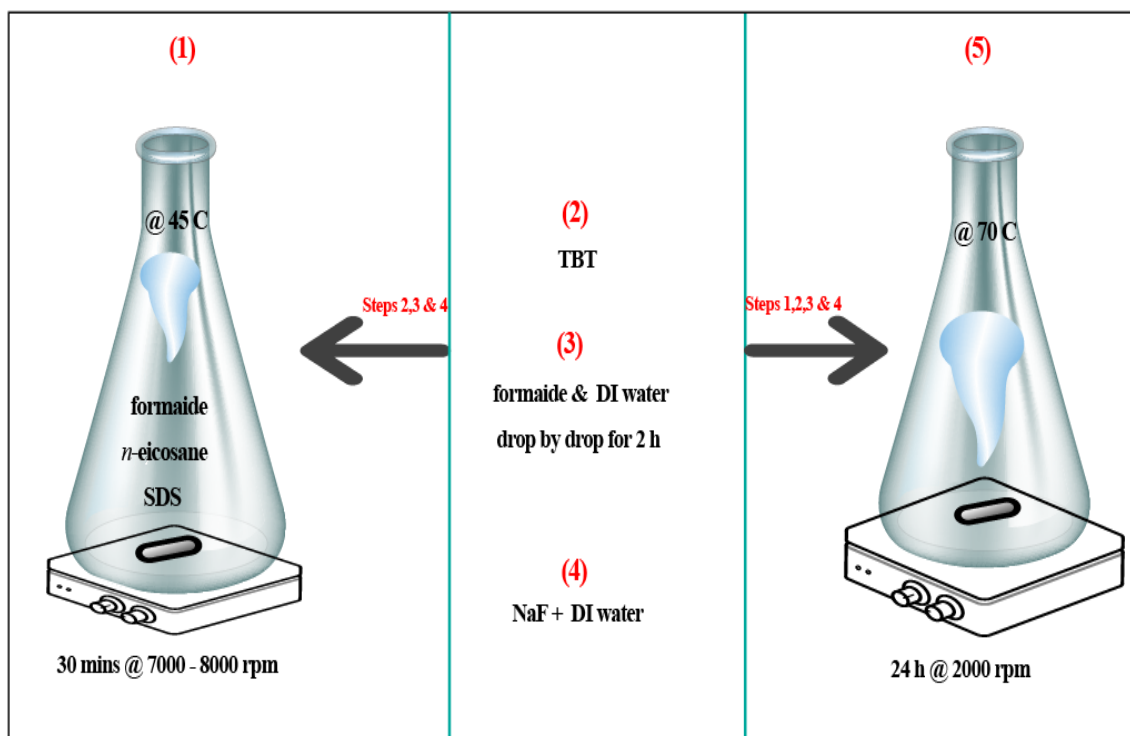


Figure 40: Preparation of Microencapsulation of TiO<sub>2</sub> Shell with *n*-eicosane as Core.

Then, 50.0 mL of formamide mixed with 4.1 mL of pure deionized water was added drop by drop to the flask over a period of 1.5 h under vigorous stirring (around 8000 rpm). The stirring operation was continued for 4.7 h maintaining the temperature at 47 °C. A white residue was the product at this stage. Next, 5.0 mL of deionized water containing 1.66 sodium fluoride NaF was poured into the suspension. The temperature was then increased to 70 °C with the stirring speed reduced to around 2000 rpm for 24 h to finalize the shape of the crystalline TiO<sub>2</sub> shell (Figure. 41). The final product was a white powder which was then washed many times with ethanol followed by pure deionized water and dried at 45 °C overnight in preparation for testing and characterization.

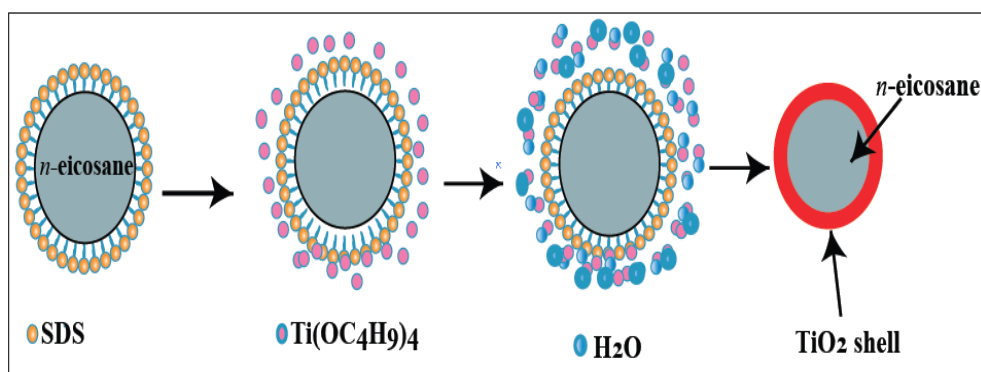


Figure 41: Schematic Diagram of the PCM Encapsulation Process Using a TiO<sub>2</sub> Shell.

### 3.4.3 Results and Discussion

#### 3.4.3.1 Fourier Transform Infrared (FTIR) Spectroscopy

FTIR spectra of the core n-eicosane and that of the TiO<sub>2</sub> encapsulated n-eicosane were recorded (Figure 42) to understand the encapsulation behavior of TiO<sub>2</sub>. It is clearly observed that the number of absorption peaks for the encapsulated n-eicosane has been reduced as compared to pure n-eicosane. There are very narrow absorption peaks at 3560, 3490 and 3430 cm<sup>-1</sup> for the encapsulated n-eicosane. However, tentatively, these can be referred to as the peaks due to hydroxyl affiliation as distinct absorption peaks and shoulders are observed at similar positions

of the spectrum of the core system. The pure core may possess both inter- and intra- molecular hydrogen bonding as evident from the distinct absorption peak and shoulders [214, 215, 220]. Assuming similar quantities have been used to obtain the FTIR spectra of the pure and encapsulated *n*-eicosane, it may be inferred that the narrow nature of the absorptions in the range from 3400 – 3600  $\text{cm}^{-1}$  is possibly due to the decrease of the intermolecular hydrogen bonding. The peak at 3560  $\text{cm}^{-1}$  explains the extending stretching vibration of the hydrogen bonding of the hydroxy functional group in the  $\text{TiO}_2$  shell. The other peaks at 3490 and 3430  $\text{cm}^{-1}$  may be due to the stretching vibration of the O-H bond of intermolecular bonding in water. On the other hand, the peaks located at 2901 and 1375  $\text{cm}^{-1}$  are seen in the infrared spectral range and could be assigned to the alkyl C-H due to the stretching phase behavior of the methyl functional group.

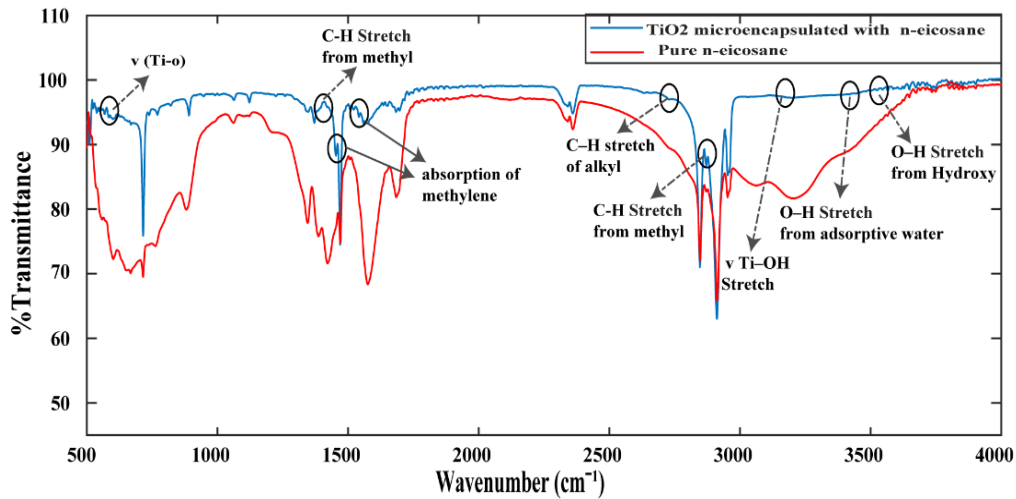


Figure 42: FTIR Spectra of the Pure and  $\text{TiO}_2$  Microencapsulated PCM *n*-Eicosane.

Moreover, the two narrow absorption peaks present in the infrared spectra at 1601 and 1480  $\text{cm}^{-1}$  may also be assigned as the absorption of the methylene group. On the other hand, the absorption range at 720  $\text{cm}^{-1}$  is marked as planar methylene fluctuation vibration as evident from the relatively broad absorption of pure *n*-eicosane. The appearance of the sharp absorption near 740  $\text{cm}^{-1}$  and the narrow absorption near 900  $\text{cm}^{-1}$  may also be interpreted as the stretching

vibrations [242] of bonded TiO<sub>2</sub> present in the shell as the crystalline TiO<sub>2</sub> shows (theoretically calculated) two bands at ~730 and ~880 cm<sup>-1</sup> [242] which may be shifted towards a lower frequency due to bonding which practically happens here (Figure 42). Moreover, the symmetric bonding nature of TiO<sub>2</sub> shell with the core, n-eicosane, possibly minimizes the number of absorption peaks of the FTIR spectrum of the microencapsulated n-eicosane (Figure 42). The rest of the characteristic absorption peaks of the plain n-eicosane are in good agreement with respect to those of pure n-eicosane. In addition, the microencapsulated sample shows absorption at ~600 cm<sup>-1</sup> because of the additional IR vibration of Ti-O. However, the very narrow peak at 3300 cm<sup>-1</sup> would clarify the stretching vibration of the hydroxyl group bonded to Ti, although it signifies the intermolecular hydrogen bonding. It is crucial to infer about the absorption peaks located at 1110 and 1405 cm<sup>-1</sup> because it may be assigned to the C-H wavelength extending vibrations specified from the formamide solvent. Finally, it may be inferred that comparative FTIR spectra of the plain and encapsulated n-eicosane seems to reveal the formation of a shell by TiO<sub>2</sub>.

#### 3.4.3.2 X-ray Diffraction (XRD)

The crystallinity of TiO<sub>2</sub> can impact photocatalytic performance. On the other hand, hydrothermal synthesis can yield an amorphous TiO<sub>2</sub> shell. The reason for adding NaF electrolyte is to improve crystallization enabled by the presence of Na<sup>+</sup> and F<sup>-</sup> ions. Figure 43 shows the X-ray diffraction patterns of the plain and encapsulated products. The data is matched with the JCPDS database to identify magnetite crystal diffractions for 2θ taken from XRD [216, 217]. In general, the results support that the TiO<sub>2</sub> shell is the crystallized moiety due to effects of fluoride ions. The XRD of pure n-eicosane shows sharp crystalline peaks of (111) and (020) Miller indices at the 2θ values of 21.2° and 22.2°, respectively, and these are well matched with the C<sub>20</sub>H<sub>42</sub> rotator phase as reported by Giambattista [243]. The metal oxide encapsulated PCM

samples showed predominantly the titania peaks of both structural phases such as anatase and brookite [244]. In the present work, the PCM favors a (020) orientation, and there is a significant shift that occurs from the relaxation behavior of this rotator phase due to the TiO<sub>2</sub> encapsulation [59]. It is noteworthy to mention that the TiO<sub>2</sub> encapsulated PCM shows nanostructural crystallites when compared to the highly crystalline plain PCM phase. The crystallite sizes and lattice strain calculations are under study and will be reported in future communications.

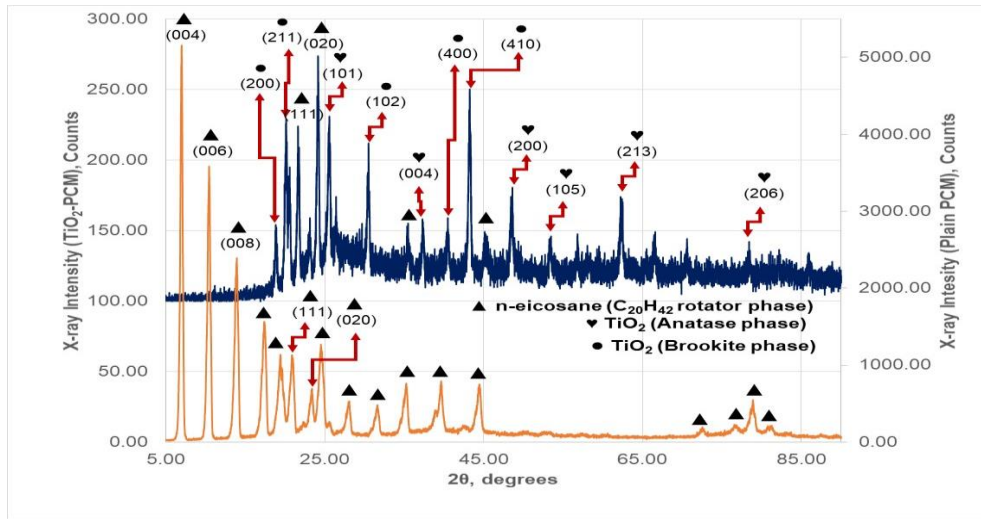


Figure 43: XRD of TiO<sub>2</sub> Microencapsulated *n*-eicosane and Plain *n*-Eicosane.

### 3.4.3.3 Differential Scanning Calorimetry (DSC)

The DSC heating profile patterns of the pure *n*-eicosane and the TiO<sub>2</sub> microencapsulated *n*-eicosane are shown in Figure 44. The pure *n*-eicosane PCM shows melting of *n*-eicosane starting at around 43 °C with an endothermic peak transition at 44.2 °C (Figure 44) and crystallization with an exothermic peak around 40 °C (cooling curve DSC profile of Figure 45). For the case of the TiO<sub>2</sub> encapsulated PCM, the DSC profile shows an endothermic melting transition with an on-set, peak and end-set temperatures are at 42.0°C, 45.4°C and 50.0°C, respectively. The broader integral area of the DSC curves and the change in the heat flow values were from -221.01 J/g for plain *n*-eicosane to -83.11 J/g for the TiO<sub>2</sub> encapsulated *n*-eicosane.

Moreover, the possibility of reliance on the microcapsules' thermal stability was verified by different cycle scans. Figure 45 illustrates DSC results of various thermal cycles for the microencapsulated and pure *n*-eicosane materials. Many cycles were carried out, for both heating and cooling transitions, in order to study the samples' behavior.

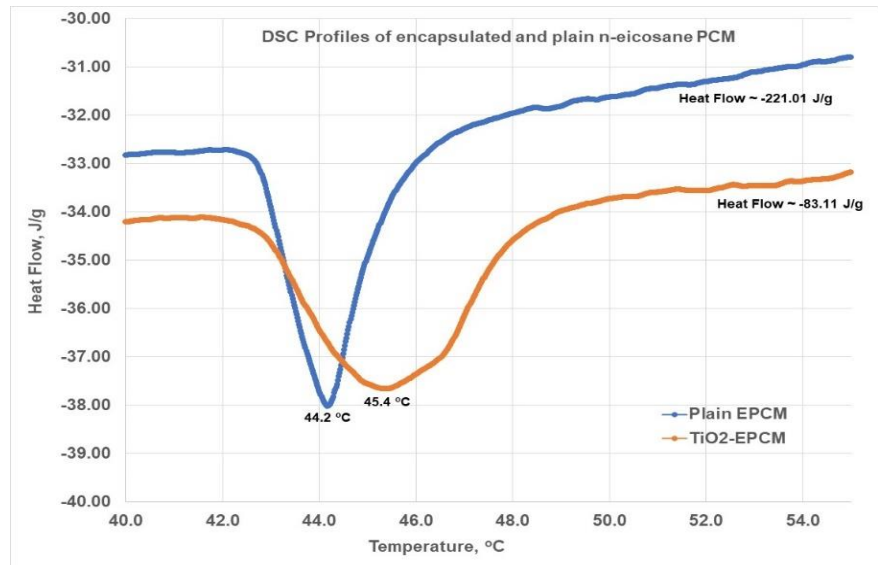


Figure 44: Heating DSC Curves of the Microencapsulated *n*-Eicosane and Plain *n*-Eicosane.

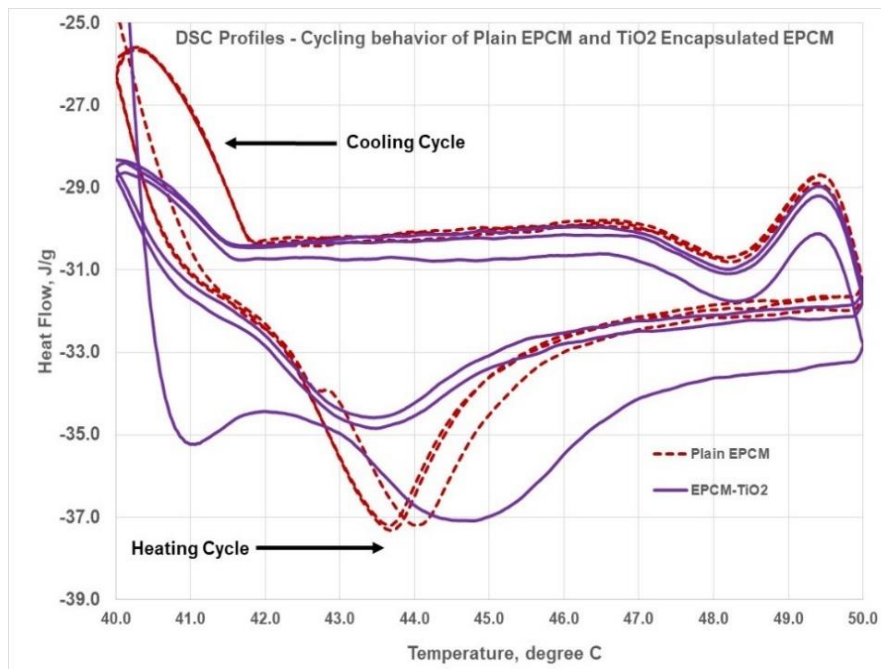


Figure 45: Heating and Cooling Cycling Behavior from DSC Profiles of Encapsulated and Plain PCM.

### 3.4.3.4 Scanning Electron Microscopy (SEM)

The surface morphology of the PCM microcapsules were verified by SEM imaging recorded at different magnifications, as shown in Figure 46. At higher magnifications, for example, 100-500 microns (Figure 46a-b), the morphologies reveal agglomerated particles, however, at lower magnification, 30-40 microns (Figure 46c-f), they appear as foamy type microstructures with a porous nature, allowing the shell metal oxide layer to adhere to the core PCM. Figure 48a shows the EDS map of the elements, with  $\text{TiO}_2$  being about 15.70 wt%, encapsulating the core PCM material. The microstructure suggests that, if the images were magnified, then the nanosized *n*-eicosane could possibly be visualized. The image would also exhibit features of the  $\text{TiO}_2$  shell. The elements of Na and F are shown in the EDS images, since NaF was used to prepare the  $\text{TiO}_2$  shells. The sulfur, at low concentration, from the residual surfactants and the excess carbon are also present because of the  $\text{C}_{20}$  *n*-eicosane organic phase (Figure 48b).

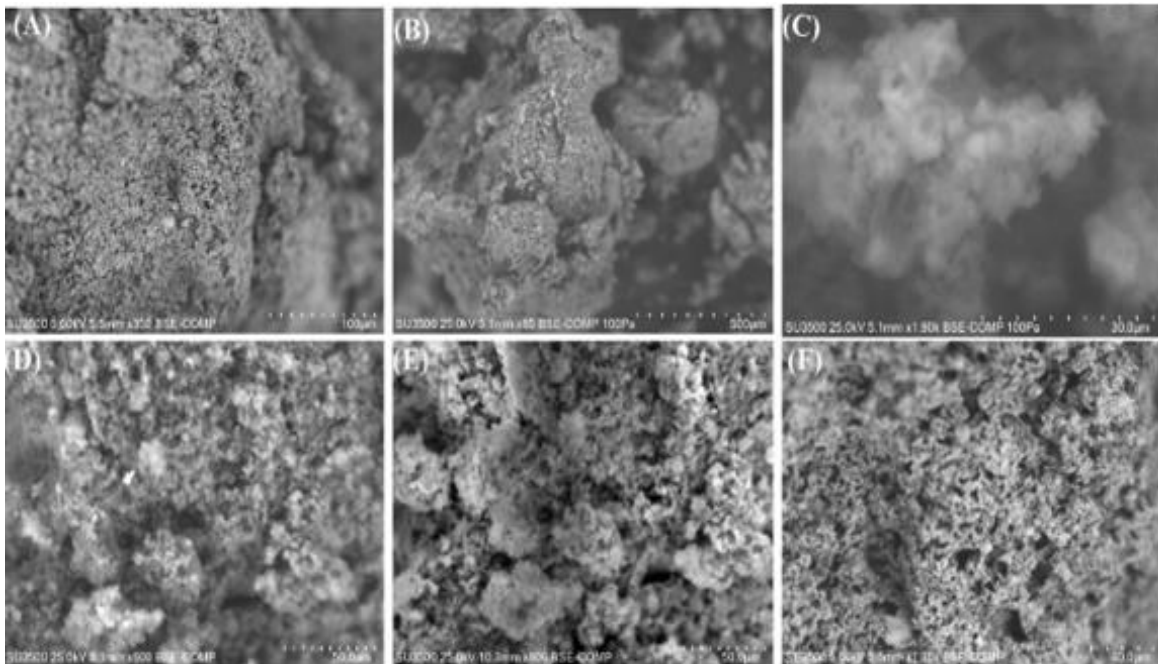


Figure 46: SEM Micrographs of the Plain *n*-Eicosane at Different Magnifications (a) to (f).

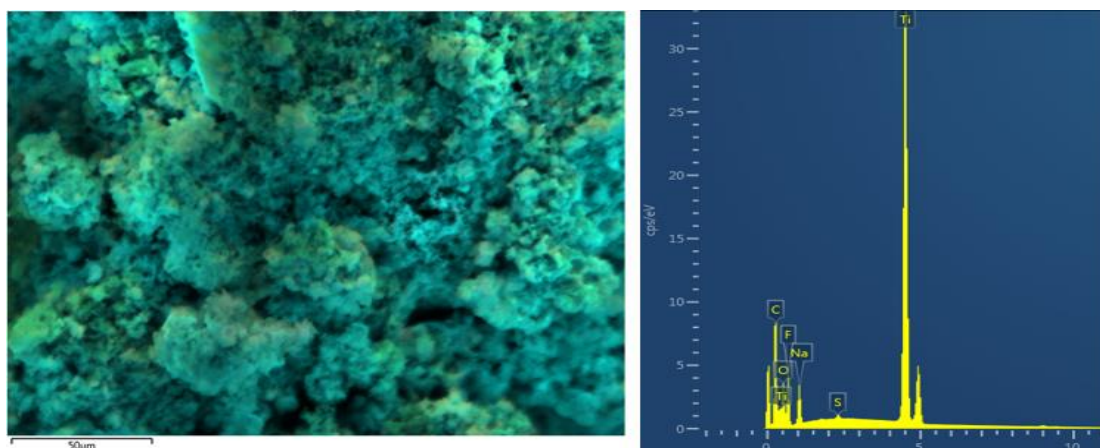


Figure 47: EDS Map Sum Image and Spectrum of the Microencapsulated *n*-Eicosane (A).

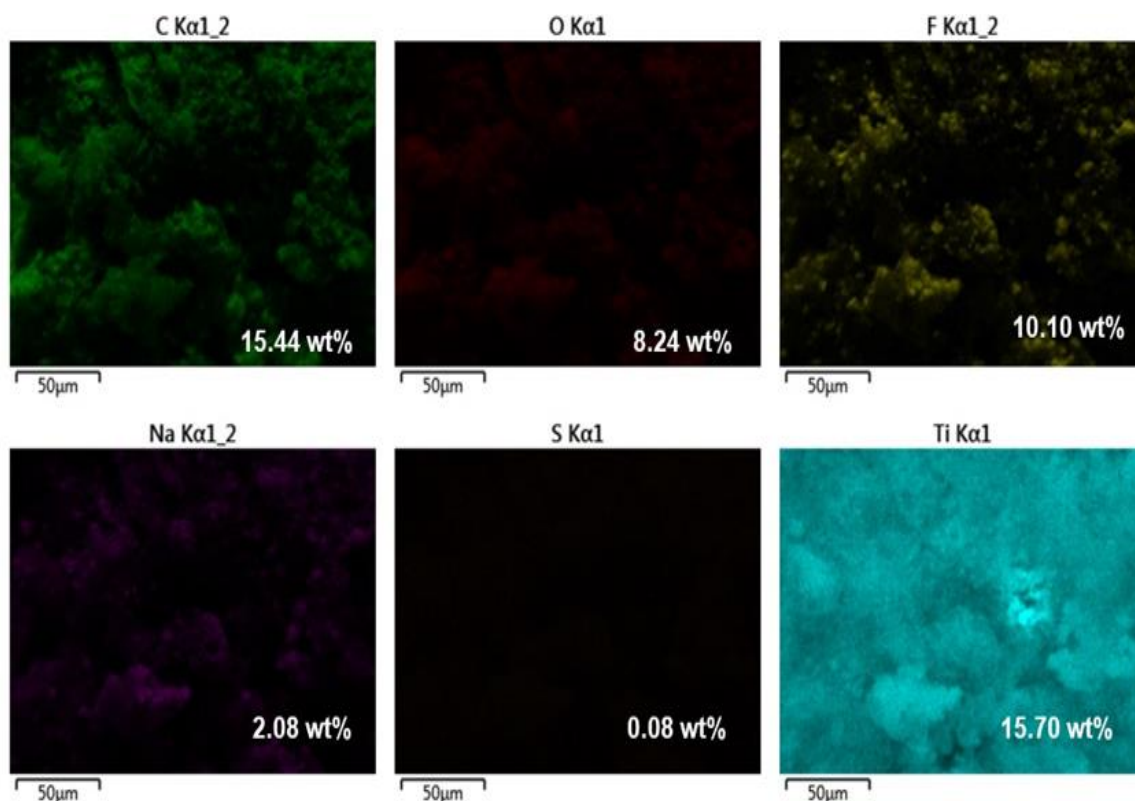


Figure 48: EDS Elemental Mapping of TiO<sub>2</sub> Encapsulated *n*-Eicosane Wt% Inserted in the Images (B).

### 3.5 Effect of Surfactant on the TiO<sub>2</sub> Microencapsulation of ThermoChromic

This work investigates the effect of surfactant on the microencapsulation of thermoChromic materials (TCMs) by TiO<sub>2</sub>. Two types of surfactants, namely Cetrimonium

Bromide (CTAB) and Sodium Dodecyl Benzene Sulphonate (SDBS), are deployed during the microemulsion process for the formation of a TiO<sub>2</sub> shell layer on a commercial dye TCM (CDTCM). These off-the-shelf CDTCMs are primarily Leuco dye particles that exhibit a color change (black to white) behavior at around 33 °C. The role of TiO<sub>2</sub> shell material encapsulation is not only to protect the CDTCMs from solar-irradiated photodegradation but also to provide self-cleaning photocatalytic benefits.

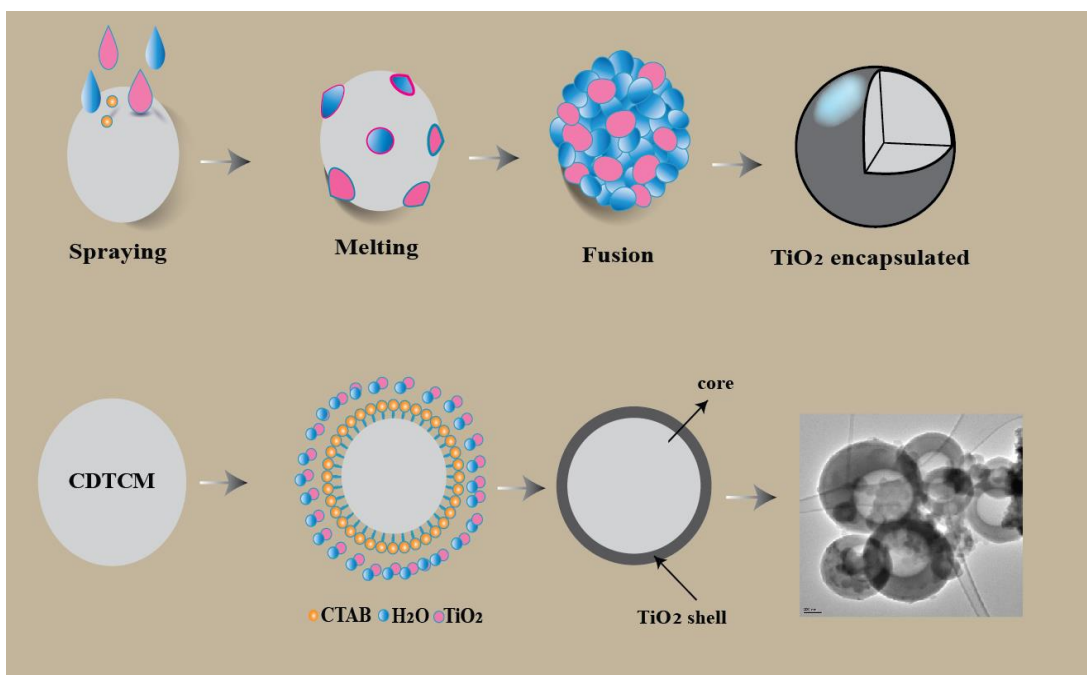


Figure 49: Microencapsulation Process of CDTCM@TiO<sub>2</sub> Using Different Surfactants.

In this study, focused on using a commercial dye, thermochromic black powder as the core CDTCM, and a sol-gel TiO<sub>2</sub> precursor for the formation of crystalline TiO<sub>2</sub> as a shell, using a microemulsion process. The process for the establishment of a core-shell structure requires solubilization of the core in the surfactant solutions for micelles formation with the core species. There are several methods that can be used to microencapsulate TCMs, as shown in Figure 49. Two of these methods are spray-drying and solvent evaporation, but they may have limitations with respect to controlling the particle size. As an example, for a surfactant, Figure 50 [245]

illustrates this interaction on the TiO<sub>2</sub> microencapsulation of thermochromic phase change materials. Moreover, initially, the CDTCM core material along with its polymer shell will be identified through detailed characterization to establish the hydrophobic or hydrophilic character of the CDTCM core. After that, a suitable surfactant is selected to enable the formation of micelles to produce TiO<sub>2</sub> microcapsules. In this research, innovative work of CDTCM@TiO<sub>2</sub> is presented, using two different types of cationic and anionic surfactants, CTAB and SDBS, respectively, for the formation of stable micelles leading to thermal stability.

Table 3: Nomenclature.

TCM	Thermochromic Material
CDTCMs	Commercial Dye Thermochromic Materials
PCM	Phase change Material
PCTCMs	Phase-Change Thermochromic Materials
MPCTCM	Microencapsulated Phase Change Thermochromic Material
EPCMs	Encapsulated Phase Change Materials

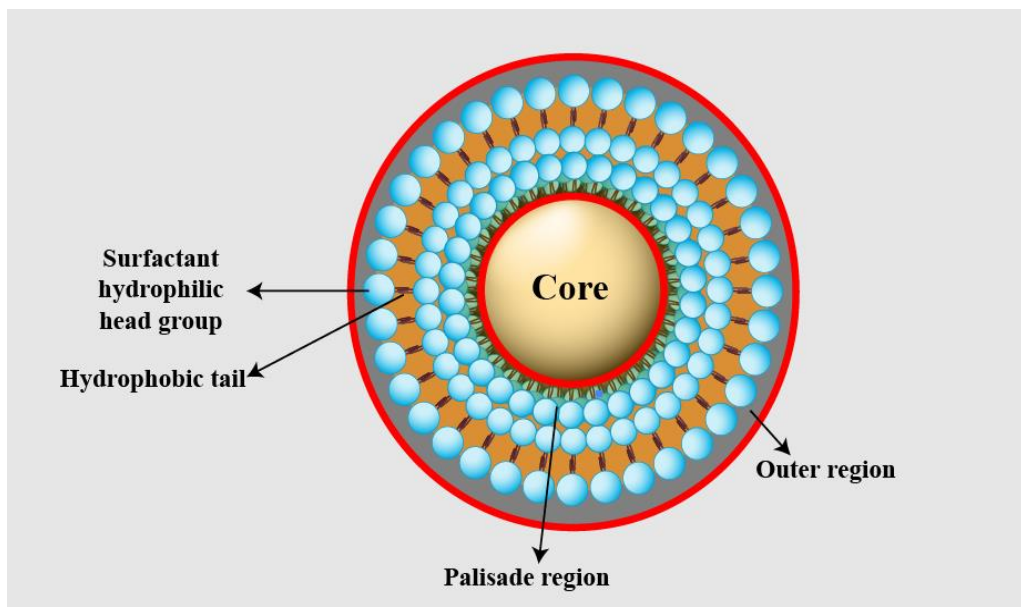


Figure 50: A Surfactant Micelle in Water: Three Different Regions of a Micelle are Identified as the Outer Region, the Palisade Region, and the Core.

### 3.5.1 Preparation of TiO<sub>2</sub> Precursor Solution, Encapsulation and Filtration

The first step was to place 80 mL beaker on a stirrer and pour in 10.0 mL toluene and 10.0 mL 2-propanol followed by stirring at a rate of 200 rpm at room temperature for 30 minutes. Then, 3.0 mL titanium isopropoxide and 1 drop of HCl were added to the solution (name this step TTIP\*). The stirring was continued for 1 hour and the solution was covered. The CTAB and SDBS were individually mixed with 80.0 mL DI water in a beaker maintaining several mass ratios of the components as per Table 4 and under continuous stirring. Next, the hot plate was set to around 80 °C and stirred at 900 rpm until the water temperature reached 75 °C. Then, the hot plate temperature was reduced to 60°C and 1.0g commercial TC dye, CDTCM, was added at constant temperature over a 30-minute time interval for complete dissolution. The surfactant amount for each system was kept the same (2.0 g). Around one drop (0.2 mL) of NaOH solution was added for pH adjustment and stirred for 1 hour. Finally, 3.0 mL of TTIP\* was added drop by drop every 5 seconds between and stirring was continued for 4 hours before filtration. A funnel was set on an empty flask on which a Whatman filter paper was placed. Then, the solution was poured through the filter paper to separate the powder. Lastly, the filter paper was washed with 10% ethanol solution three times in order to ensure proper filtration. The filtered powder was then placed overnight in an incubator at around 70 °C. Different types of microcapsules were prepared by this microemulsion process. The product weight of the microcapsules was specified to be around 1.0 g for each sample. Figure 51 shows the preparation of the TiO<sub>2</sub> precursor solution at each steps A, B and C.

Table 4: The Compositions of the TTIP\* and Surfactant Types.

Surfactants (g)		TTIP* (mL)	Deionized water (mL)	CDTCM (g)	NaOH (mL)
CTAB	2.0	3.0	80.0	1.0	0.2
SDBS	2.0	3.0	80.0	1.0	0.2

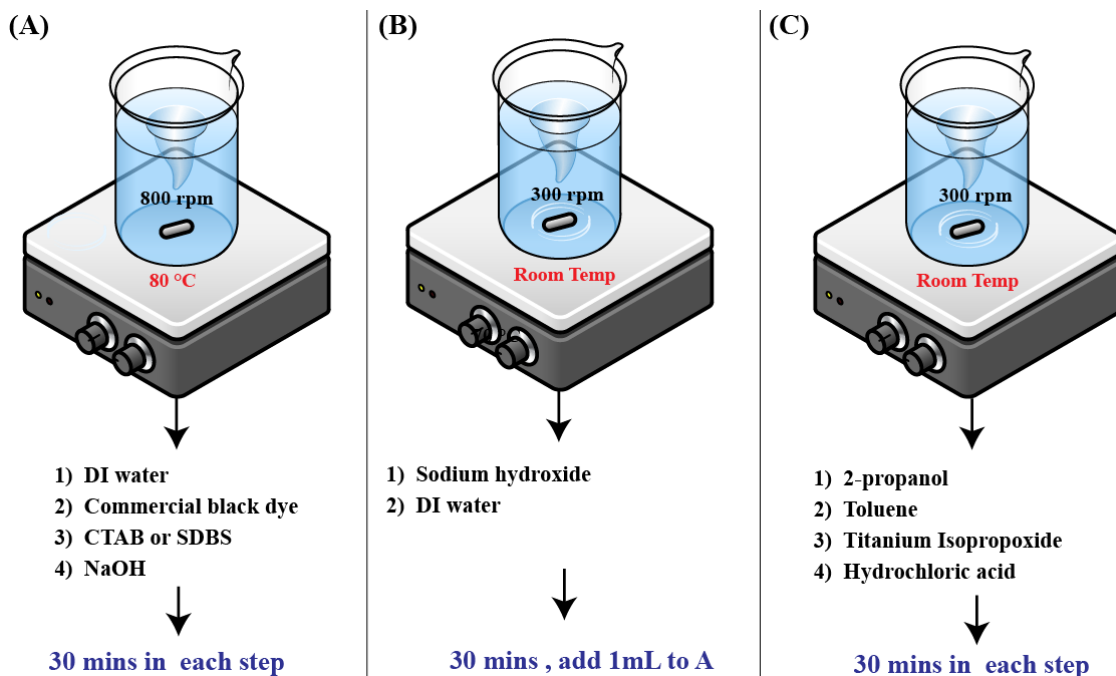


Figure 51: Preparation of TiO<sub>2</sub> Encapsulated Black Dye.

### 3.5.2 Results and Discussion

An investigation on the identification of an ideal surfactant for the TiO<sub>2</sub> encapsulation process was undertaken. We have tested CTAB and SDBS as potential surfactant options and used scanning electron microscopy (SEM), high-resolution transmission electron microscopy (HRTEM) and energy-dispersive x-ray spectroscopy (EDS) to evaluate their effectiveness in encapsulating commercial thermochromic powders, by observing the surface morphologies and microstructures. A few physico-chemical characterization methods, such as XRD, FTIR, UV-Vis, CIE LAB, optical microscopy, and DSC were used to understand the structural, chemical, optical and thermal chromic color change behavior of TiO<sub>2</sub> microencapsulated systems.

#### 3.5.2.1 SEM, HRTEM, EDS

SEM and HRTEM were utilized to investigate the composite surface morphology and core-shell structure of the microcapsules, with the resultant micrographs presented in Figures 52 and 53. The SEM-HRTEM micrographs of the CDTCM@TiO<sub>2</sub> (using CTAB) show a smooth

morphology with a core-shell structure and symmetric spherical particles with particle size of ~3.7 nm. Moreover, the samples synthesized with CDTCM@TiO<sub>2</sub> using SDBS, shown in Figure 53, resulted in a mixture of amorphous CDTCM@TiO<sub>2</sub> nanoparticles. It is noted that the inorganic TiO<sub>2</sub> shell can effectively increase the thermal conductivity of the CDTCM [210]. Figures 52e and 53h show that the TiO<sub>2</sub> nanosheets display a transparent thin layered structure with corrugations and waves.

Furthermore, the core-shell microstructure of CDTCM@TiO<sub>2</sub> microcapsules obtained by using the CTAB and SDBS surfactants had a thickness of about 3.7-3.9 nm, obtained from the images of the HRTEM, Figure 2f for the CTAB and Figure 53d for the SDBS, respectively. Figure 52a clearly shows that the CTAB surfactant produces distinct particles with core and shell as compared to the particles produced by using the SDBS surfactant. In general, the microcapsules' core and shell structure can be seen in Figure 52b-g for the CTAB and in Figure 53e-f-g for the SDBS. The darker shell is TiO<sub>2</sub>, and the lighter is the CDTCM particle inside the shell, shown in some small areas in Figure 52d (encapsulated) and Figure 53b (unencapsulated) CDTCM crystals. The high-resolution TEM micrographs as exhibited in Figures 52g-h and 53e show lattice fringes with d-spacings 2.5 Å (101), 2.2 Å (111) corresponding to the TiO<sub>2</sub> anatase phase for the CTAB surfactant, and 3.5Å (101) corresponding to the TiO<sub>2</sub> rutile phase for the SDBS, according to Hanawalt et al [246]. It can be observed that the TiO<sub>2</sub> encapsulated microcapsules have a spherical shape with a particle diameter of 3-4 nm, according to the HRTEM and SEM images. Moreover, it can be noticed that the structure and particle topography of CDTCM@TiO<sub>2</sub> microcapsules are successfully synthesized by self-assembly for CTAB and contain mix of amorphous media for SDBS. Figures 54 and 55 show the EDS spectral results of CDTCM@TiO<sub>2</sub> using CTAB and SDBS together with the wt% of the titanium composition. The

EDS images in Figures 54 and 55 show all the sample zone elements such as carbon, copper, oxygen, and titanium contained in the shell chemical composition. The titanium and oxygen elemental compositions are of the appropriate weight ratios corresponding to an effective encapsulant shell layer.

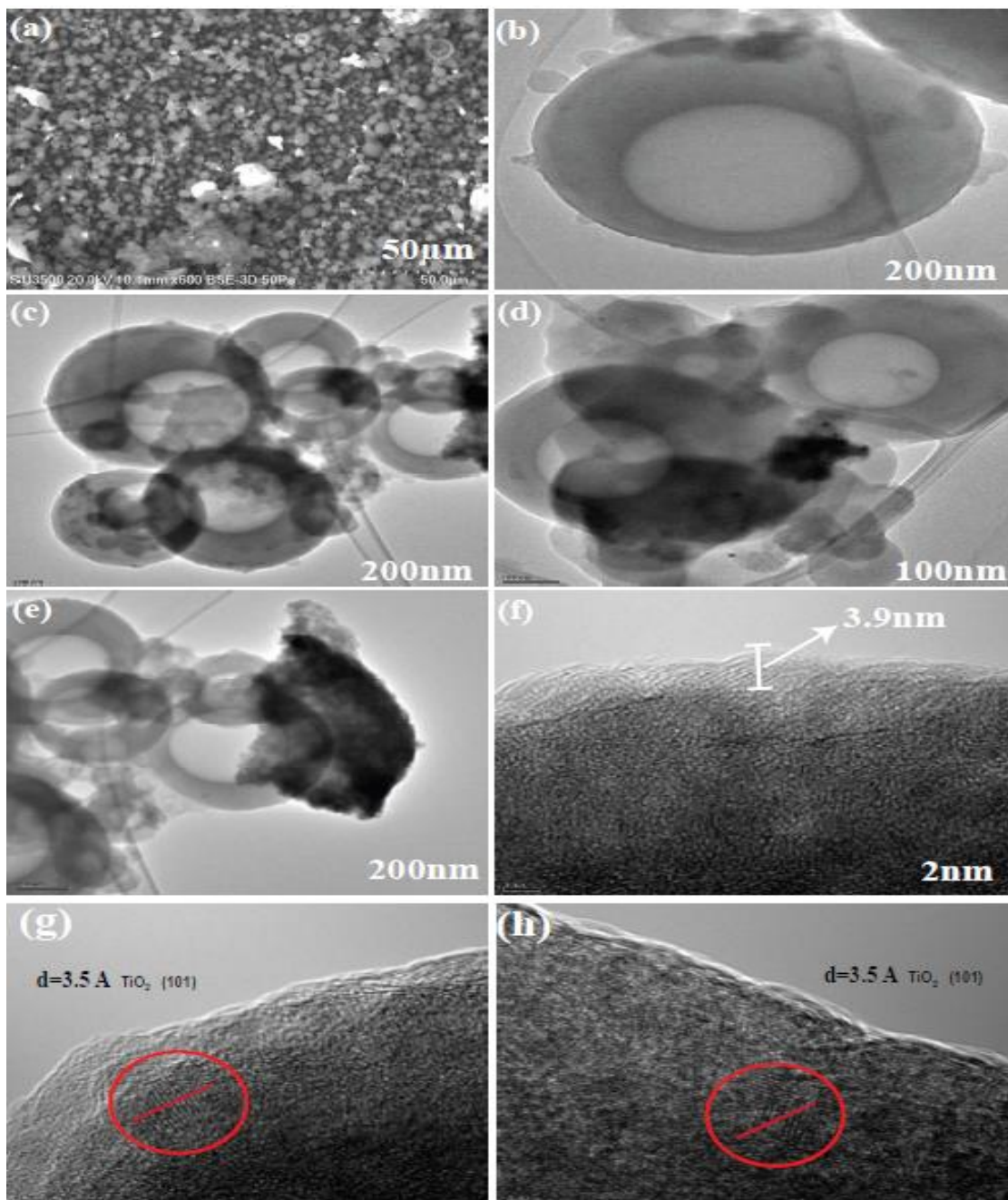


Figure 52: SEM-HRTEM Micrographs of CDTCM@TiO<sub>2</sub> by Using CTAB Surfactant.

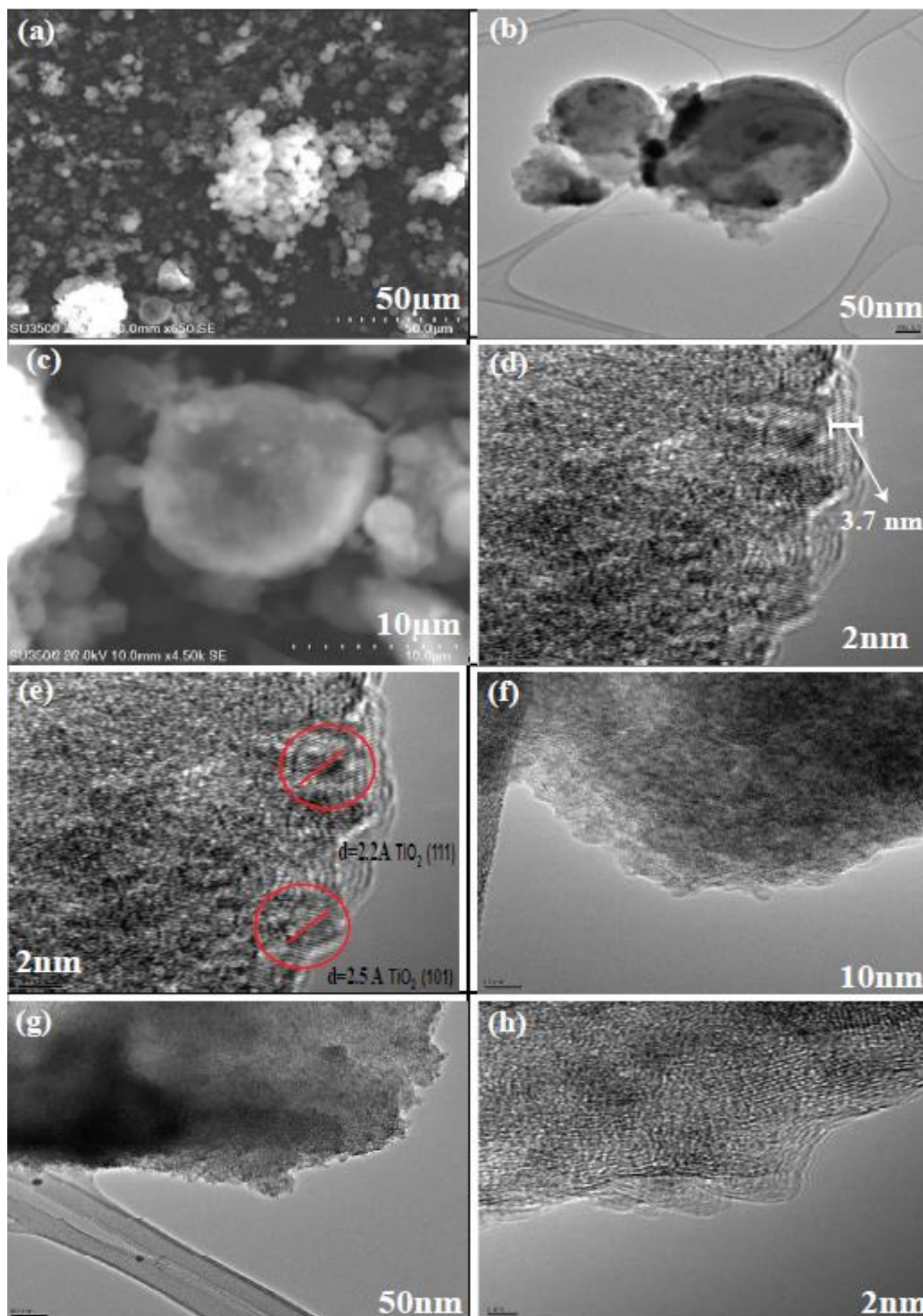


Figure 53: SEM-HRTEM Micrographs of CDTCM@TiO<sub>2</sub> by Using a SDBS Surfactant.

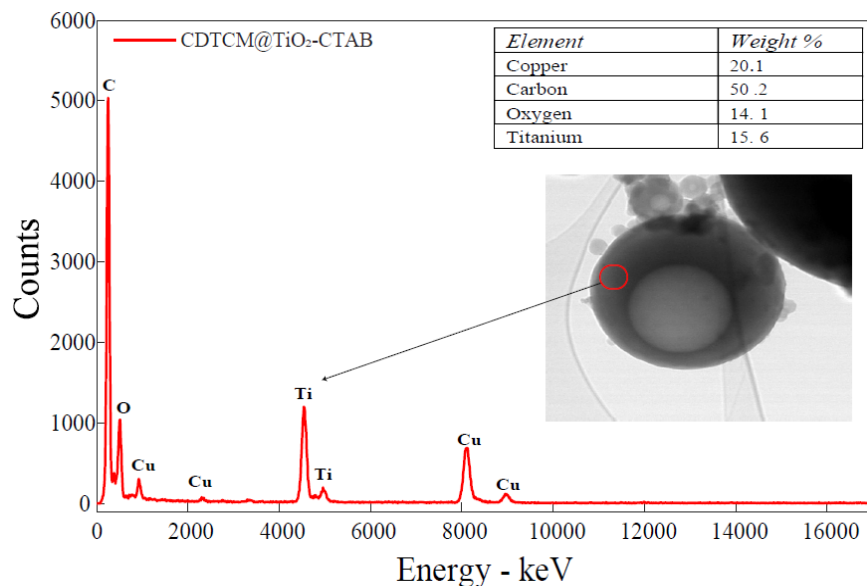


Figure 54: EDS Spectrum of the Microencapsulated CDTCM with a Crystalline TiO<sub>2</sub> Shell CTAB.

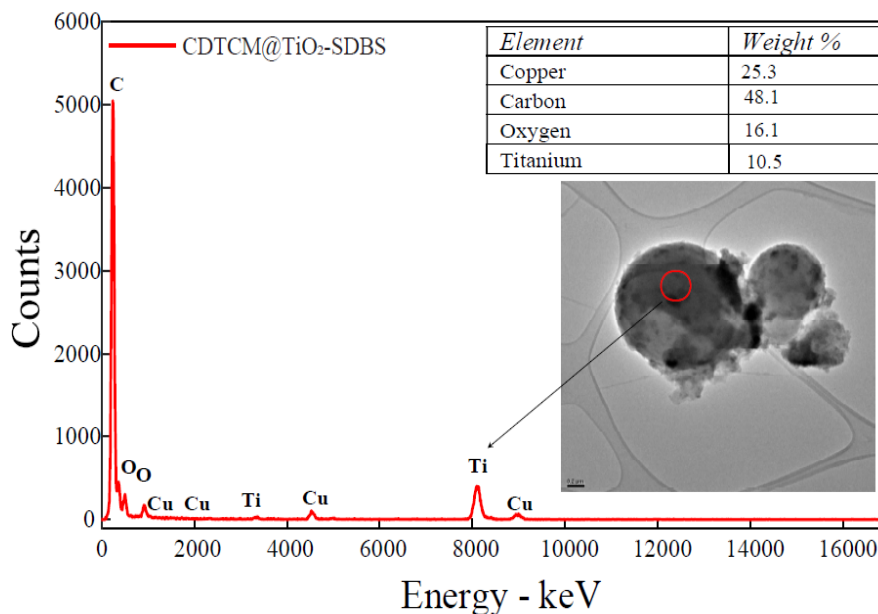


Figure 55: EDS Spectrum of the Microencapsulated CDTCM with a Crystalline TiO<sub>2</sub> Shell SDBS.

### 3.5.2.2 DSC - Thermal Heat Flow

The TCM phase change from solid to liquid, when the solvent melts, is responsible for the color change [41, 247]. Differential scanning calorimetry (DSC) was utilized to analyze different types of materials, such as the CDTCM encapsulated with TiO<sub>2</sub> using CTAB and SDBS

as surfactants. Table 5 shows the peak temperatures and the enthalpy values associated with the phase transition for samples, plain CDTCM and CDTCM@TiO<sub>2</sub> encapsulated using CTAB and SDBS, respectively.

Table 5: Peak Temperatures and Enthalpy Values for the Plain and Encapsulated CDTCM for Surfactants, CTAB and SDBS.

Sample	Heating Curve	
	Solid-Liquid Phase Change Transition Peak Temperature (°C)	Enthalpy Stored at the Solid-Liquid Phase Transition (J/g)
CDTCM	32.50	43.06
CDTCM@TiO <sub>2</sub> -CTAB	33.86	68.01
CDTCM@TiO <sub>2</sub> -SDBC	34.66	53.83

The DSC results shown in Figure 56 are compared with the color change properties for different samples. The plain commercial CDTCM material changes color from black to white and undergoes phase transition at around 32.50 °C with a change in heat flow enthalpy of 43.06 J/g. The solid to liquid transition peak temperature of the TiO<sub>2</sub> encapsulated CDTCM using CTAB was around 33.86 °C with the heat flow value of 68.01 J/g. The TiO<sub>2</sub> encapsulated CDTCM using SDBS changes color from black to white at a peak melting temperature of about 34.66 °C and the heat flow enthalpy is of 53.83 J/g. As it can be seen in Figure 56, the dye encapsulated with TiO<sub>2</sub> using CTAB as surfactant has the best performance at the solid-liquid phase transition with a larger integrated area than the plain CDTCM. This indicates that the TiO<sub>2</sub> encapsulated CDTCM using CTAB has a larger latent heat storage per the unit weight of all the samples. This is because of the additional TiO<sub>2</sub> - shell layer on the CDTCM core. Moreover, the DSC curve of all the CDTCM@TiO<sub>2</sub> encapsulated samples are asymmetrical sharp peaks and are narrower in peak transition than the bulk plain CDTCM. Overall, it is noteworthy to mention that

the DSC profiles of the TiO<sub>2</sub> microencapsulated CDTCM using different surfactants, such as CTAB and SDBS, demonstrate higher heat flow enthalpies of at least 10-20 J/g with the peak transition temperature increasing by 1 to 2 °C.

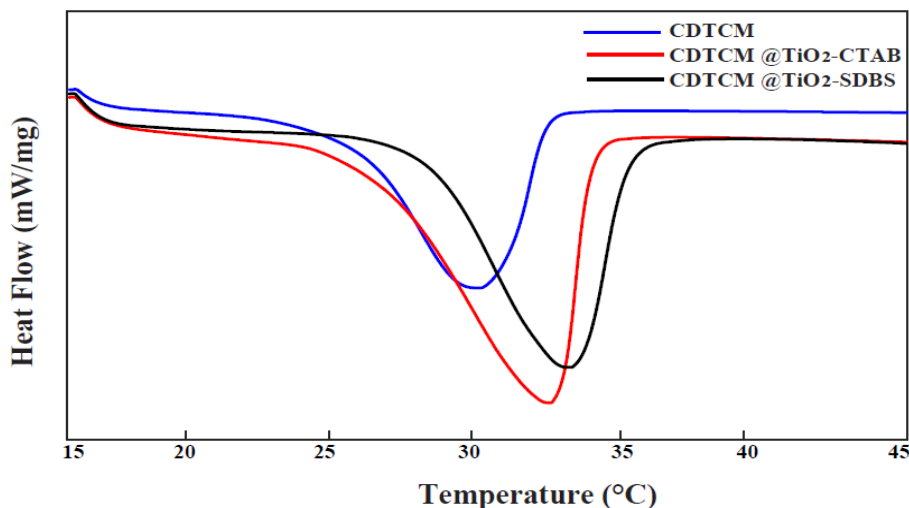


Figure 56: DSC Profiles of CDTCM & CDTCM@TiO<sub>2</sub> Encapsulated.

### 3.5.2.3 CIE LAB Color Simulation

The plain and encapsulated TCM color changes, during the phase change transition, were determined by the International Commission on Illumination (CIE LAB) color space coordinates for both the CTAB and SDBS surfactants [219]. The plain CDTCM was used as a standard for the color variation analysis [248]. Figure 57 shows the results of these studies taken at room temperature and at 50 °C. The six types of colors shown in Figure 57 and in Table 6 exhibited a dynamic linear shift in the coordinates and  $h$ , which are highly sensitive to temperature change (room temperature to 50 °C). From the Table 6, it is observed that the change in lightness index,  $dL^*$  consistently increases for all the samples heated at 50 °C from room temperature and hence demonstrates the chromic color change behavior. Out of the two surfactants used for the TiO<sub>2</sub> encapsulation, the CTAB shows greater effect in terms of lightness change (from 5.048 at room temperature to 21.598 at 50 °C) than the SDBS prepared samples

(from 11.807 to 15. 217). This data is well supported by Figure 57 where the CTAB sample at 50 °C qualitatively has more color contrast on the brighter scale than the SDBS sample. The other color coordinator parametric values such as dE\*, da\*, db\*, dc\* and dh\* in Table 6, has the same trend as dL\* in differentiating the CDTCMs or TiO<sub>2</sub> microencapsulated CDTCMs at room temperature and samples heated at the transition temperature of 50 °C.



Figure 57: CIE LAB Color Simulation of the Samples at Room Temp & at 50 °C.

Table 6: C.I.E. L\*a\*b\* Data Sets for the Samples at Room Temperature (Standard) and at 50 °C (Sample).

Standard CDTCM: L* =12.135, a* = 5.129, b* = 0.839, c*= 5.197, h* = 9.286						
Sample Name	dE*	dL*	da*	db*	dc*	dh*
CDTCM 50 °C	32.865	32.647	-2.412	2.909	-0.568	3.736
CDTCM@TiO <sub>2</sub> -SDBC Room Temp	12.105	11.807	-2.497	0.953	-2.013	1.758
CDTCM@TiO <sub>2</sub> -SDBC 50 °C	15.332	15.217	-1.867	0.194	-1.776	0.609
CDTCM@TiO <sub>2</sub> -CTAB Room Temp	5.913	5.048	0.127	3.077	1.357	2.764
CDTCM@TiO <sub>2</sub> -CTAB 50 °C	22.388	21.598	-0.723	5.850	2.813	5.180

#### 3.5.2.4 UV-Visible Spectrophotometer Absorbance and Reflectance

Figures 58A and 58B shows the UV-Vis absorption and reflectance spectra of the plain CDTCM and TiO<sub>2</sub> microencapsulated CDTCM at around room temperature and at 50 °C. The absorption band at around 625 nm with a shoulder band at around 580 nm are due to the chromic color change behavior of the thermochromic dye particle (CVL lactone ring opening) as a core constituent. The spectra of the decolored CDTCM at room temperature and also at 50 °C do not show any characteristic absorption band for CVL as it is the lactone of a closed ring, this behavior is similar to that of the theoretical and experimental spectra of CVL where the lactone ring is closed [213]. The presence of CVL as a leuco dye microencapsulated by a polymer in CDTCM can be supported by the XRD pattern reported elsewhere [8] and also in the present study (next section).

If the leuco dye in the CDTCM is CVL, one can assume its hydrophilic nature. Hence it needs a cationic surfactant for the microemulsion process [245] to generate shell formation around the CVL. Therefore, smooth micelle formation occurs with the cationic surfactant, CTAB and TiO<sub>2</sub> precursor to form a TiO<sub>2</sub> shell around the CVL core. In this case, all the opened lactone rings are utilized and would not show any absorption bands, even after the melting / phase change shown in Figure 58A. Therefore, the absorbance curves at room as well as elevated temperatures should be the same. On the other hand, the use of an anionic surfactant, SDBS, for the microemulsion process for the hydrophilic CVL would create very weak interaction between the CVL and the surfactant. In this case, the next interaction with the titania precursor would generate a porous and inhomogeneous shell structure around CVL. Accordingly, then the developed shells would have different optical density without any characteristic bands Figure 58A. Utilization of the UV-Visible spectrophotometer (Cary 5000 UV-Vis-NIR) can also be

applied to the energy-saving efficiency of coatings [249, 250]. Reflectance spectra of all the samples are replicas of their corresponding absorbance spectra Figure 58B. Variation of intensities are due to the possession of different refractive indices. The CTAB-based, core-shell material shows relatively high reflectance while the SDBS-based core-shell material shows relatively low reflectance. This observation indicates that CTAB forms a uniform  $\text{TiO}_2$  shell layer while SDBS forms a negligible  $\text{TiO}_2$  shell layer as its reflectance is close to that of the untreated CDTCM (Figure 58B). The thickness of the shell layer is around 300 nm estimated from the processing system.

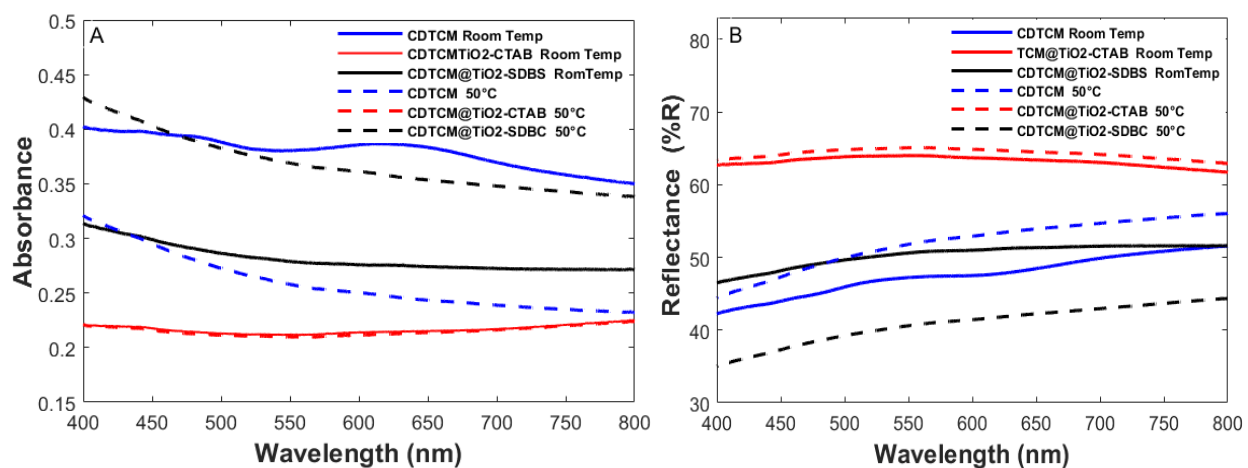


Figure 58: Absorbance (A), Reflectance (B) Spectra of CDTCM and CDTCM@TiO<sub>2</sub> Room Temp and 50 °C.

### 3.5.2.5 XRD Phase Analysis

The phase behavior and structure of the CDTCM and CDTCM@TiO<sub>2</sub> with different surfactants, namely CTAB and SDBS, were characterized by XRD as shown in Figure 59. The XRD curves exhibit diffraction patterns of relatively high intensity. Comparison of the diffraction patterns of the present work with those of the amino aldehyde prepolymer based microencapsulated CVL [40] show great similarity. The presence of strong diffraction peaks at the same angles, along with similar intensity ratios, as given in Figure 59, is an indication of the

same crystalline phase in all cases. All of the diffraction patterns seem to be independent of the microencapsulation materials. However, the small difference at around  $19^\circ$  is possibly due to the decolored and colored types [213]. Moreover, the peak near  $19.8^\circ$  with relatively low intensity suggests the presence of PMMA [251] as microencapsulates in all the systems of CDTCM as shown in Figure 59. As the nanostructured  $\text{TiO}_2$  shell thickness is very small [vide supra-in the section, HRTEM Microstructure Discussion], the X-ray diffraction pattern (Figure 59) cannot be used to identify the formation of anatase or rutile  $\text{TiO}_2$  crystal faces.

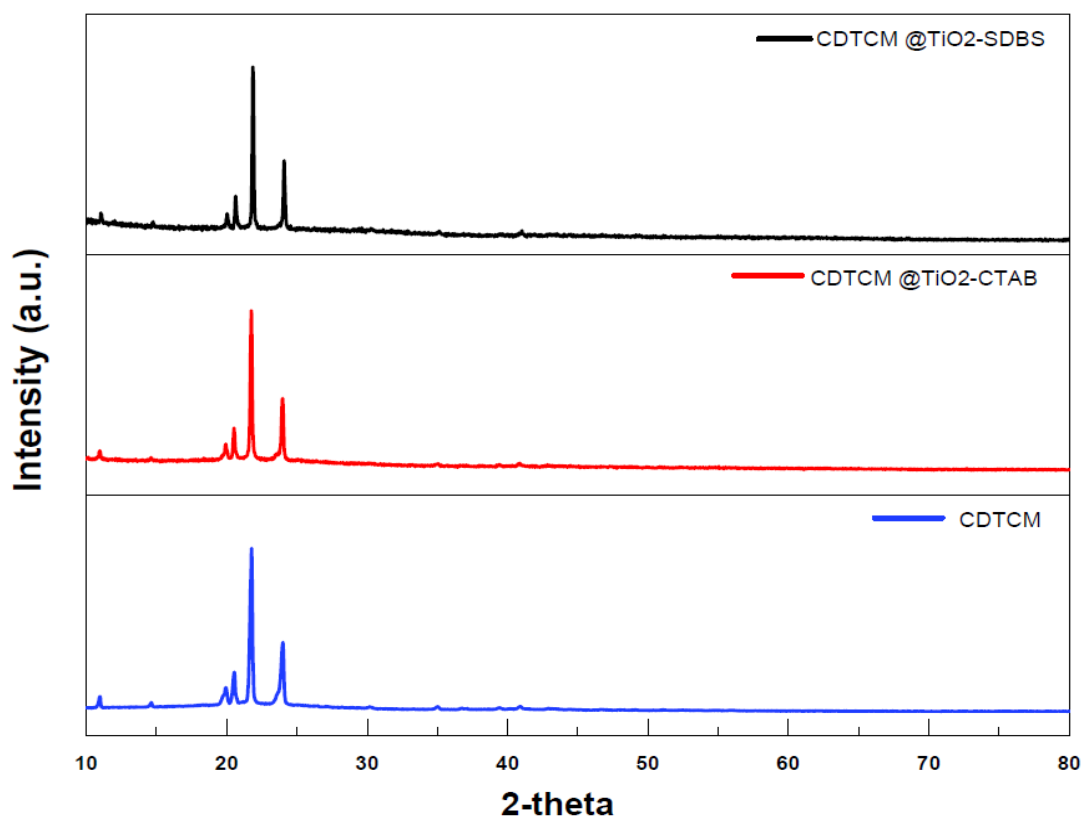


Figure 59: The XRD Patterns of CDTCM, CDTCM@TiO<sub>2</sub>-CTAB and SDBS.

### 3.5.2.6 FTIR Spectral Data Analysis

Figure 60 shows the FTIR spectra of the composite microcapsule materials, CDTCM and CDTCM@TiO<sub>2</sub>, using the CTAB surfactant and the CDTCM@TiO<sub>2</sub> using the SDBS surfactant. It is expected that the polymer encapsulated leuco dye in commercially available CDTCM has a

PMMA polymer shell, as the carbonyl group of the ester group of PMMA responds to the appearance of a band at around  $1740\text{ cm}^{-1}$  in the FTIR spectra of CDTCM, CDTCM@TiO<sub>2</sub> (CTAB surfactant) and CDTCM@TiO<sub>2</sub> (SDBS surfactant), as shown in Figure 60, due to the symmetric stretching mode of the carbonyl group [251, 252].

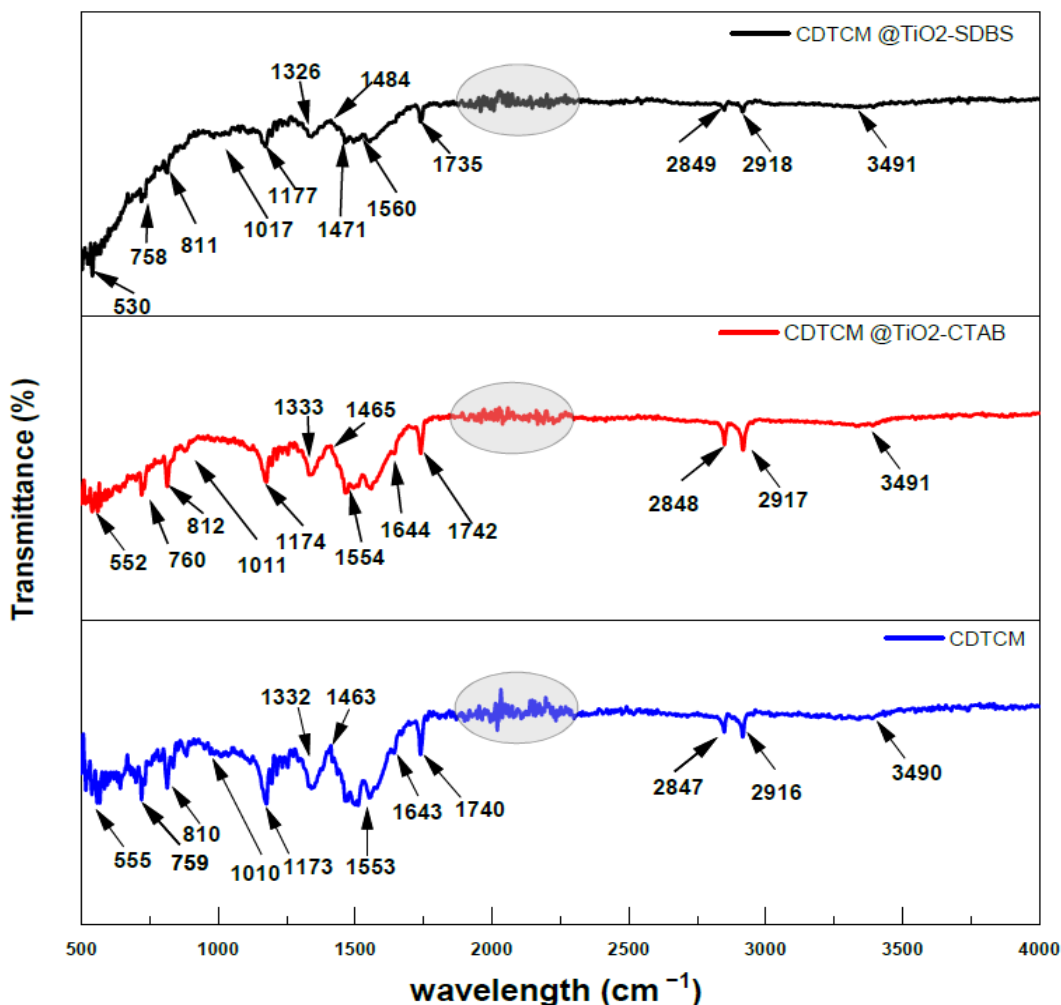


Figure 60: The FTIR Spectra CDTCM, CDTCM@TiO<sub>2</sub>-CTAB and SDBS.

Moreover, for the black dye, a colored state occurs due to the opening of lactone ring of dye, and there is a possibility to exhibit the asymmetric stretching vibration of the carbonyl group. Practically, appearance of the FTIR absorption (a weak shoulder) near  $1640\text{ cm}^{-1}$  for all systems confirms the presence of a dye system having a lactone ring which is opened in the

colored state. The nature of a positive shift of this type of vibrational mode indicates the dye takes part in a reaction of the composite to establish a bond. On the other hand, the absorption near  $1340\text{ cm}^{-1}$  is possibly for the symmetric vibrational mode of the carbonyl group of the existing dye. In this case, considerable negative shifting is observed which supports the above type of reaction in the system. From the previous discussion on UV-Visible spectra and XRD patterns, we suggest that the above vibrational modes appearing at  $1640$  and  $1340\text{ cm}^{-1}$  are for the carbonyl group of CVL. The very weak and broad absorption near  $3500\text{ cm}^{-1}$  may be for the stretching vibration of hydrogen bonded hydroxyl groups. On the other hand, the absorption peaks at  $\sim 2848\text{ cm}^{-1}$  and  $\sim 2917\text{ cm}^{-1}$  are for the stretching vibration of C-H. After encapsulation of CDTCM by the anatase  $\text{TiO}_2$  shell, the FTIR absorption feature of CDTCM near  $650$  and  $750\text{ cm}^{-1}$  are changed (Figure 60) due to the bonding of the  $\text{TiO}_2$  shell with the outer surface of CDTCM. As the stretching vibrational modes of  $\text{TiO}_2$  appear near  $650$  and  $750\text{ cm}^{-1}$ , the above change in the absorption feature after encapsulation, is possibly due to the  $\text{TiO}_2$  encapsulation [242, 244].

## **Chapter 4: Effects of Multilayer Thin Film Coatings on Different Thermochromic Materials for Thermal Energy Storage Applications<sup>3</sup>**

### **4.1 Introduction**

Nowadays, there is an increased use of heating and cooling systems needed to provide comfortable environments in buildings. This leads to increased power consumption and greenhouse gas emissions [253]. Over the past decade, considerable research has focused on this topic [254] leading to new technological approaches and reduction of the “heat island” effect [255]. Different materials used as smart coatings significantly impact a building’s thermal envelop [256] with smart windows and cool roofs being the best known applications [257].

Highly reflective fenestration obtained by applying different coatings are commonly used in various types of construction, and urban settings. This also provides more comfortable temperatures at outside surfaces and their immediate surroundings [258]. Moreover, the layers of different coating materials have suitable absorptive, reflective and transmissive properties, positively impact energy savings during hot seasons [259]. Thermochromic smart materials can play a significant role and can help reduce a building’s energy needs during both hot and cold seasons [260]. By using smart thermochromic materials on external window glass surfaces, a reduction in the room temperature can occur as the glass surface color changes.

---

<sup>3</sup>This chapter was before published in *SPIE Proceedings* (Hakami, A., Srinivasan, S.S., Marildi, H., Biswas, P. K., Wallen, S. L., & Stefanakos, E. K.) (2021, August). Effects of multilayer thin film coatings on different thermochromic materials for thermal storage applications. In *Current Developments in Lens Design and Optical Engineering XXII* (Vol. 11814, p. 118140F). International Society for Optics and Photonics. Permission is included in Appendix A.

Although windows cover a small part of a building's surface, the amount of energy saved by the application of different thermochromic materials can be significant. In the past few years, the use of thermochromic coatings on the roofs and windows of buildings is gradually increasing [164]. In the present study, a thick glass (2 mm) has been used as the substrate for thermochromic coatings. The optical components of the developed coatings are tested. Two kinds of dye, namely, (1) commercially available black dye and (2) lab synthesized three component based blue dye have been used as thermochromic materials.  $\text{TiO}_2$  or  $\text{SiO}_2$  were chosen to protect the polymer based thermochromic materials from photodegradation or thermal degradation.

## **4.2 Experimental**

In this study, several samples were prepared by applying different thermochromic coatings on 2 mm thick glass surfaces. Powdered titanium dioxide ( $\text{TiO}_2$ ) (purity  $\geq 98.9\%$ , Sigma-Aldrich, Inc), silicon dioxide ( $\text{SiO}_2$ ) (Purity 99% from TEOS precursor, Sigma-Aldrich, Inc) encapsulated blue dye prepared via a wet chemistry route, a 3-component blue dye, and a commercially available black dye (with and without a  $\text{TiO}_2$  second layer coating). These were studied by mixing selected components with a sodium silicate binder. The blue dye three component system included 1-tetradecanol as the solvent, crystal violet lactone (CVL) as the basic dye system, and bisphenol A (BPA) as a color developer. All the chemicals were purchased from Sigma-Aldrich, Inc (Purity  $\geq 99.0\%$ ). The encapsulation process of the blue dye has been previously reported [41]. The black dye (Atlanta Chemical Engineering Company) was used both for its color change and its phase change when heated above 30 °C. The sodium silicate was used as binder in both black and blue dye thermochromic samples. The wt% of the dye was

calculated using equation (1) [261]. The details of the studied system components along with their mass are shown in Table 7.

$$\text{wt \% of dye} = \frac{\text{mass of dye}}{\text{Total mass of solution}} \times 100 \quad (1)$$

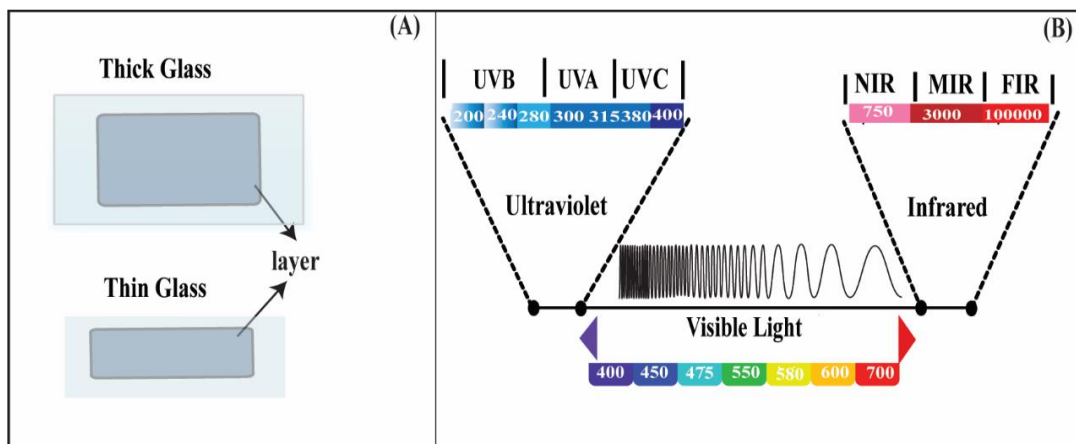


Figure 61: Schematic Showing Thick and Thin Glass with Layers (A), UV-VIS Spectrophotometer Wavelength Range (B).

Table 7: Compositions of All Components with a Binder.

Components	Mass of dye components (g)	Total mass of solution (g) (Mass of each component increased due to addition of water)
Plain black dye with binder	13.08	17.03
Plain blue dye with binder	12.85	15.01
TiO <sub>2</sub> powder with binder	12.55	15.20
SiO <sub>2</sub> with blue dye gel (wet chemistry)	13.08	16.09
TiO <sub>2</sub> with blue dye (multilayer coating)	13.75	16.33
TiO <sub>2</sub> with black dye (multilayer coating)	14.08	16.90

Brief descriptions for the preparation of the precursor of the black and blue dyes are given below. The fundamental formulation (in wt%) of the precursor for the glass coating is 1.5 wt%. The binder, 0.7-0.8 ml sodium silicate, was mixed with water. Each component was mixed

using a round bottom flask and stirred at an average rpm speed of 800 rpm for 2 hours. Next, the requisite amount of TiO<sub>2</sub> pure powder was added to the mixture and stirred for 45 min. Then, the stirring speed was reduced to 700 rpm, and a small amount, ~0.1%, of pure black/blue dye was added to the mixture. Finally, a homogeneous solution containing all the components was obtained and used for coating. Stirring was continued during the whole process.

In this study, six types of samples were prepared Table: 7. The glass substrate was set in a film applicator (doctor blade) to apply a uniform 300 μm coating (schematic in Figure 61A). The samples were dried at room temperature, 20 °C, for at least 6 hours. All samples were protected by a suitable parafilm cover. The main purpose of this work is to study the performance of different types of glass-coated dyes. Analytical tools such as UV-Visible spectrophotometer (schematic in Figure 61B), Differential Scanning Calorimeter, Scanning Electron Microscope, and Energy Dispersive x-ray detector have been employed for the characterization of these thin films. The CIE L\*a\*b\* (International Commission on Illumination) was used to quantify the color coordinates of the samples, where L\* represents the lightness index while a\* and b\* indicate the values for the green-red and blue-yellow color components[218].

### **4.3 Results and Discussion**

A series of the samples' optical spectra were obtained using a UV-Visible spectrophotometer (Cary 5000 UV-Vis-NIR). The spectra of both colored (20 °C) and colorless coatings (30-40 °C) deposited on 2mm glass were measured and analyzed. Figure 62-64 (A-F) shows the UV-Vis spectra of all thin film samples listed in Table 7, at 20 °C and 40 °C. These samples are binder and CVL leuco dye-based black and blue dyes which are also encapsulated individually by SiO<sub>2</sub> and TiO<sub>2</sub> except in one case where the black dye was not encapsulated by

SiO<sub>2</sub>. To obtain a more precise evaluation of the binder-TiO<sub>2</sub> coating, its absorption, transmission, and reflection spectra were also recorded, not shown due to page limitation. In the three-component system we have used CVL as the leuco dye while the commercially available black dye needs a validation regarding the nature of dye [213]. A comparative study of the absorption behavior of the blue dye, black dye and also of the CVL, theoretically and experimentally carried out by K. Takaoka et al. Figure 51 helped us understand the nature of the dye used in black dye. Basically, CVL possesses lactone rings which are colorless. The lactone ring opens with proton addition through a change of temperature of the system. This leads to a change of color giving rise to the thermochromic effect. Three absorption bands can be observed at around 620 nm, 570 nm, and 470 nm. The bands are assigned  $\pi \rightarrow \pi^*$  transitions of the aminophenyl rings of CVL, occurring from the HOMO to LUMO levels, as per the molecular orbital calculations. The CVL lactone ring opening and closing in a reversible manner in the presence of a proton.

Figure 62A shows that the black dye coated a glass substrate exhibits two major absorption bands at approximately 450 nm and 625 nm with a weak shoulder at around 570 nm, having overall absorption close to 0.8 due to the thickness of around 300  $\mu\text{m}$ . This shows the black dye has higher absorption at these wavelengths due to the resonance of the canonical structures of the ring opening form [213].

These absorption bands disappear (Figure 62B) and the overall absorbance reduced from 0.8 to 0.6 when the black dye was heated to 40 °C. This observation suggests that the black dye contains CVL leuco dye with the ring opening and closing mechanism occurring at 20 °C and 40 °C, respectively. In the case of the three-component system, (blue dye with the binder) at room temperature, Figure 62A shows a broad absorption band in the range of 500 nm to 650 nm with a

peak maximum of approximately 625 nm and a shoulder at 550 nm for the ring opening structure of CVL. The absorbance (0.8-0.95) of the blue dye with binder at room temperature Figure 62A is reduced by at least 50% when the same sample is heated to 40 °C, as shown in Figure 62B, due to the ring closure. The SiO<sub>2</sub> encapsulated blue dye shows no change in the absorbance when going from room temperature to 40 °C, due to the very low concentration of the dye particles. This physical effect can be explained by the presence of the dye in the very low refractive index ( $\eta$ ) material, i.e.,  $\eta$  of SiO<sub>2</sub> (1.46). Similarly, for the black or the blue dye coated glass substrates with multiple TiO<sub>2</sub> layers, the figure shows a smooth UV-Vis absorbance spectrum in the range of 0.2-0.6 in the wavelength range of 400 – 800 nm. However, their absorptions are relatively high when encapsulated by particles of relatively high refractive index ( $\eta = \sim 2.0$ , TiO<sub>2</sub>). Spectra plotted as percent transmission versus wavelength are given in Figure 63 (C and D). Overall, the transmission curves of the plain dye/binder samples show an increase in the percent transmission from 10-20% to 20-50% because of the color change characteristics from black or blue to white which is highly reflective and desirable for building applications. The color change behavior would create dispersion in the visible causing a change in the refractive index. In this case, an increase in refractive index would signify a change in reflectance behavior. For an individual metal oxide encapsulated thermochromic dyes, there is little or no change of visible transmission for the samples heated to 40 °C when compared to those at room temperature. But there is a change in transmission behavior in the case of encapsulation made by different oxide systems. Usually, for the silica-based encapsulation, transmission will be high as its refractive index is very low (1.46) while for the titania-based encapsulation, transmission will be lower as its refractive index is near 2.0. In the case of reflectance spectra, the effect will be reciprocal.

Figure 64 (E and F) shows the UV-Vis reflectance spectra of the samples at temperatures of 20 °C (room temperature) and 40 °C for wavelengths ranging from 400-800 nm. Though the samples have been transported to the UV-Vis instrument at a temperature close to 40 °C, these sample intrinsically loose heat due to the long scanning process to cover the wavelength range. Therefore, some discrepancies noted in terms of reflectance were observed in Figure 64 (E and F). Overall, the plain dye with binder coated on the glass substrate shows a higher reflectance due to the chromogenic behavior, i. e. changing color from black or blue to white and, thereby, generating dispersion and relatively high reflectance. For the metal oxide encapsulated or multilayer coatings of these dyes, no drastic change was observed in terms of the reflectance. The band at around 625 nm is very prominent for the blue dye.

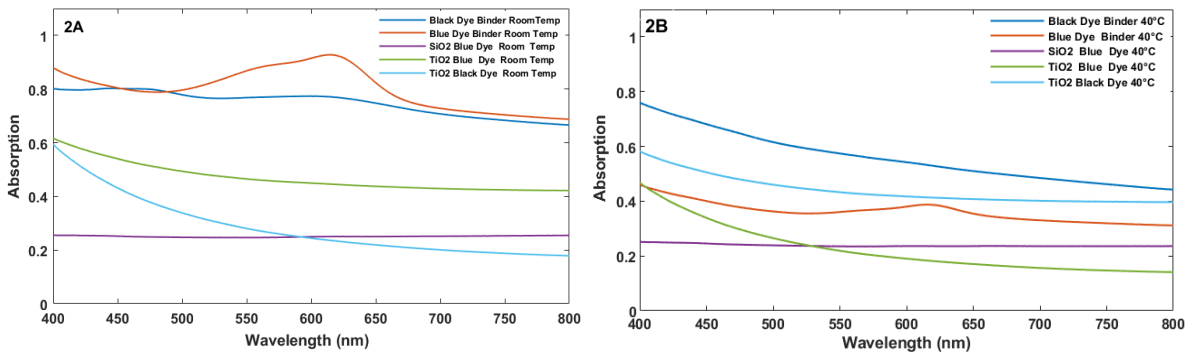


Figure 62: Absorbance Spectra of Plain Black Dye, Plain Blue Dye, SiO<sub>2</sub>/Blue Dye, TiO<sub>2</sub>/Black Dye, and TiO<sub>2</sub>/Blue Dye at (A) Room Temperature and at (B) 40 °C.

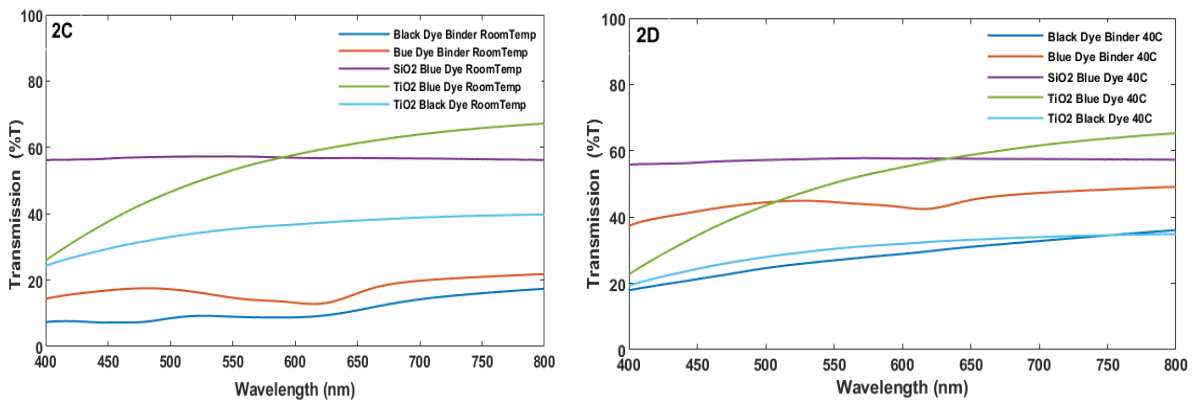


Figure 63: Transmission Spectra of Plain Black Dye, Plain Blue Dye, SiO<sub>2</sub>/Blue Dye, TiO<sub>2</sub>/Black Dye, and TiO<sub>2</sub>/Blue Dye at (C) Room Temperature and at (D) 40 °C

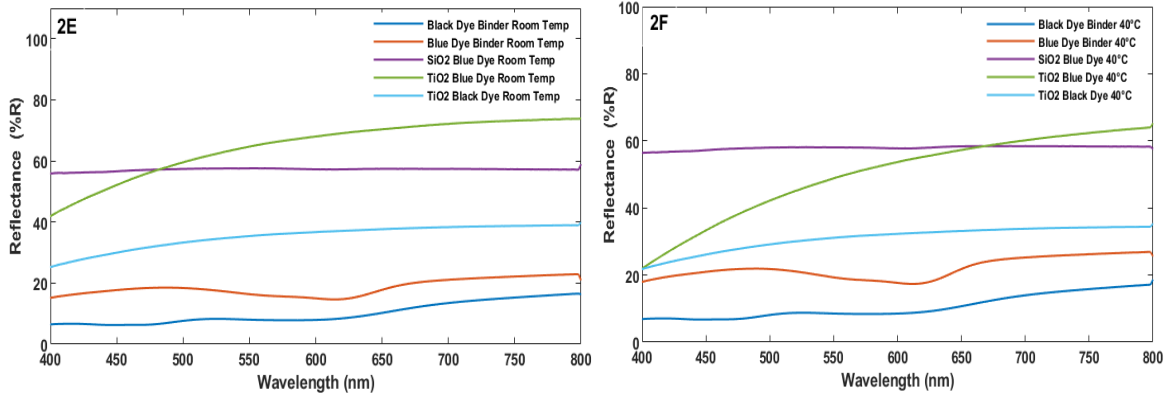


Figure 64: Reflection Spectra of Plain Black Dye, Plain Blue Dye, SiO<sub>2</sub>/Blue Dye, TiO<sub>2</sub>/Black Dye, and TiO<sub>2</sub>/Blue Dye at (E) Room Temperature and at (F) 40 °C.

Two of the films coated on the glass substrates were examined by microstructural imaging and chemical (elemental) analysis via scanning electron microscopy and energy dispersive X-ray spectroscopy. One type of film considered was the plain commercial black dye, mixed using sodium silicate as a binder, and coated with a thickness of ~ 300 μm. The second type of film was the blue dye, mixed with sodium silicate binder, and coated with the same thickness of ~300 μm on the thick glass substrate.

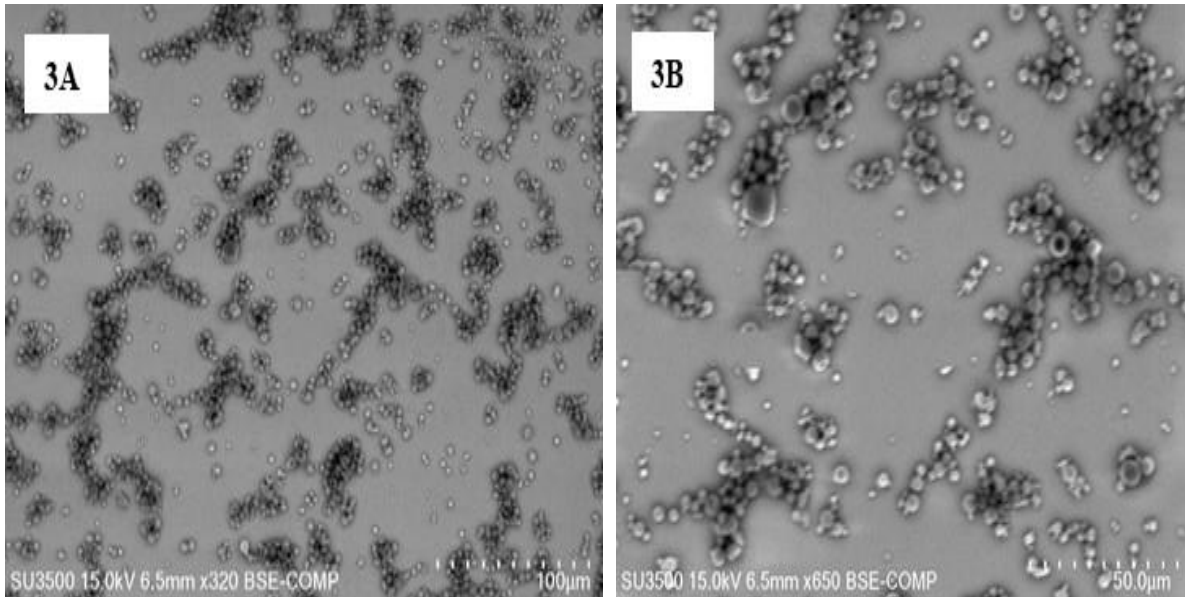


Figure 65: SEM Micrographs of Black Dye with Sodium Silicate Binder Coated on a Thick Glass Substrate at (A) Lower Magnification and (B) Higher Magnification.

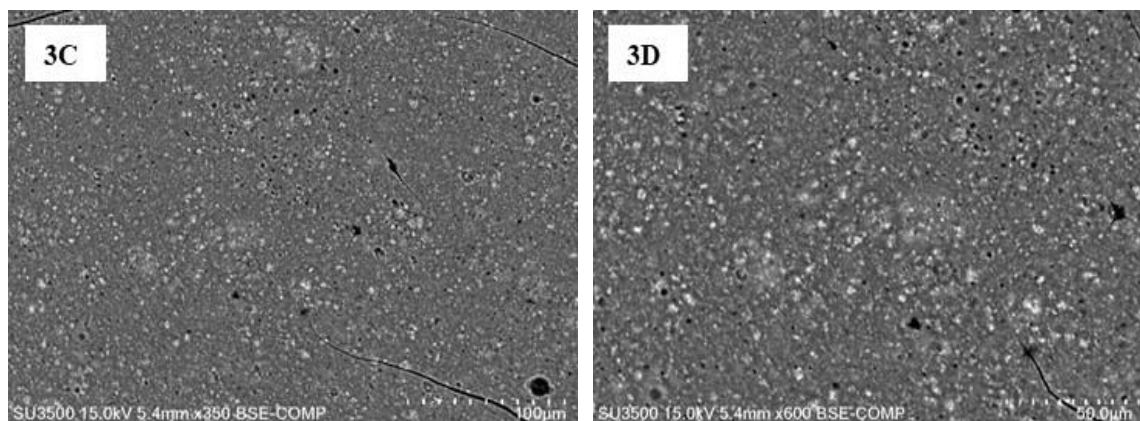


Figure 66: SEM Micrographs of Blue Dye with Sodium Silicate Binder Coated on a Thick Glass Substrate at (C) Lower Magnification and (D) Higher Magnification.

From Figure 65 (A & B), the coated black dye/binder films show some island effects due to the fact that these commercial black dyes have been pre-encapsulated with a polymer layer that separates each individual spherical dye particle and maintains its thermochromic characteristics. On the other hand, the blue dye synthesized in the lab, using the three-component system, and then mixed with a sodium silicate binder, and coated on a glass substrate exhibits very homogeneous surface morphology as shown in Figure 66 (C & D). The EDS spectra show signatures of carbon, oxygen, and other stoichiometric elements such as silicon, and sodium due to the presence of the black or blue dyes and the sodium silicate binder. These spectral results are not shown here due to page limits of this manuscript.

Table 8: C.I.E.  $L^*a^*b^*$  Data Sets for the Samples Treated at Room Temperature (Standard) and at 40 °C (Sample).

A: Standard Name: Black Dye/Binder, $L^*=47.827$ , $a^*=3.800$ , $b^*=5.152$ , $c^*=6.402$ , $h^*=53.588$							
No.	Sample Name	dE*	dL*	da*	db*	dc*	dh*
1	1	21.043	20.879	-2.589	0.422	-0.698	2.529
2	2	25.079	24.857	-3.332	-0.136	-1.364	3.043
Average (D65/ $\mu$ 8mm,		23.061	22.868	-2.961	0.143	-1.031	2.786

Table 8: (Continued)

B: Standard: Blue Dye/Binder, L*=45.151, a*=6.682, b*=-33.463, c*=34.123, h*=281.292							
No.	Sample Name	dE*	dL*	da*	db*	dc*	dh*
1	1	45.920	23.555	-5.471	39.037	-28.419	27.316
2	2	47.721	27.533	-6.214	38.479	-29.085	25.947
Average (D65/ $\mu$ 8mm,		46.820	25.544	-5.842	38.758	-28.752	26.631

C: Standard: TiO <sub>2</sub> /Binder, L*=34.281, a*=-2.938, b*=-3.136, c*=4.297, h*=226.871							
No.	Sample Name	dE*	dL*	da*	db*	dc*	dh*
1	1	35.751	34.425	4.148	8.710	1.407	9.544
2	2	39.406	38.403	3.406	8.152	0.741	8.804
Average (D65/ $\mu$ 8mm		37.578	36.414	3.777	8.431	1.074	9.174

D: Standard: SiO <sub>2</sub> /Blue Dye, L*=48.400, a*=-1.513, b*=-2.324, c*=2.773, h*=236.942							
No.	Sample Name	dE*	dL*	da*	db*	dc*	dh*
1	1	21.958	20.306	2.724	7.898	2.931	7.824
2	2	25.446	24.284	1.981	7.340	2.265	7.258
Average (D65/ $\mu$ 8mm		23.702	22.295	2.352	7.619	2.598	7.541

E: Standard: TiO <sub>2</sub> /Blue Dye, L*=38.629, a*=-1.643, b*=-3.231, c*=3.624, h*=243.051							
No	Sample Name	dE*	dL*	da*	db*	dc*	dh*
1	1	31.469	30.077	2.853	8.805	2.080	9.019
2	2	35.103	34.055	2.111	8.247	1.413	8.395
Average (D65/ $\mu$ 8mm,		33.286	32.066	2.482	8.526	1.746	8.707

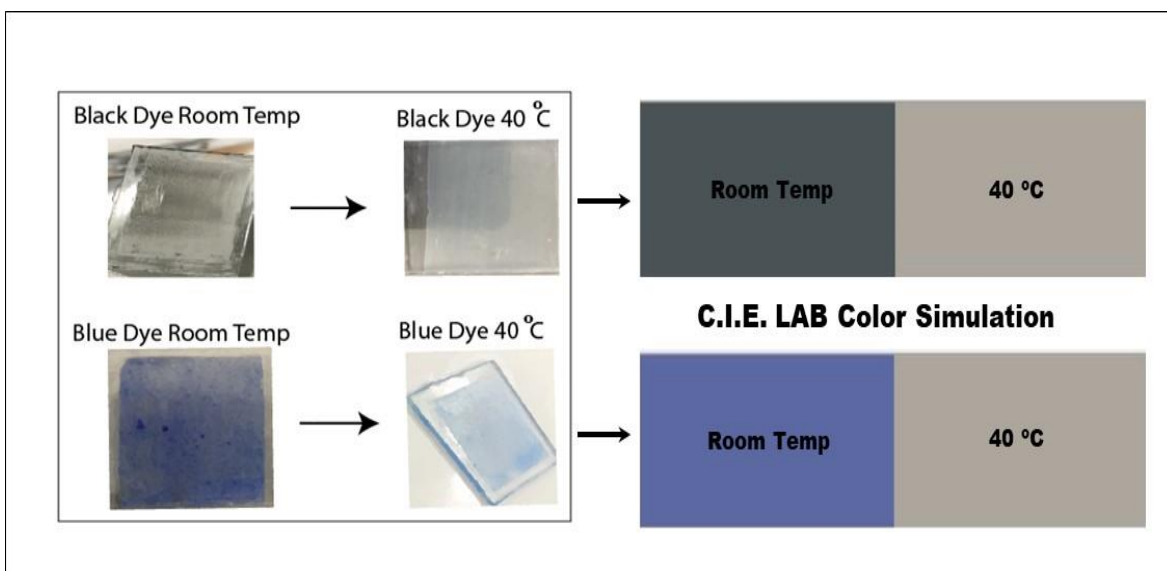


Figure 67: Photographic Images of the Coated Samples at Room Temperature (Left) and 40 °C (Right) CIE LAB Color Simulation of the Samples.

Table 8 (A-E) represents the color coordinate values of the standards (at room temperature, 20 °C) and sample iterations 1 and 2 of the heat-treated samples at 40 °C. We will elaborate on the first two sets of table values (Table 8(A & B) and Figure 67) with the rest being similar. The lightness index  $L^*$  of the black dye/binder coated glass substrate (Table 8A) shows the value of 47.827, however, these samples, heat-treated at 40 °C, turned white and show an increase in the  $L^*$  (70.689) value with an average difference,  $dL^*=22.862$ . Similarly, for this sample, the  $dE^*$  value shows a positive difference of 23.061 indicating a clear color change of these heat-treated samples. Examining Table 8B, the blue dye/binder system at room temperature exhibits a blue color and, upon heating to 40 °C, becomes white with a change in color coordinates as obtained from the CIE LAB instrument (Figure 67B). In this particular case, the lightness index of the blue dye/binder system is 45.151, whereas, in the heat-treated white sample counterpart the difference in lightness index is found to be  $dL^*=25.444$  with  $dE^*=46.820$ . Tables 8D, 2E and 2E show similar patterns of increasing lightness index values due to the fact that these composite materials are either encapsulated or in a multilayer

configuration that encloses the black or blue dye particles in the core. For Table 8C, without dye incorporation, the TiO<sub>2</sub> ad-mixed with the sodium silicate binder shows positive values of  $dL^*=36.414$  and  $dE^*=37.578$  because of the interaction of TiO<sub>2</sub> particles with the binder increasing the whiteness. Moreover, the opacity is enhanced as inferred from the UV-Vis spectra discussed above.

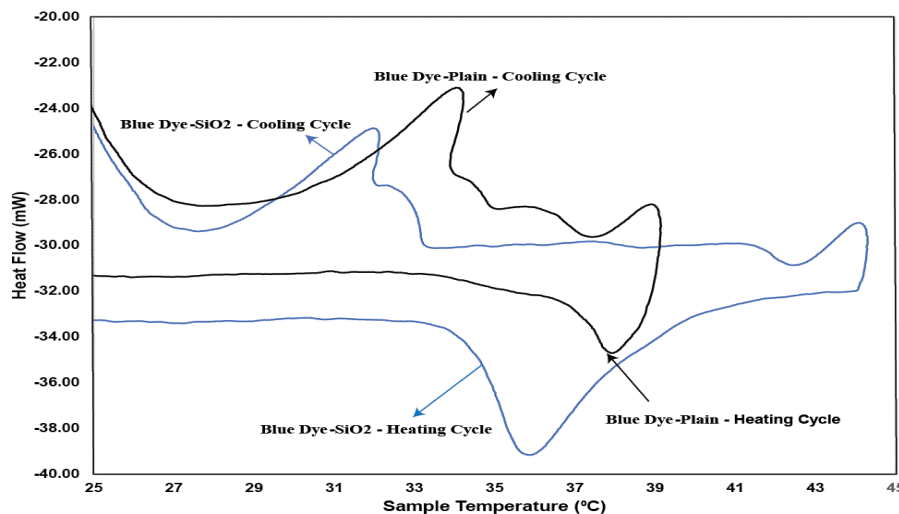


Figure 68: DSC Profiles of Plain Blue Dye and SiO<sub>2</sub> Encapsulated Blue Dye in Both Heating and Cooling Cycles Exhibit Thermal Storage Characteristics While Changing its Color from Blue to White and Vice-Versa.

The thermal storage characteristics of the candidate dye particles and their encapsulated metal oxide counterparts were systematically examined using differential scanning calorimetry at ambient pressure and a ramping temperature rate of 1 °C/min from room temperature to at least up to 45 °C in a dynamic scanning mode. Figure 68 shows the DSC profiles of the three component plain blue dye system synthesized in the laboratory and the silicon dioxide encapsulated blue dye particles. The amount of SiO<sub>2</sub> is controlled to obtain uniform encapsulation for subsequent characterization procedures. The plain blue dye particles exhibit an endothermic transition at around 38 °C where the color changes from blue to white, whereas in the cooling cycle, the blue dye is reconstructed by regaining its color and, hence, the exothermic

transition appears indicating complete reversibility of the thermochromic transition. In the case of the SiO<sub>2</sub> encapsulated blue dye particles, a similar endothermic transition was observed 2 °C earlier (36 °C) and this transition appears wider when compared to the pristine blue dye. The cooling curve of the SiO<sub>2</sub> encapsulated blue dye shows an earlier exothermic transition around 31 °C and reversibility is observed in this system as well. However, due to the low thermal conductivity of the silica system, the encapsulation of the dye by silica would favor relatively high thermal storage. The heat flow observed in this process for both pristine and encapsulated blue dye are approximately from -10.35 to -14.10 mW°C.

## Chapter 5: Conclusions and Recommendations for Future Work

### 5.1 Conclusions

Several strategies must be used for the improvement of TCM properties to make them more effective. Several processes have been developed for the synthesis and microencapsulation of TCMs in recent years, but further investigation is required to overcome the limitations of the methods in the pursuit of making them more efficient by increasing their stability and durability, particularly from photodegradation and thermal degradation. In addition, the application areas may be increased in the near future by tuning the properties of thermochromic materials. A sound understanding of nanotechnology, nanoengineering, colloidal science, polymer chemistry, and process engineering would play an important role in the improvement of all these processes leading to the improvement of the performance of TCMs for future applications.

Various experiments have been addressed in this dissertation. The first part was a three-component thermochromic blue dye was successfully synthesized by in-situ polycondensation and was encapsulated by PMMA. The results strongly suggest that the blue dye not only can be used as a thermochromic material, but also, by utilizing the latent heat absorbed during the color change transition, as a thermal storage material. The encapsulated TCM material was extensively characterized and its latent heat, at the transition temperature, determined by using differential scanning calorimetry (DSC). In the second part of this chapter, the *n*-eicosane phase change material (PCM) was microencapsulated by TiO<sub>2</sub>. The microencapsulated PCM was synthesized by a sol-gel TiO<sub>2</sub> based precursor used for the TiO<sub>2</sub> shell formation, with TBT being the starting

material of the sol-gel precursor. The encapsulated particles were characterized to understand the core-shell features and, by DSC measurements, evaluate the thermal and heat energy storage properties of the material. The third part is microencapsulation, characterization and testing of commercially available black thermochromic dyes (transition temperature) by  $\text{TiO}_2$  by individual surfactant were used successfully to construct a titanium oxide shell. These off-the-shelf thermochromic materials involve Leuco dye particles that demonstrate color change (black to white) behavior at the low transition temperature of about  $32.50\text{ }^\circ\text{C}$ . the final part, were six types of thin films fabricated and their UV-Vis spectral responses were studied in terms of absorbance, percent transmission, and percent reflectance with incident wavelengths ranging from 200 to 800 nm at room temperature and heat-treated at  $40.0\text{ }^\circ\text{C}$ . The absorption spectra show distinct features for the plain black and blue dyes.

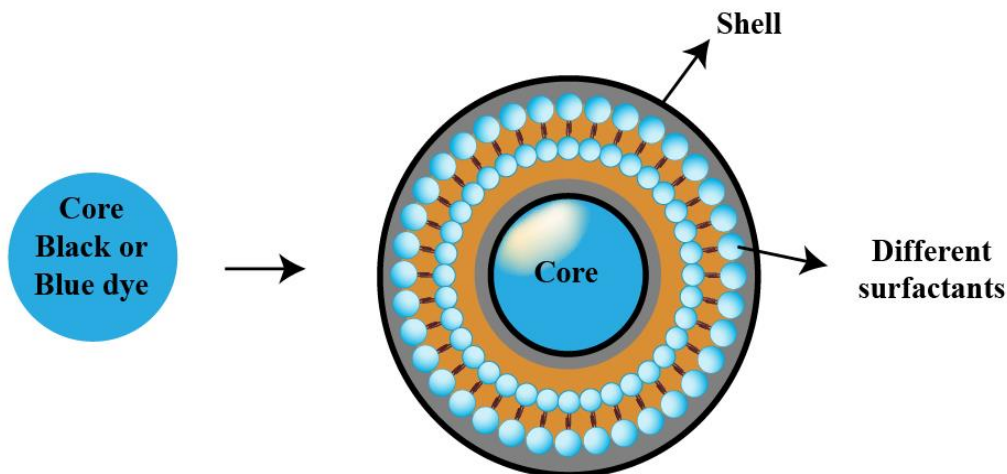


Figure 69: Different Surfactants Beside TCM@ $\text{TiO}_2$ .

## 5.2 Recommendations for Future Work

To continue work for the thermochromic microcapsules development, further research and study are needed to comprehend the behavior of the chemical components (i.e., surfactants and shell types). It is important to control the thickness of microcapsules with several kinds of

components as long as the shell thickness is uniform overall. There is an ample scope of research to find new solutions for how to control the shell of TiO<sub>2</sub>. Also, the different surfactants, such as PEG 1000, SDS, and PEG 200, can be successfully utilized between the core and shell. The suggested solutions are listed below for both black and blue dyes as shown in Figure 69.

### 5.3 Abbreviation

- TCM's - Thermochromic Materials
- HOMO – Highest Occupied Molecular Orbital
- LUMO – Lowest Occupied Molecular Orbital
- LCAO - Linar Combination of Atomic Orbitals
- CN – Coordination Number
- ITCM - Inorganic Thermochromic Material
- OTCM - Organic Thermochromic Material
- CVL – Crystal Violet Lactone
- UV- Ultraviolet
- XRD – X-ray Diffraction
- FESEM – Field Emission Scanning Electron Microscope
- SEE-C – Continuous supercritical emulsion extraction
- CTPCM - Composite thermochromic and phase-change materials
- TLD – Thermochromic leuco dye
- PVD – Physical Vapor Deposition
- PLD – Pulsed Laser Deposition
- CVD – Chemical Vapor Deposition

## References

- [1] J. Cleland, "World population growth; past, present and future," *Environmental and Resource Economics*, vol. 55, no. 4, pp. 543-554, 2013.
- [2] B. Güneralp *et al.*, "Global scenarios of urban density and its impacts on building energy use through 2050," *Proceedings of the National Academy of Sciences*, vol. 114, no. 34, pp. 8945-8950, 2017.
- [3] D. Urge-Vorsatz *et al.*, "Energy end-use: buildings," in *Global Energy Assessment-Toward a Sustainable Future*: Cambridge University Press, 2012.
- [4] Y. Y. Smolin, K. K. Lau, and M. Soroush, "First-principles modeling for optimal design, operation, and integration of energy conversion and storage systems," *AIChE Journal*, vol. 65, no. 7, p. e16482, 2019.
- [5] U. Desideri and F. Asdrubali, *Handbook of energy efficiency in buildings: a life cycle approach*. Butterworth-Heinemann, 2018.
- [6] P. S. Aklujkar and B. Kandasubramanian, "A review of microencapsulated thermochromic coatings for sustainable building applications," *Journal of Coatings Technology and Research*, vol. 18, no. 1, pp. 19-37, 2021.
- [7] M. Aburas, V. Soebarto, T. Williamson, R. Liang, H. Ebendorff-Heidepriem, and Y. Wu, "Thermochromic smart window technologies for building application: A review," *Applied Energy*, vol. 255, p. 113522, 2019.
- [8] B. Liu, A. Rasines Mazo, P. A. Gurr, and G. G. Qiao, "Reversible nontoxic thermochromic microcapsules," *ACS applied materials & interfaces*, vol. 12, no. 8, pp. 9782-9789, 2020.
- [9] O. Panák, M. Držková, R. Svoboda, and M. K. Gunde, "Combined colorimetric and thermal analyses of reversible thermochromic composites using crystal violet lactone as a colour former," *Journal of Thermal Analysis and Calorimetry*, vol. 127, no. 1, pp. 633-640, 2017.
- [10] D. C. MacLaren and M. A. White, "Dye-developer interactions in the crystal violet lactone-lauryl gallate binary system: implications for thermochromism," *Journal of Materials Chemistry*, vol. 13, no. 7, pp. 1695-1700, 2003.
- [11] W. Ibrahim, "An investigation into textile applications of thermochromic pigments," Heriot-Watt University, 2012.
- [12] J. C. Crano, R. J. Guglielmetti, and R. Guglielmetti, "Organic photochromic and thermochromic compounds: volume 2: physicochemical studies, biological applications, and thermochromism," 1999.
- [13] M. A. Chowdhury, B. S. Butola, and M. Joshi, "Application of thermochromic colorants on textiles: temperature dependence of colorimetric properties," *Coloration Technology*, vol. 129, no. 3, pp. 232-237, 2013.

- [14] S. M. Burkinshaw, J. Griffiths, and A. D. Towns, "Reversibly thermochromic systems based on pH-sensitive functional dyes," *Journal of materials chemistry*, vol. 8, no. 12, pp. 2677-2683, 1998.
- [15] J. Luthern and A. Peredes, "Determination of the stoichiometry of a thermochromic color complex via Job's method," *Journal of materials science letters*, vol. 19, no. 3, pp. 185-188, 2000.
- [16] A. Seeboth, D. Löttsch, E. Potechius, and R. Vetter, "Thermochromic effects of leuco dyes studied in polypropylene," *Chinese journal of polymer science*, vol. 24, no. 04, pp. 363-368, 2006.
- [17] I. Malherbe, R. D. Sanderson, and E. Smit, "Reversibly thermochromic micro-fibres by coaxial electrospinning," *Polymer*, vol. 51, no. 22, pp. 5037-5043, 2010.
- [18] Z. Liu, F. Bao, and F. Fu, "Study of manufacturing thermochromic wood," *Wood and fiber science*, vol. 43, no. 3, pp. 239-243, 2011.
- [19] A. N. Bourque and M. A. White, "Control of thermochromic behaviour in crystal violet lactone (CVL)/alkyl gallate/alcohol ternary mixtures," *Canadian Journal of Chemistry*, vol. 93, no. 1, pp. 22-31, 2015.
- [20] D. MacLaren and M. A. White, "Design rules for reversible thermochromic mixtures," *Journal of materials science*, vol. 40, no. 3, pp. 669-676, 2005.
- [21] F. Li, Y. Zhao, S. Wang, D. Han, L. Jiang, and Y. Song, "Thermochromic core-shell nanofibers fabricated by melt coaxial electrospinning," *Journal of Applied Polymer Science*, vol. 112, no. 1, pp. 269-274, 2009/04/05 2009, doi: 10.1002/app.29384.
- [22] H. Tang, D. C. MacLaren, and M. A. White, "New insights concerning the mechanism of reversible thermochromic mixtures," *Canadian Journal of Chemistry*, vol. 88, no. 11, pp. 1063-1070, 2010.
- [23] K. Bašneć, M. Hajžeri, and M. K. Gunde, "Thermal and colour properties of leuco dye-based thermochromic composite with dodecanol solvent," *Journal of Thermal Analysis and Calorimetry*, vol. 127, no. 1, pp. 55-61, 2017.
- [24] O. Panák, N. Hauptman, M. Klanjšek Gunde, and M. Kaplanová, "Colorimetric characterization of thermochromic composites with different molar ratios of components," *J Print Media Technol Res*, vol. 1, no. 2, pp. 113-20, 2012.
- [25] F. Azizian, A. J. Field, B. M. Heron, and C. Kilner, "Intrinsically thermochromic fluorans," *Chemical Communications*, vol. 48, no. 5, pp. 750-752, 2012.
- [26] F. Azizian, A. J. Field, and B. M. Heron, "Reductive alkylation of aminofluorans: A simple route to intrinsically thermochromic fluorans," *Dyes and Pigments*, vol. 99, no. 2, pp. 432-439, 2013.
- [27] E. A. Kandirmaz, A. Ozcan, and D. E. Ulusoy, "Production of thermochromic microcapsulated inks for smart packaging and examination of printability properties," *Pigment & Resin Technology*, 2020.
- [28] A. Nawade, K. Ramya, and S. Mukhopadhyay, "Design of thermochromic materials and coatings for cool building applications," in *Energy Saving Coating Materials*: Elsevier, 2020, pp. 197-226.
- [29] G. Pérez, V. R. Allegro, M. Corroto, A. Pons, and A. Guerrero, "Smart reversible thermochromic mortar for improvement of energy efficiency in buildings," *Construction and Building Materials*, vol. 186, pp. 884-891, 2018.

- [30] X. Zhu, Y. Liu, Z. Li, and W. Wang, "Thermochromic microcapsules with highly transparent shells obtained through in-situ polymerization of urea formaldehyde around thermochromic cores for smart wood coatings," *Scientific reports*, vol. 8, no. 1, pp. 1-10, 2018.
- [31] M. Fan and F. Fu, *Advanced high strength natural fibre composites in construction*. Woodhead Publishing, 2016.
- [32] R. Muthyala, *Chemistry and applications of leuco dyes*. Springer Science & Business Media, 2006.
- [33] G. Jorgenson, "Thermochromic materials and devices inorganic systems," in *Large-Area Chromogenics: Materials and Devices for Transmittance Control*, 1990, vol. 10304: International Society for Optics and Photonics, p. 1030408.
- [34] R. Kulčar, M. Friškovec, N. Hauptman, A. Vesel, and M. K. Gunde, "Colorimetric properties of reversible thermochromic printing inks," *Dyes and pigments*, vol. 86, no. 3, pp. 271-277, 2010.
- [35] W. Zhang, X. Ji, C. Zeng, K. Chen, Y. Yin, and C. Wang, "A new approach for the preparation of durable and reversible color changing polyester fabrics using thermochromic leuco dye-loaded silica nanocapsules," *Journal of Materials Chemistry C*, 10.1039/C7TC02077E vol. 5, no. 32, pp. 8169-8178, 2017, doi: 10.1039/C7TC02077E.
- [36] C. Yu, Y. Zhang, D. Cheng, X. Li, Y. Huang, and J. A. Rogers, "All-Elastomeric, Strain-Responsive Thermochromic Color Indicators," *Small*, vol. 10, no. 7, pp. 1266-1271, 2014/04/01 2014, doi: 10.1002/sml.201302646.
- [37] A. Seeboth, D. Löttsch, R. Ruhmann, and O. Muehling, "Thermochromic Polymers—Function by Design," *Chemical Reviews*, vol. 114, no. 5, pp. 3037-3068, 2014/03/12 2014, doi: 10.1021/cr400462e.
- [38] Q. M. Zhou *et al.*, "Dual Emissions and Thermochromic Luminescence Behavior of Chloroplumbate Organic–Inorganic Hybrid Crystals," *European Journal of Inorganic Chemistry*, vol. 2018, no. 33, pp. 3748-3756, 2018.
- [39] J. H. Day, "Thermochromism," *Chemical Reviews*, vol. 63, no. 1, pp. 65-80, 1963.
- [40] J. H. Day, "Thermochromism of inorganic compounds," *Chemical Reviews*, vol. 68, no. 6, pp. 649-657, 1968.
- [41] A. Hakami *et al.*, "Microencapsulation of Thermochromic Material by Silicon Oxide Nanoparticles," in *Key Engineering Materials*, 2021, vol. 878: Trans Tech Publ, pp. 41-48.
- [42] K. Nassau. "Physical And Chemical Causes Of Colour." Encyclopædia Britannica, inc. <https://www.britannica.com/science/color> (accessed 07 Oct, 2020).
- [43] G. Mastrotheodoros, K. Beltsios, and N. Zacharias, "Assessment of the production of antiquity pigments through experimental treatment of ochres and other iron based precursors," *Mediterranean Archaeology and Archaeometry*, vol. 10, no. 1, pp. 37-59, 2010.
- [44] F. Rahman, "Zinc oxide light-emitting diodes: a review," *Optical Engineering*, vol. 58, no. 1, p. 010901, 2019. [Online]. Available: <https://doi.org/10.1117/1.OE.58.1.010901>.
- [45] A. Ahmad, "Phase transition study in a [Cu<sub>2</sub>HgI<sub>4</sub>·xAgI] mixed composite system," *Bulletin of Materials Science*, vol. 33, no. 4, pp. 419-425, 2010.

- [46] R. D. Willett, J. A. Haugen, J. Lebsack, and J. Morrey, "Thermochromism in copper(II) chlorides. Coordination geometry changes in tetrachlorocuprate(2-)anions," *Inorganic Chemistry*, vol. 13, no. 10, pp. 2510-2513, 1974/10/01 1974, doi: 10.1021/ic50140a040.
- [47] Y. Tapuhi, O. Kalisky, and I. Agranat, "Thermochromism and thermal E,Z isomerizations in bianthrones," *The Journal of Organic Chemistry*, vol. 44, no. 12, pp. 1949-1952, 1979/06/01 1979, doi: 10.1021/jo01326a012.
- [48] V. K. Seiler, N. Tumanov, K. Robeyns, J. Wouters, B. Champagne, and T. Leyssens, "A Structural Analysis of Spiropyran and Spirooxazine Compounds and Their Polymorphs," *Crystals*, vol. 7, no. 3, p. 84, 2017, doi: 10.3390/cryst7030084.
- [49] H. Xia, K. Xie, and G. Zou, "Advances in Spiropyrans/Spirooxazines and Applications Based on Fluorescence Resonance Energy Transfer (FRET) with Fluorescent Materials," (in eng), *Molecules*, vol. 22, no. 12, p. 2236, 2017, doi: 10.3390/molecules22122236.
- [50] I. Sage, "Thermochromic liquid crystals," *Liquid crystals*, vol. 38, no. 11-12, pp. 1551-1561, 2011.
- [51] A. N. Bourque and W. M. Anne, "Control of thermochromic behaviour in crystal violet lactone (CVL)/alkyl gallate/alcohol ternary mixtures," *Canadian Journal of Chemistry*, vol. 93, no. 1, pp. 22-31, 2014, doi: 10.1139/cjc-2014-0251.
- [52] C. G. Granqvist, "Transparent conductors as solar energy materials: A panoramic review," *Solar Energy Materials and Solar Cells*, vol. 91, no. 17, pp. 1529-1598, 2007/10/15/ 2007, doi: <https://doi.org/10.1016/j.solmat.2007.04.031>.
- [53] S.-Y. Li, G. A. Niklasson, and C. G. Granqvist, "Nanothermochromics with VO<sub>2</sub>-based core-shell structures: Calculated luminous and solar optical properties," *Journal of Applied Physics*, vol. 109, no. 11, p. 113515, 2011, doi: 10.1063/1.3592350.
- [54] A. Raditoiu, V. Raditoiu, C. A. Nicolae, M. F. Raduly, V. Amariutei, and L. E. Wagner, "Optical and structural dynamical behavior of Crystal Violet Lactone – Phenolphthalein binary thermochromic systems," *Dyes and Pigments*, vol. 134, pp. 69-76, 2016/11/01/ 2016, doi: <https://doi.org/10.1016/j.dyepig.2016.06.046>.
- [55] A. Seeboth, R. Ruhmann, and O. Mühlhling, "Thermotropic and Thermochromic Polymer Based Materials for Adaptive Solar Control," (in eng), *Materials (Basel)*, vol. 3, no. 12, pp. 5143-5168, 2010, doi: 10.3390/ma3125143.
- [56] S. Mehta, A. Kushwaha, R. R. Kisannagar, and D. Gupta, "Fabrication of a reversible thermochromism based temperature sensor using an organic–inorganic composite system," *Rsc Advances*, vol. 10, no. 36, pp. 21270-21276, 2020.
- [57] J. Yang and D. Sweeney, "Infrared holography using the thermochromic material Cu<sub>2</sub>HgI<sub>4</sub>," *Applied optics*, vol. 18, no. 14, pp. 2398-2406, 1979.
- [58] D. K. Nguyen, H. Lee, and I.-T. Kim, "Synthesis and Thermochromic properties of Cr-doped Al<sub>2</sub>O<sub>3</sub> for a reversible thermochromic sensor," *Materials*, vol. 10, no. 5, p. 476, 2017.
- [59] Y. Ji, A. Mattsson, G. A. Niklasson, C. G. Granqvist, and L. Österlund, "Synergistic TiO<sub>2</sub>/VO<sub>2</sub> window coating with thermochromism, enhanced luminous transmittance, and photocatalytic activity," *Joule*, vol. 3, no. 10, pp. 2457-2471, 2019.
- [60] C.-Y. Kim, T. Slusar, J. Cho, and H.-T. Kim, "Mott Switching and Structural Transition in the Metal Phase of VO<sub>2</sub> Nanodomain," *ACS Applied Electronic Materials*.

- [61] F. Xu, X. Cao, H. Luo, and P. Jin, "Recent advances in VO<sub>2</sub>-based thermochromic composites for smart windows," *Journal of Materials Chemistry C*, vol. 6, no. 8, pp. 1903-1919, 2018.
- [62] C. Batista and V. Teixeira, "VO<sub>2</sub>-Based Thermochromic Thin Films for Energy Efficient Windows."
- [63] W. S. Xi *et al.*, "Cytotoxicity of vanadium oxide nanoparticles and titanium dioxide-coated vanadium oxide nanoparticles to human lung cells," *Journal of Applied Toxicology*, vol. 40, no. 5, pp. 567-577, 2020.
- [64] D. Wu *et al.*, "Toxicity assessment and mechanistic investigation of engineered monoclinic VO<sub>2</sub> nanoparticles," *Nanoscale*, vol. 10, no. 20, pp. 9736-9746, 2018.
- [65] S. A. Ahmed, R. M. Okasha, K. S. Khairou, T. H. Afifi, A.-A. H. Mohamed, and A. S. Abd-El-Aziz, "Design of Thermochromic Polynorbornene Bearing Spiropyran Chromophore Moieties: Synthesis, Thermal Behavior and Dielectric Barrier Discharge Plasma Treatment," (in eng), *Polymers (Basel)*, vol. 9, no. 11, p. 630, 2017, doi: 10.3390/polym9110630.
- [66] O. Panák, M. Držková, M. Kaplanová, U. Novak, and M. Klanjšek Gunde, "The relation between colour and structural changes in thermochromic systems comprising crystal violet lactone, bisphenol A, and tetradecanol," *Dyes and Pigments*, vol. 136, pp. 382-389, 2017/01/01/ 2017, doi: <https://doi.org/10.1016/j.dyepig.2016.08.050>.
- [67] C. F. Zhu and A. B. Wu, "Studies on the synthesis and thermochromic properties of crystal violet lactone and its reversible thermochromic complexes," *Thermochimica Acta*, vol. 425, no. 1, pp. 7-12, 2005/01/20/ 2005, doi: <https://doi.org/10.1016/j.tca.2003.08.001>.
- [68] R. Gavara, C. A. T. Laia, A. J. Parola, and F. Pina, "Formation of a leuco Spirolactone from 4-(2-Carboxyphenyl)-7-diethylamino-4'-dimethylamino-1-benzopyrylium: Design of a Phase-Change Thermochromic System Based on a Flavylum Dye," *Chemistry – A European Journal*, vol. 16, no. 26, pp. 7760-7766, 2010, doi: 10.1002/chem.200903482.
- [69] I. J. Kim, R. Manivannan, and Y. A. Son, "Thermally Reversible Fluorans: Synthesis, Thermochromic Properties and Real Time Application," (in eng), *Journal of nanoscience and nanotechnology*, vol. 18, no. 5, pp. 3299-3305, May 1 2017, doi: 10.1166/jnn.2018.14705.
- [70] M. R. di Nunzio, P. L. Gentili, A. Romani, and G. Favaro, "Photochromism and Thermochromism of some Spirooxazines and Naphthopyrans in the Solid State and in Polymeric Film," *The Journal of Physical Chemistry C*, vol. 114, no. 13, pp. 6123-6131, 2010/04/08 2010, doi: 10.1021/jp9109833.
- [71] L. Kortekaas and W. R. Browne, "The evolution of spiropyran: fundamentals and progress of an extraordinarily versatile photochrome," *Chemical Society Reviews*, 10.1039/C9CS00203K vol. 48, no. 12, pp. 3406-3424, 2019, doi: 10.1039/C9CS00203K.
- [72] K. Li *et al.*, "Crystal Violet Lactone Salicylaldehyde Hydrazone Zn(II) Complex: a Reversible Photochromic Material both in Solution and in Solid Matrix," *Scientific Reports*, vol. 5, no. 1, p. 14467, 2015/09/28 2015, doi: 10.1038/srep14467.
- [73] D. Tipikin, "Mechanochromism of organic compounds by the example of spiropyran," vol. 75, pp. 1876-1880, 01/01 2001.

- [74] F. M. Raymo and S. Giordani, "Signal Processing at the Molecular Level," *Journal of the American Chemical Society*, vol. 123, no. 19, pp. 4651-4652, 2001/05/01 2001, doi: 10.1021/ja005699n.
- [75] V. I. Minkin, "Photo-, Thermo-, Solvato-, and Electrochromic Spiroheterocyclic Compounds," *Chemical Reviews*, vol. 104, no. 5, pp. 2751-2776, 2004/05/01 2004, doi: 10.1021/cr020088u.
- [76] J. T. C. Wojtyk *et al.*, "Elucidating the Mechanisms of Acidochromic Spiropyran-Merocyanine Interconversion," *The Journal of Physical Chemistry A*, vol. 111, no. 13, pp. 2511-2516, 2007/04/01 2007, doi: 10.1021/jp068575r.
- [77] T. Mizutani, H. Takagi, Y. Ueno, T. Horiguchi, K. Yamamura, and H. Ogoshi, "Hydrogen-bonding-based thermochromic phenol-amine complexes," *Journal of physical organic chemistry*, vol. 11, no. 10, pp. 737-742, 1998.
- [78] A. Seeboth and D. Löttsch. "Thermochromic phenomena in polymers." Smithers Rapra. <http://www.books24x7.com/marc.asp?bookid=28292> (accessed).
- [79] H. Yu, Z. Wei, Y. Hao, Z. Liang, Z. Fu, and H. Cai, "Reversible solid-state thermochromism of a 2D organic-inorganic hybrid perovskite structure based on iodoplumbate and 2-aminomethyl-pyridine," *New Journal of Chemistry*, vol. 41, no. 18, pp. 9586-9589, 2017.
- [80] S. Ke, M. Li, W. Rao, Z. Wei, and H. Cai, "A square-pyramidal coordinated copper (ii) hydrazine dimeric complex showing reversible phase transition, dielectric anomaly and thermochromism," *New Journal of Chemistry*, vol. 44, no. 48, pp. 21288-21292, 2020.
- [81] J. C. Liu *et al.*, "A molecular thermochromic ferroelectric," *Angewandte Chemie*, vol. 132, no. 9, pp. 3523-3527, 2020.
- [82] M. Mączka, M. Ptak, A. Gağor, D. Stefańska, and A. Sieradzki, "Layered lead iodide of [Methylhydrazinium] 2PbI<sub>4</sub> with a reduced band gap: thermochromic luminescence and switchable dielectric properties triggered by structural phase transitions," *Chemistry of Materials*, vol. 31, no. 20, pp. 8563-8575, 2019.
- [83] J. W. Goodby, "Chirality in liquid crystals," *Journal of Materials Chemistry*, 10.1039/JM9910100307 vol. 1, no. 3, pp. 307-318, 1991, doi: 10.1039/JM9910100307.
- [84] H. Finkelmann and G. Rehage, "Investigations on liquid crystalline polysiloxanes, 2. Optical properties of cholesteric phases and influence of the flexible spacer on the mobility of the mesogenic groups," *Die Makromolekulare Chemie, Rapid Communications*, vol. 1, no. 12, pp. 733-740, 1980/12/05 1980, doi: 10.1002/marc.1980.030011206.
- [85] T.-A. Yamagishi and P. Sixou, "Preparation and characteristics of cholesteric gel from pentyl ether of hydroxypropyl cellulose," *Polymer*, vol. 36, no. 11, pp. 2315-2317, 1995/01/01/ 1995, doi: [https://doi.org/10.1016/0032-3861\(95\)95313-P](https://doi.org/10.1016/0032-3861(95)95313-P).
- [86] R. A. M. Hikmet and R. Polesso, "Patterned Multicolor Switchable Cholesteric Liquid Crystal Gels," *Advanced Materials*, vol. 14, no. 7, pp. 502-504, 2002/04/04 2002, doi: 10.1002/1521-4095(20020404)14:7<502::AID-ADMA502>3.0.CO;2-G.
- [87] H. Park, J. S. Lee, H. Choi, D. J. Ahn, and J. M. Kim, "Rational Design of Supramolecular Conjugated Polymers Displaying Unusual Colorimetric Stability upon Thermal Stress," *Advanced Functional Materials*, vol. 17, no. 17, pp. 3447-3455, 2007/11/23 2007, doi: 10.1002/adfm.200700242.

- [88] J. W. Y. Lam, J. Luo, Y. Dong, K. K. L. Cheuk, and B. Z. Tang, "Functional Polyacetylenes: Synthesis, Thermal Stability, Liquid Crystallinity, and Light Emission of Polypropiolates," *Macromolecules*, vol. 35, no. 22, pp. 8288-8299, 2002/10/01 2002, doi: 10.1021/ma021011a.
- [89] J. W. Y. Lam and B. Z. Tang, "Functional Polyacetylenes," *Accounts of Chemical Research*, vol. 38, no. 9, pp. 745-754, 2005/09/01 2005, doi: 10.1021/ar040012f.
- [90] X. Chen and J. Yoon, "A thermally reversible temperature sensor based on polydiacetylene: Synthesis and thermochromic properties," *Dyes and Pigments*, vol. 89, no. 3, pp. 194-198, 2011/06/01/ 2011, doi: <https://doi.org/10.1016/j.dyepig.2009.12.015>.
- [91] H. Wang, S. Han, Y. Hu, Z. Qi, and C. Hu, "Polydiacetylene-based periodic mesoporous organosilicas with colorimetric reversibility under multiple stimuli," *Colloids and Surfaces A: Physicochemical and Engineering Aspects*, vol. 517, pp. 84-95, 2017/03/20/ 2017, doi: <https://doi.org/10.1016/j.colsurfa.2017.01.006>.
- [92] R. D. Miller *et al.*, "The solution and solid-state thermochromism of unsymmetrically substituted polysilanes," *Journal of Inorganic and Organometallic Polymers*, vol. 1, no. 4, pp. 505-530, 1991/12/01 1991, doi: 10.1007/BF00683514.
- [93] T. Sanji, K. Sakamoto, H. Sakurai, and K. Ono, "A Statistical Model for the Cooperative Thermochromic Transition of Polysilanes," *Macromolecules*, vol. 32, no. 11, pp. 3788-3794, 1999/06/01 1999, doi: 10.1021/ma981466t.
- [94] B. Lucht, W. Euler, and O. Gregory, "Investigation of the thermochromic properties of polythiophenes in host polymers," *Polym. Prep.*, vol. 43, no. 1, pp. 59-60, 01/01 2002.
- [95] X. Zhao, "Synthesis, characterization and structure dependence of thermochromism of polythiophene derivatives," *Journal of Materials Science*, vol. 40, no. 13, pp. 3423-3428, 2005/07/01 2005, doi: 10.1007/s10853-005-2849-z.
- [96] J. M. Leger, A. L. Holt, and S. A. Carter, "Reversible thermochromic effects in poly(phenylene vinylene)-based polymers," *Applied Physics Letters*, vol. 88, no. 11, p. 111901, 2006, doi: 10.1063/1.2183360.
- [97] C.-C. Wang *et al.*, "Thermochromism of a Poly(phenylene vinylene): Untangling the Roles of Polymer Aggregate and Chain Conformation," *The Journal of Physical Chemistry B*, vol. 113, no. 50, pp. 16110-16117, 2009/12/17 2009, doi: 10.1021/jp906645d.
- [98] P. Naumov, N. Ishizawa, J. Wang, L. Pejov, M. Pumera, and S. C. Lee, "On the Origin of the Solid-State Thermochromism and Thermal Fatigue of Polycyclic Overcrowded Enes," *The Journal of Physical Chemistry A*, vol. 115, no. 30, pp. 8563-8570, 2011/08/04 2011, doi: 10.1021/jp2040339.
- [99] D. C. MacLaren and M. A. White, "Design rules for reversible thermochromic mixtures," *Journal of Materials Science*, vol. 40, no. 3, pp. 669-676, 2005/02/01 2005, doi: 10.1007/s10853-005-6305-x.
- [100] P. S. Aklujkar and B. Kandasubramanian, "A review of microencapsulated thermochromic coatings for sustainable building applications," *Journal of Coatings Technology and Research*, pp. 1-19, 2020.
- [101] S. Ohkawa, F. Yang, K. Kawabata, and H. Goto, "Synthesis of polymers from chiral monomers in chiral liquid crystals," *Journal of Applied Polymer Science*, vol. 128, no. 6, pp. 3586-3591, 2013/06/15 2013, doi: 10.1002/app.38561.

- [102] H.-B. Duan, S.-S. Yu, S.-X. Liu, and H. Zhang, "An inorganic–organic hybrid crystal with a two-step dielectric response and thermochromic luminescence," *Dalton Transactions*, 10.1039/C6DT03691K vol. 46, no. 7, pp. 2220-2227, 2017, doi: 10.1039/C6DT03691K.
- [103] N. Traiphol, N. Rungruangviriyaya, R. Potai, and R. Traiphol, "Stable polydiacetylene/ZnO nanocomposites with two-steps reversible and irreversible thermochromism: The influence of strong surface anchoring," *Journal of Colloid and Interface Science*, vol. 356, no. 2, pp. 481-489, 2011/04/15/ 2011, doi: <https://doi.org/10.1016/j.jcis.2011.01.028>.
- [104] A. Chanakul, N. Traiphol, and R. Traiphol, "Controlling the reversible thermochromism of polydiacetylene/zinc oxide nanocomposites by varying alkyl chain length," *Journal of Colloid and Interface Science*, vol. 389, no. 1, pp. 106-114, 2013/01/01/ 2013, doi: <https://doi.org/10.1016/j.jcis.2012.08.066>.
- [105] S. Gadžurić, M. Vraneš, and S. Dožić, "Thermochromic cobalt(II) chloro-complexes in different media: Possible application for auto-regulated solar protection," *Solar Energy Materials and Solar Cells*, vol. 105, pp. 309-316, 2012/10/01/ 2012, doi: <https://doi.org/10.1016/j.solmat.2012.06.035>.
- [106] T. Yokoyama, A. Masuhara, T. Onodera, H. Kasai, and H. Oikawa, "Development of fabrication process for Ag/polydiacetylene (core/shell) hybridized nanocrystals," *Synthetic Metals*, vol. 159, no. 9, pp. 897-899, 2009/05/01/ 2009, doi: <https://doi.org/10.1016/j.synthmet.2009.01.058>.
- [107] A. K. Vishwakarma, R. Kumari, P. S. Ghalsasi, and N. Arulsamy, "Crystal structure, thermochromic and magnetic properties of organic-inorganic hybrid compound: (C<sub>7</sub>H<sub>7</sub>N<sub>2</sub>S)<sub>2</sub>CuCl<sub>4</sub>," *Journal of Molecular Structure*, vol. 1141, pp. 93-98, 2017/08/05/ 2017, doi: <https://doi.org/10.1016/j.molstruc.2017.03.076>.
- [108] Q.-M. Zhou *et al.*, "Dual Emissions and Thermochromic Luminescence Behavior of Chloroplumbate Organic–Inorganic Hybrid Crystals," *European Journal of Inorganic Chemistry*, vol. 2018, no. 33, pp. 3748-3756, 2018/09/09 2018, doi: 10.1002/ejic.201800606.
- [109] S. Usseglio, A. Damin, D. Scarano, S. Bordiga, A. Zecchina, and C. Lamberti, "(I<sub>2</sub>)<sub>n</sub> Encapsulation inside TiO<sub>2</sub>: A Way To Tune Photoactivity in the Visible Region," *Journal of the American Chemical Society*, vol. 129, no. 10, pp. 2822-2828, 2007/03/01 2007, doi: 10.1021/ja066083m.
- [110] S. Nagamine and E. Sasaoka, "Synthesis of Nanostructured Titania Templated by Anionic Surfactant in Acidic Conditions," *Journal of Porous Materials*, vol. 9, no. 3, pp. 167-173, 2002/10/01 2002, doi: 10.1023/A:1020966016542.
- [111] A. Zielińska *et al.*, "Silver-doped TiO<sub>2</sub> prepared by microemulsion method: Surface properties, bio- and photoactivity," *Separation and Purification Technology*, vol. 72, no. 3, pp. 309-318, 2010/05/11/ 2010, doi: <https://doi.org/10.1016/j.seppur.2010.03.002>.
- [112] X. Li, W. Zheng, G. He, R. Zhao, and D. Liu, "Morphology Control of TiO<sub>2</sub> Nanoparticle in Microemulsion and Its Photocatalytic Property," *ACS Sustainable Chemistry & Engineering*, vol. 2, no. 2, pp. 288-295, 2014/02/03 2014, doi: 10.1021/sc400328u.

- [113] H. Arami, M. Mazloumi, R. Khalifehzadeh, and S. K. Sadrnezhad, "Sonochemical preparation of TiO<sub>2</sub> nanoparticles," *Materials Letters*, vol. 61, no. 23, pp. 4559-4561, 2007/09/01/ 2007, doi: <https://doi.org/10.1016/j.matlet.2007.02.051>.
- [114] J. Guo *et al.*, "Sonochemical synthesis of TiO<sub>2</sub> nanoparticles on graphene for use as photocatalyst," *Ultrasonics Sonochemistry*, vol. 18, no. 5, pp. 1082-1090, 2011/09/01/ 2011, doi: <https://doi.org/10.1016/j.ultsonch.2011.03.021>.
- [115] J. Yang, H. Peterlik, M. Lomoschitz, and U. Schubert, "Preparation of mesoporous titania by surfactant-assisted sol-gel processing of acetaldoxime-modified titanium alkoxides," *Journal of Non-Crystalline Solids*, vol. 356, no. 25, pp. 1217-1227, 2010/06/01/ 2010, doi: <https://doi.org/10.1016/j.jnoncrysol.2010.04.035>.
- [116] D. P. Macwan, P. N. Dave, and S. Chaturvedi, "A review on nano-TiO<sub>2</sub> sol-gel type syntheses and its applications," *Journal of Materials Science*, vol. 46, no. 11, pp. 3669-3686, 2011/06/01 2011, doi: 10.1007/s10853-011-5378-y.
- [117] Z. Zhao *et al.*, "Surfactant-assisted solvo- or hydrothermal fabrication and characterization of high-surface-area porous calcium carbonate with multiple morphologies," *Microporous and Mesoporous Materials*, vol. 138, no. 1, pp. 191-199, 2011/02/01/ 2011, doi: <https://doi.org/10.1016/j.micromeso.2010.09.006>.
- [118] R. Gao, Z. Jiao, Y. Wang, L. Xu, S. Xia, and H. Zhang, "Eco-friendly synthesis of rutile TiO<sub>2</sub> nanostructures with controlled morphology for efficient lithium-ion batteries," *Chemical Engineering Journal*, vol. 304, pp. 156-164, 2016/11/15/ 2016, doi: <https://doi.org/10.1016/j.cej.2016.06.051>.
- [119] L. Yang *et al.*, "Functionalizing slag wool fibers with photocatalytic activity by anatase TiO<sub>2</sub> and CTAB modification," *Ceramics International*, vol. 44, no. 6, pp. 5842-5847, 2018/04/15/ 2018, doi: <https://doi.org/10.1016/j.ceramint.2017.11.036>.
- [120] L.-y. Chai, Y.-f. Yu, G. Zhang, B. Peng, and S.-w. Wei, "Effect of surfactants on preparation of nanometer TiO<sub>2</sub> by pyrohydrolysis," *Transactions of Nonferrous Metals Society of China*, vol. 17, no. 1, pp. 176-180, 2007/01/01/ 2007, doi: [https://doi.org/10.1016/S1003-6326\(07\)60068-5](https://doi.org/10.1016/S1003-6326(07)60068-5).
- [121] C. Saiwan, S. Krathong, T. Anukulprasert, rsquo, and I. I. I. E. A. rear, "Nano-Titanium Dioxide Synthesis in AOT Microemulsion System with Salinity Scan," *JOURNAL OF CHEMICAL ENGINEERING OF JAPAN*, vol. 37, no. 2, pp. 279-285, 2004, doi: 10.1252/jcej.37.279.
- [122] A. Mitra, A. Bhaumik, and B. K. Paul, "Synthesis and characterization of mesoporous titanium dioxide using self-assembly of sodium dodecyl sulfate and benzyl alcohol systems as templates," *Microporous and Mesoporous Materials*, vol. 109, no. 1, pp. 66-72, 2008/03/01/ 2008, doi: <https://doi.org/10.1016/j.micromeso.2007.04.052>.
- [123] W. Lekphet *et al.*, "Morphology control studies of TiO<sub>2</sub> microstructures via surfactant-assisted hydrothermal process for dye-sensitized solar cell applications," *Applied Surface Science*, vol. 382, pp. 15-26, 2016/09/30/ 2016, doi: <https://doi.org/10.1016/j.apsusc.2016.04.115>.
- [124] J. Zhang *et al.*, "One-step synthesis of rutile nano-TiO<sub>2</sub> with exposed {111} facets for high photocatalytic activity," *Journal of Alloys and Compounds*, vol. 632, pp. 133-139, 2015/05/25/ 2015, doi: <https://doi.org/10.1016/j.jallcom.2015.01.170>.

- [125] J. Yuenyongsuwan, N. Nithiyakorn, P. Sabkird, E. A. O'Rear, and T. Pongprayoon, "Surfactant effect on phase-controlled synthesis and photocatalyst property of TiO<sub>2</sub> nanoparticles," *Materials Chemistry and Physics*, vol. 214, pp. 330-336, 2018/08/01/ 2018, doi: <https://doi.org/10.1016/j.matchemphys.2018.04.111>.
- [126] G. Peng, R. Du, Q. Peng, S. Wu, and C. Yu, "A surfactant free method for rutile TiO<sub>2</sub> microspheres-graphene oxide composite and its photocatalytic performance," *Materials Chemistry and Physics*, vol. 214, pp. 34-40, 2018/08/01/ 2018, doi: <https://doi.org/10.1016/j.matchemphys.2018.04.092>.
- [127] S. Meng, J. Mansouri, Y. Ye, and V. Chen, "Effect of templating agents on the properties and membrane distillation performance of TiO<sub>2</sub>-coated PVDF membranes," *Journal of Membrane Science*, vol. 450, pp. 48-59, 2014/01/15/ 2014, doi: <https://doi.org/10.1016/j.memsci.2013.08.036>.
- [128] C. Della-Casa, A. Fraleoni, P. Costa-Bizzarri, and M. Lanzi, "New 3-alkylthiophene copolymers functionalized with a NLO chromophore," *Synthetic Metals*, vol. 124, no. 2, pp. 467-470, 2001/10/22/ 2001, doi: [https://doi.org/10.1016/S0379-6779\(01\)00401-5](https://doi.org/10.1016/S0379-6779(01)00401-5).
- [129] V. C. Gonçalves, L. M. M. Costa, M. R. Cardoso, C. R. Mendonca, and D. T. Balogh, "Synthesis and characterization of copolymers of alkyl- and azo-thiophenes: Chromic properties and photoinduced birefringence," *Journal of Applied Polymer Science*, vol. 114, no. 2, pp. 680-687, 2009/10/15 2009, doi: 10.1002/app.30575.
- [130] E. G. Morales-Espinoza, E. Aguilar-Ortíz, A. Vázquez-Arce, E. Rodríguez-Alba, H. Vázquez-Torres, and E. Rivera, "Synthesis and characterization of novel luminescent polythiophenes containing pyrene units and oligo(ethylene glycol) spacers: Thermal and optical properties", *Synthetic Metals*, vol. 199, pp. 223-231, 2015/01/01/ 2015, doi: <https://doi.org/10.1016/j.synthmet.2014.11.038>.
- [131] E. G. Morales-Espinoza, J. Castellón-Urbe, M. Fuentes-Pérez, and M. E. Nicho, "Synthesis and characterization of thermochromic thiophene copolymers containing pyrene groups," *Materials Today Communications*, vol. 24, p. 101166, 2020/09/01/ 2020, doi: <https://doi.org/10.1016/j.mtcomm.2020.101166>.
- [132] A. Hakami, S. Indrakar, A. Krishnegowda, P. K. Biswas, E. Stefanakos, and S. Srinivasan, "Microencapsulation of the as-synthesized and off-the-shelf thermochromic dyes by nanosized SiO<sub>2</sub> thermal energy savings applications," *International Journal of Materials Science and Engineering*, 2020.
- [133] S. A. Kahani and F. Abdevali, "Mechanochemical synthesis and characterization of a nickel(ii) complex as a reversible thermochromic nanostructure," *RSC Advances*, 10.1039/C5RA22606F vol. 6, no. 6, pp. 5116-5122, 2016, doi: 10.1039/C5RA22606F.
- [134] O. Mapazi, P. K. Matabola, R. M. Moutloali, and C. J. Ngila, "A urea-modified polydiacetylene-based high temperature reversible thermochromic sensor: Characterisation and evaluation of properties as a function of temperature," *Sensors and Actuators B: Chemical*, vol. 252, pp. 671-679, 2017/11/01/ 2017, doi: <https://doi.org/10.1016/j.snb.2017.05.095>.
- [135] S. Zhu, Y. Chen, J. Sun, Y. Yang, and C. Yue, "Synthesis, Characterization, Thermochromism, and Photochromism of Aromatic Aldehyde Hydrazone Derivatives," *Journal of Chemistry*, vol. 2016, p. 8460462, 2016/08/18 2016, doi: 10.1155/2016/8460462.

- [136] L. Mehta, K. Wadgaonkar, M. Suryawanshi, and R. Jagtap, "Solvent-free microwave-assisted synthesis and characterization of polybenzoxazine as a thermochromic material for smart coatings," *Colloid and Polymer Science*, vol. 297, no. 5, pp. 795-798, 2019/05/01 2019, doi: 10.1007/s00396-019-04491-9.
- [137] G. Peng, G. Dou, Y. Hu, Y. Sun, and Z. Chen, "Phase Change Material (PCM) Microcapsules for Thermal Energy Storage," *Advances in Polymer Technology*, vol. 2020, p. 9490873, 2020/01/12 2020, doi: 10.1155/2020/9490873.
- [138] M. S. Tözüm, S. A. Aksoy, and C. Alkan, "Microencapsulation of Three-Component Thermochromic System for Reversible Color Change and Thermal Energy Storage," *Fibers and Polymers*, vol. 19, no. 3, pp. 660-669, 2018/03/01 2018, doi: 10.1007/s12221-018-7801-3.
- [139] X. Zhu, Y. Liu, Z. Li, and W. Wang, "Thermochromic microcapsules with highly transparent shells obtained through in-situ polymerization of urea formaldehyde around thermochromic cores for smart wood coatings," *Scientific Reports*, vol. 8, no. 1, p. 4015, 2018/03/05 2018, doi: 10.1038/s41598-018-22445-z.
- [140] M. M. Umair, Y. Zhang, K. Iqbal, S. Zhang, and B. Tang, "Novel strategies and supporting materials applied to shape-stabilize organic phase change materials for thermal energy storage—A review," *Applied Energy*, vol. 235, pp. 846-873, 2019/02/01/ 2019, doi: <https://doi.org/10.1016/j.apenergy.2018.11.017>.
- [141] R. Campardelli, G. Della Porta, V. Gomez, S. Irusta, E. Reverchon, and J. Santamaria, "Encapsulation of titanium dioxide nanoparticles in PLA microspheres using supercritical emulsion extraction to produce bactericidal nanocomposites," *Journal of Nanoparticle Research*, vol. 15, no. 10, p. 1987, 2013/09/15 2013, doi: 10.1007/s11051-013-1987-5.
- [142] B. Wu, L. Shi, Q. Zhang, and W.-J. Wang, "Microencapsulation of 1-hexadecanol as a phase change material with reversible thermochromic properties," *RSC Advances*, 10.1039/C7RA06764J vol. 7, no. 67, pp. 42129-42137, 2017, doi: 10.1039/C7RA06764J.
- [143] S. Wu, L. Yuan, A. Gu, Y. Zhang, and G. Liang, "Synthesis and characterization of novel epoxy resins-filled microcapsules with organic/inorganic hybrid shell for the self-healing of high performance resins," *Polymers for Advanced Technologies*, vol. 27, no. 12, pp. 1544-1556, 2016/12/01 2016, doi: 10.1002/pat.3829.
- [144] S. Yi, S. Sun, Y. Deng, and S. Feng, "Preparation of composite thermochromic and phase-change materials by the sol-gel method and its application in textiles," *The Journal of The Textile Institute*, vol. 106, no. 10, pp. 1071-1077, 2015/10/03 2015, doi: 10.1080/00405000.2014.965501.
- [145] A. Arshad, M. Jabbal, Y. Yan, and J. Darkwa, "The micro-/nano-PCMs for thermal energy storage systems: A state of art review," *International Journal of Energy Research*, vol. 43, no. 11, pp. 5572-5620, 2019/09/01 2019, doi: 10.1002/er.4550.
- [146] Y. Zhang, X. Wang, and D. Wu, "Design and fabrication of dual-functional microcapsules containing phase change material core and zirconium oxide shell with fluorescent characteristics," *Solar Energy Materials and Solar Cells*, vol. 133, pp. 56-68, 2015.
- [147] T. Chang *et al.*, "Mitigating Deterioration of Vanadium Dioxide Thermochromic Films by Interfacial Encapsulation," *Matter*, vol. 1, no. 3, pp. 734-744, 2019/09/04/ 2019, doi: <https://doi.org/10.1016/j.matt.2019.04.004>.

- [148] S. S. Latthe, S. Liu, C. Terashima, K. Nakata, and A. Fujishima, "Transparent, adherent, and photocatalytic SiO<sub>2</sub>-TiO<sub>2</sub> coatings on polycarbonate for self-cleaning applications," *Coatings*, vol. 4, no. 3, pp. 497-507, 2014.
- [149] M. Shahnooshi, A. Eshaghi, and A. A. Aghaei, "Transparent anti-fogging and anti-scratch SiO<sub>2</sub>/SiO<sub>2</sub>-TiO<sub>2</sub> thin film on polycarbonate substrate," *Materials Research Express*, vol. 6, no. 8, p. 086447, 2019.
- [150] T. Yuranova, R. Mosteo, J. Bandara, D. Laub, and J. Kiwi, "Self-cleaning cotton textiles surfaces modified by photoactive SiO<sub>2</sub>/TiO<sub>2</sub> coating," *Journal of Molecular Catalysis A: Chemical*, vol. 244, no. 1-2, pp. 160-167, 2006.
- [151] R. Palkovits *et al.*, "Polymerization of w/o Microemulsions for the Preparation of Transparent SiO<sub>2</sub>/PMMA Nanocomposites," *Langmuir*, vol. 21, no. 13, pp. 6048-6053, 2005/06/01 2005, doi: 10.1021/la050630k.
- [152] S. M. Khaled, R. Sui, P. A. Charpentier, and A. S. Rizkalla, "Synthesis of TiO<sub>2</sub>-PMMA Nanocomposite: Using Methacrylic Acid as a Coupling Agent," *Langmuir*, vol. 23, no. 7, pp. 3988-3995, 2007/03/01 2007, doi: 10.1021/la062879n.
- [153] Q. Yin *et al.*, "Fabrication and Performance of Composite Microencapsulated Phase Change Materials with Palmitic Acid Ethyl Ester as Core," *Polymers (Basel)*, vol. 10, no. 7, 2018, doi: 10.3390/polym10070726.
- [154] G. Alva, Y. Lin, L. Liu, and G. Fang, "Synthesis, characterization and applications of microencapsulated phase change materials in thermal energy storage: A review," *Energy and Buildings*, vol. 144, pp. 276-294, 2017/06/01/ 2017, doi: <https://doi.org/10.1016/j.enbuild.2017.03.063>.
- [155] M. N. A. Hawlader, M. S. Uddin, and M. M. Khin, "Microencapsulated PCM thermal-energy storage system," *Applied Energy*, vol. 74, no. 1, pp. 195-202, 2003/01/01/ 2003, doi: [https://doi.org/10.1016/S0306-2619\(02\)00146-0](https://doi.org/10.1016/S0306-2619(02)00146-0).
- [156] A. M. Borreguero, J. L. Valverde, J. F. Rodríguez, A. H. Barber, J. J. Cubillo, and M. Carmona, "Synthesis and characterization of microcapsules containing Rubitherm®RT27 obtained by spray drying," *Chemical Engineering Journal*, vol. 166, no. 1, pp. 384-390, 2011/01/01/ 2011, doi: <https://doi.org/10.1016/j.cej.2010.10.055>.
- [157] T. Y. Wang and J. Huang, "Synthesis and characterization of microencapsulated sodium phosphate dodecahydrate," *Journal of Applied Polymer Science*, vol. 130, no. 3, pp. 1516-1523, 2013/11/05 2013, doi: 10.1002/app.39249.
- [158] Y. Lin, C. Zhu, G. Alva, and G. Fang, "Microencapsulation and thermal properties of myristic acid with ethyl cellulose shell for thermal energy storage," *Applied Energy*, vol. 231, pp. 494-501, 2018.
- [159] V. Suganya and V. Anuradha, "Microencapsulation and Nanoencapsulation: A Review," *International Journal of Pharmaceutical and Clinical Research*, vol. 9, pp. 233-239 03/25 2017, doi: 10.25258/ijpcr.v9i3.8324.
- [160] A. Wiatrowski, A. Obstarczyk, M. Mazur, D. Kaczmarek, and D. Wojcieszak, "Characterization of HfO<sub>2</sub> Optical Coatings Deposited by MF Magnetron Sputtering," *Coatings*, vol. 9, no. 2, 2019, doi: 10.3390/coatings9020106.
- [161] X. Tang, W. Li, X. Zhang, and H. Shi, "Fabrication and characterization of microencapsulated phase change material with low supercooling for thermal energy storage," *Energy*, vol. 68, pp. 160-166, 2014/04/15/ 2014, doi: <https://doi.org/10.1016/j.energy.2014.03.002>.

- [162] H. Wang, J. Luo, Y. Yang, L. Zhao, G. Song, and G. Tang, "Fabrication and characterization of microcapsulated phase change materials with an additional function of thermochromic performance," *Solar Energy*, vol. 139, pp. 591-598, 2016.
- [163] X. Huang, C. Zhu, Y. Lin, and G. Fang, "Thermal properties and applications of microencapsulated PCM for thermal energy storage: A review," *Applied Thermal Engineering*, vol. 147, pp. 841-855, 2019/01/25/ 2019, doi: <https://doi.org/10.1016/j.applthermaleng.2018.11.007>.
- [164] Y. Ma, B. Zhu, and K. Wu, "Preparation of reversible thermochromic building coatings and their properties," *Journal of Coatings Technology*, vol. 72, no. 911, pp. 67-71, 2000.
- [165] M. Vasei, P. Das, H. Cherfouth, B. Marsan, and J. P. Claverie, "TiO<sub>2</sub>@C core-shell nanoparticles formed by polymeric nano-encapsulation," (in English), *Frontiers in Chemistry*, Original Research vol. 2, no. 47, 2014-July-11 2014, doi: 10.3389/fchem.2014.00047.
- [166] N. Falco, E. Reverchon, and G. Della Porta, "Continuous Supercritical Emulsions Extraction: Packed Tower Characterization and Application to Poly(lactic-co-glycolic Acid) + Insulin Microspheres Production," *Industrial & Engineering Chemistry Research*, vol. 51, no. 25, pp. 8616-8623, 2012/06/27 2012, doi: 10.1021/ie300482n.
- [167] J. T. McCann, M. Marquez, and Y. Xia, "Melt Coaxial Electrospinning: A Versatile Method for the Encapsulation of Solid Materials and Fabrication of Phase Change Nanofibers," *Nano Letters*, vol. 6, no. 12, pp. 2868-2872, 2006/12/01 2006, doi: 10.1021/nl0620839.
- [168] D. I. Braghirolli, D. Steffens, and P. Pranke, "Electrospinning for regenerative medicine: a review of the main topics," *Drug discovery today*, vol. 19, no. 6, pp. 743-753, 2014.
- [169] K. Sahebkar, S. Indrakar, S. Srinivasan, S. Thomas, and a. E. K. Stefanakos, "Electrospun Microfibers with Embedded Leuco Dye-Based Thermochromic Material for Textile Applications," *Journal of Industrial Textiles*, October, 06, 2020 2020.
- [170] J. Hu and X. B. Yu, "Adaptive thermochromic roof system: Assessment of performance under different climates," *Energy and Buildings*, vol. 192, pp. 1-14, 2019.
- [171] P. Kiri, G. Hyett, and R. Binions, "Solid State Thermochromic Materials," *Advanced Materials Letters*, vol. 1, pp. 86-105, 09/01 2010, doi: 10.5185/amlett.2010.8147.
- [172] J. K. Kana *et al.*, "Thermochromic VO<sub>2</sub> thin films synthesized by rf-inverted cylindrical magnetron sputtering," *Applied Surface Science*, vol. 254, no. 13, pp. 3959-3963, 2008.
- [173] M. G. Krishna, Y. Debaugé, and A. Bhattacharya, "X-ray photoelectron spectroscopy and spectral transmittance study of stoichiometry in sputtered vanadium oxide films," *Thin solid films*, vol. 312, no. 1-2, pp. 116-122, 1998.
- [174] G. Jorgenson and J. Lee, "Doped vanadium oxide for optical switching films," *Solar Energy Materials*, vol. 14, no. 3-5, pp. 205-214, 1986.
- [175] K. Wasa, M. Kitabatake, and H. Adachi, *Thin film materials technology: sputtering of control compound materials*. Springer Science & Business Media, 2004.
- [176] M. Borek, F. Qian, V. Nagabushnam, and R. K. Singh, "Pulsed laser deposition of oriented VO<sub>2</sub> thin films on R-cut sapphire substrates," *Applied Physics Letters*, vol. 63, no. 24, pp. 3288-3290, 1993, doi: 10.1063/1.110177.
- [177] D. H. Kim and H. S. Kwok, "Pulsed laser deposition of VO<sub>2</sub> thin films," *Applied Physics Letters*, vol. 65, no. 25, pp. 3188-3190, 1994/12/19 1994, doi: 10.1063/1.112476.

- [178] S. Lu, L. Hou, and F. Gan, "Preparation and optical properties of phase-change VO<sub>2</sub> thin films," *Journal of Materials Science*, vol. 28, no. 8, pp. 2169-2177, 1993/04/01 1993, doi: 10.1007/BF00367579.
- [179] S. B. Bhaduri, *The Physics And Chemistry Of Sol-Gel Processing edited by C.J. Brinker and G.W. Scherer* San Diego, CA: Academic Press, Inc, 1990.
- [180] C. B. Greenberg, "Undoped and doped VO<sub>2</sub> films grown from VO(OC<sub>3</sub>H<sub>7</sub>)<sub>3</sub>," *Thin Solid Films*, vol. 110, no. 1, pp. 73-82, 1983/12/02/ 1983, doi: [https://doi.org/10.1016/0040-6090\(83\)90175-X](https://doi.org/10.1016/0040-6090(83)90175-X).
- [181] Y. Takahashi, M. Kanamori, H. Hashimoto, Y. Moritani, and Y. Masuda, "Preparation of VO<sub>2</sub> films by organometallic chemical vapour deposition and dip-coating," *Journal of Materials Science*, vol. 24, no. 1, pp. 192-198, 1989/01/01 1989, doi: 10.1007/BF00660953.
- [182] D. Barreca *et al.*, "Highly Oriented V<sub>2</sub>O<sub>5</sub> Nanocrystalline Thin Films by Plasma-Enhanced Chemical Vapor Deposition," *Chemistry of Materials*, vol. 12, no. 1, pp. 98-103, 2000/01/01 2000, doi: 10.1021/cm991095a.
- [183] P. Martin, "Deposition technologies: an overview," *Handbook of deposition technologies for films and coatings*, vol. 3, 2010.
- [184] D. M. Mattox, *Handbook of physical vapor deposition (PVD) processing*. William Andrew, 2010.
- [185] T. J. Jackson and S. B. Palmer, "Oxide superconductor and magnetic metal thin film deposition by pulsed laser ablation: a review," *Journal of Physics D: Applied Physics*, vol. 27, no. 8, pp. 1581-1594, 1994/08/14 1994, doi: 10.1088/0022-3727/27/8/001.
- [186] S. S. Kanu and R. Binions, "Thin films for solar control applications," *Proceedings of the Royal Society A: Mathematical, Physical and Engineering Sciences*, vol. 466, no. 2113, pp. 19-44, 2010/01/08 2010, doi: 10.1098/rspa.2009.0259.
- [187] R. Binions, C. Carmalt, and I. Parkin, "A comparison of the gas sensing properties of solid state metal oxide semiconductor gas sensors produced by atmospheric pressure chemical vapour deposition and screen printing," *Measurement Science and Technology*, vol. 18, p. 190, 11/30 2007, doi: 10.1088/0957-0233/18/1/024.
- [188] K. L. Choy, "Chemical vapour deposition of coatings," *Progress in Materials Science*, vol. 48, no. 2, pp. 57-170, 2003/01/01/ 2003, doi: [https://doi.org/10.1016/S0079-6425\(01\)00009-3](https://doi.org/10.1016/S0079-6425(01)00009-3).
- [189] J. Pospsil and S. Nespurek, "Photostabilization of coatings. Mechanisms and performance," *Progress in Polymer Science*, vol. 25, pp. 1261-1335 11/01 2000, doi: 10.1016/S0079-6700(00)00029-0.
- [190] C. Fabiani, A. Pisello, E. Bou-Zeid, J. Yang, and F. Cotana, "Adaptive measures for mitigating urban heat islands: The potential of thermochromic materials to control roofing energy balance," *Applied Energy*, vol. 247, pp. 155-170, 2019.
- [191] G. Pérez, C. Mota-Heredia, J. Sánchez-García, and A. Guerrero, "Compatibility between thermochromic pigments and Portland cement-based materials," *Construction and Building Materials*, vol. 251, p. 119038, 2020.
- [192] J. F. Rabek, *Photodegradation of Polymers: Physical Characteristics and Applications*. Springer Berlin Heidelberg, 1996.

- [193] H. B. Olayan, H. S. Hami, and E. D. Owen, "Photochemical and Thermal Crosslinking of Polymers," *Journal of Macromolecular Science, Part C*, vol. 36, no. 4, pp. 671-719, 1996/11/01 1996, doi: 10.1080/15321799608014858.
- [194] N. S. Allen and J. F. McKellar, *Photochemistry of Dyed and Pigmented Polymers*. Applied Science Publishers, 1980.
- [195] J. G. Williams, "Polymeric Materials Encyclopedia Edited by Joseph C. Salamone. CRC Press: Boca Raton, FL. 1996. ISBN 0-8493-2470-X," *Journal of the American Chemical Society*, vol. 120, no. 27, pp. 6848-6849, 1998/06/13 1998, doi: 10.1021/ja985901a.
- [196] J. J. Florio and D. J. Miller, *Handbook Of Coating Additives*. Taylor & Francis, 2004.
- [197] M. A. Villetti, J. S. Crespo, M. S. Soldi, A. T. N. Pires, R. Borsali, and V. Soldi, "Thermal Degradation of Natural Polymers," *Journal of Thermal Analysis and Calorimetry*, vol. 67, no. 2, pp. 295-303, 2002/02/01 2002, doi: 10.1023/A:1013902510952.
- [198] K. Li, Y. Xu, Y. Liu, M. M. Mohideen, H. He, and S. Ramakrishna, "Dissipative particle dynamics simulations of centrifugal melt electrospinning," *Journal of Materials Science*, vol. 54, no. 13, pp. 9958-9968, 2019.
- [199] C. G. Granqvist, "Electrochromics and Thermo-chromics: Towards a New Paradigm for Energy Efficient Buildings," *Materials Today: Proceedings*, vol. 3, pp. S2-S11, 2016/01/01/ 2016, doi: <https://doi.org/10.1016/j.matpr.2016.01.002>.
- [200] C. G. Granqvist, "Recent progress in thermo-chromics and electrochromics: A brief survey," *Thin Solid Films*, vol. 614, pp. 90-96, 2016/09/01/ 2016, doi: <https://doi.org/10.1016/j.tsf.2016.02.029>.
- [201] T.-C. Chang, X. Cao, S.-H. Bao, S.-D. Ji, H.-J. Luo, and P. Jin, "Review on thermo-chromic vanadium dioxide based smart coatings: from lab to commercial application," *Advances in Manufacturing*, vol. 6, no. 1, pp. 1-19, 2018/03/01 2018, doi: 10.1007/s40436-017-0209-2.
- [202] J. Hu and X. B. Yu, "Adaptive building roof by coupling thermo-chromic material and phase change material: Energy performance under different climate conditions," *Construction and Building Materials*, vol. 262, p. 120481, 2020.
- [203] N. M. Rao, "BIOMEDICAL APPLICATION OF THERMOCHROMIC LIQUID CRYSTALS AND LEUCO DYES FOR TEMPERATURE MONITORING IN THE EXTREMITIES," Kent State University, 2016.
- [204] S. J. Woltman, G. D. Jay, and G. P. Crawford, "Liquid-crystal materials find a new order in biomedical applications," *Nature Materials*, vol. 6, no. 12, pp. 929-938, 2007/12/01 2007, doi: 10.1038/nmat2010.
- [205] R. Kambarami, O. Chidede, and N. Pereira, "ThermoSpot in the detection of neonatal hypothermia," (in eng), *Annals of tropical paediatrics*, vol. 22, no. 3, pp. 219-23, Sep 2002, doi: 10.1179/027249302125001516.
- [206] T. B. Mole, N. Kennedy, N. Ndoya, and A. Emond, "ThermoSpots to detect hypothermia in children with severe acute malnutrition," (in eng), *PLoS One*, vol. 7, no. 9, pp. e45823-e45823, 2012, doi: 10.1371/journal.pone.0045823.
- [207] L. Ćurković, D. Ljubas, S. Šegota, and I. Bačić, "Photocatalytic degradation of Lissamine Green B dye by using nanostructured sol-gel TiO<sub>2</sub> films," *Journal of Alloys and Compounds*, vol. 604, pp. 309-316, 2014/08/15/ 2014, doi: <https://doi.org/10.1016/j.jallcom.2014.03.148>.

- [208] L. Szatmáry, J. Šubrt, V. Kalousek, J. Mosinger, and K. Lang, "Low-temperature deposition of anatase on nanofiber materials for photocatalytic NO<sub>x</sub> removal," *Catalysis Today*, vol. 230, pp. 74-78, 2014/07/01/ 2014, doi: <https://doi.org/10.1016/j.cattod.2013.09.023>.
- [209] S. Sakthivel, B. Neppolian, M. V. Shankar, B. Arabindoo, M. Palanichamy, and V. Murugesan, "Solar photocatalytic degradation of azo dye: comparison of photocatalytic efficiency of ZnO and TiO<sub>2</sub>," *Solar Energy Materials and Solar Cells*, vol. 77, no. 1, pp. 65-82, 2003/04/30/ 2003, doi: [https://doi.org/10.1016/S0927-0248\(02\)00255-6](https://doi.org/10.1016/S0927-0248(02)00255-6).
- [210] S. Gong, X. Cheng, Y. Li, X. Wang, Y. Wang, and H. Zhong, "Effect of nano-SiC on thermal properties of expanded graphite/1-octadecanol composite materials for thermal energy storage," *Powder Technology*, vol. 367, pp. 32-39, 2020.
- [211] S. Alay Aksoy, C. Alkan, M. S. Tözüm, S. Demirbağ, R. Altun Anayurt, and Y. Ulcay, "Preparation and textile application of poly (methyl methacrylate-co-methacrylic acid)/n-octadecane and n-eicosane microcapsules," *The Journal of the Textile Institute*, vol. 108, no. 1, pp. 30-41, 2017.
- [212] C. Alkan, S. A. Aksoy, and R. A. Anayurt, "Synthesis of poly (methyl methacrylate-co-acrylic acid)/n-eicosane microcapsules for thermal comfort in textiles," *Textile Research Journal*, vol. 85, no. 19, pp. 2051-2058, 2015.
- [213] K. Takaoka, S. Maeda, H. Miura, K. Endo, and D. P. Chong, "Theoretical valence XPS and UV-visible absorption spectra of four leuco dyes using MO calculations," *Bulletin of the Chemical Society of Japan*, vol. 71, no. 4, pp. 807-816, 1998.
- [214] N. Stirbescu *et al.*, "BANANA FLOWER NECTAR-MEDIATED SYNTHESIS OF SILVER NANOPARTICLES," *Bulletin of the Transilvania University of Brasov. Engineering Sciences. Series I*, vol. 12, no. 2, pp. 55-64, 2019.
- [215] P. I. Nagy, "Competing intramolecular vs. intermolecular hydrogen bonds in solution," *International journal of molecular sciences*, vol. 15, no. 11, pp. 19562-19633, 2014.
- [216] H. Yang, F. Chen, Y. Jiao, and J. Zhang, "Investigation of phase transitions for the hydrothermal formation of TiO<sub>2</sub> in the presence of F<sup>-</sup> ions," *Chemical engineering journal*, vol. 214, pp. 229-236, 2013.
- [217] Q. Tay, X. Liu, Y. Tang, Z. Jiang, T. C. Sum, and Z. Chen, "Enhanced photocatalytic hydrogen production with synergistic two-phase anatase/brookite TiO<sub>2</sub> nanostructures," *The Journal of Physical Chemistry C*, vol. 117, no. 29, pp. 14973-14982, 2013.
- [218] O. Panák, M. Držková, and M. Kaplanová, "Insight into the evaluation of colour changes of leuco dye based thermochromic systems as a function of temperature," *Dyes and Pigments*, vol. 120, pp. 279-287, 2015.
- [219] J. Che, R. Li, and M. Senanayake, "A comparative study of the dependency of colour measurement on surface temperature," *Coloration Technology*, vol. 132, no. 2, pp. 144-152, 2016.
- [220] O. h. O. Brovarets' and D. M. Hovorun, "Conformational diversity of the quercetin molecule: A quantum-chemical view," *Journal of Biomolecular Structure and Dynamics*, vol. 38, no. 10, pp. 2817-2836, 2020.
- [221] O. Panák, M. Držková, M. Kaplanová, U. Novak, and M. K. Gunde, "The relation between colour and structural changes in thermochromic systems comprising crystal violet lactone, bisphenol A, and tetradecanol," *Dyes and Pigments*, vol. 136, pp. 382-389, 2017.

- [222] A. Watanabe, "The synthesis and the physical properties of normal higher primary alcohols. V. Thermal and X-ray studies of the polymorphism of alcohols of odd carbon numbers from undecanol to heptatriacontanol," *Bulletin of the Chemical Society of Japan*, vol. 36, no. 3, pp. 336-340, 1963.
- [223] S. Demirbağ and S. A. Aksoy, "Encapsulation of phase change materials by complex coacervation to improve thermal performances and flame retardant properties of the cotton fabrics," *Fibers and Polymers*, vol. 17, no. 3, pp. 408-417, 2016.
- [224] L. F. Cabeza, A. Castell, C. d. Barreneche, A. De Gracia, and A. Fernández, "Materials used as PCM in thermal energy storage in buildings: A review," *Renewable and Sustainable Energy Reviews*, vol. 15, no. 3, pp. 1675-1695, 2011.
- [225] D. Zhou, C.-Y. Zhao, and Y. Tian, "Review on thermal energy storage with phase change materials (PCMs) in building applications," *Applied energy*, vol. 92, pp. 593-605, 2012.
- [226] A. Sharma, V. V. Tyagi, C. Chen, and D. Buddhi, "Review on thermal energy storage with phase change materials and applications," *Renewable and Sustainable energy reviews*, vol. 13, no. 2, pp. 318-345, 2009.
- [227] A. M. Khudhair and M. M. Farid, "A review on energy conservation in building applications with thermal storage by latent heat using phase change materials," *Energy conversion and management*, vol. 45, no. 2, pp. 263-275, 2004.
- [228] K. Huang, J. Li, X. Luan, L. Liu, Z. Yang, and C. Wang, "Effect of Graphene Oxide on Phase Change Materials Based on Disodium Hydrogen Phosphate Dodecahydrate for Thermal Storage," *ACS omega*, vol. 5, no. 25, pp. 15210-15217, 2020.
- [229] C.-Y. Zhao and G. H. Zhang, "Review on microencapsulated phase change materials (MEPCMs): fabrication, characterization and applications," *Renewable and Sustainable Energy Reviews*, vol. 15, no. 8, pp. 3813-3832, 2011.
- [230] S. Himran, A. Suwono, and G. A. Mansoori, "Characterization of alkanes and paraffin waxes for application as phase change energy storage medium," *Energy sources*, vol. 16, no. 1, pp. 117-128, 1994.
- [231] S. Wu, T. Yan, Z. Kuai, and W. Pan, "Thermal conductivity enhancement on phase change materials for thermal energy storage: A review," *Energy Storage Materials*, vol. 25, pp. 251-295, 2020.
- [232] K. Cho and S. Choi, "Thermal characteristics of paraffin in a spherical capsule during freezing and melting processes," *International journal of heat and mass transfer*, vol. 43, no. 17, pp. 3183-3196, 2000.
- [233] A. Sarı, C. Alkan, and A. Karaipekli, "Preparation, characterization and thermal properties of PMMA/n-heptadecane microcapsules as novel solid-liquid microPCM for thermal energy storage," *Applied Energy*, vol. 87, no. 5, pp. 1529-1534, 2010.
- [234] M. Delgado, A. Lázaro, J. Mazo, and B. Zalba, "Review on phase change material emulsions and microencapsulated phase change material slurries: materials, heat transfer studies and applications," *Renewable and Sustainable Energy Reviews*, vol. 16, no. 1, pp. 253-273, 2012.
- [235] M. Romero-Cano and B. Vincent, "Controlled release of 4-nitroanisole from poly (lactic acid) nanoparticles," *Journal of controlled release*, vol. 82, no. 1, pp. 127-135, 2002.
- [236] Y. Zhu *et al.*, "Preparation and properties of nanoencapsulated n-octadecane phase change material with organosilica shell for thermal energy storage," *Energy conversion and Management*, vol. 105, pp. 908-917, 2015.

- [237] B. Tang, L. Wang, Y. Xu, J. Xiu, and S. Zhang, "Hexadecanol/phase change polyurethane composite as form-stable phase change material for thermal energy storage," *Solar Energy Materials and Solar Cells*, vol. 144, pp. 1-6, 2016.
- [238] F. Li, X. Wang, and D. Wu, "Fabrication of multifunctional microcapsules containing n-eicosane core and zinc oxide shell for low-temperature energy storage, photocatalysis, and antibiosis," *Energy Conversion and Management*, vol. 106, pp. 873-885, 2015.
- [239] P. Zhang, X. Xiao, and Z. Ma, "A review of the composite phase change materials: Fabrication, characterization, mathematical modeling and application to performance enhancement," *Applied Energy*, vol. 165, pp. 472-510, 2016.
- [240] S. Lashgari, H. Arabi, A. R. Mahdavian, and V. Ambrogi, "Thermal and morphological studies on novel PCM microcapsules containing n-hexadecane as the core in a flexible shell," *Applied Energy*, vol. 190, pp. 612-622, 2017.
- [241] D. Yin, L. Bai, Y. Jia, J. Liu, and Q. Zhang, "Microencapsulation through thermally sintering Pickering emulsion-based colloidosomes," *Soft matter*, vol. 13, no. 20, pp. 3720-3725, 2017.
- [242] M. Giarola *et al.*, "Vibrational dynamics of anatase TiO<sub>2</sub>: Polarized Raman spectroscopy and ab initio calculations," *Physical Review B*, vol. 81, no. 17, p. 174305, 2010.
- [243] C. Di Giambattista, R. Sanctuary, E. Perigo, and J. Baller, "Relaxations in the metastable rotator phase of n-eicosane," *The Journal of chemical physics*, vol. 143, no. 5, p. 054507, 2015.
- [244] L. Chai, X. Wang, and D. Wu, "Development of bifunctional microencapsulated phase change materials with crystalline titanium dioxide shell for latent-heat storage and photocatalytic effectiveness," *Applied Energy*, vol. 138, pp. 661-674, 2015.
- [245] A. R. Tehrani-Bagha and K. Holmberg, "Solubilization of hydrophobic dyes in surfactant solutions," *Materials*, vol. 6, no. 2, pp. 580-608, 2013.
- [246] J. Hanawalt, H. Rinn, and L. Frevel, "Chemical analysis by X-ray diffraction," *Industrial & Engineering Chemistry Analytical Edition*, vol. 10, no. 9, pp. 457-512, 1938.
- [247] K. Sahebkar, S. Indrakar, S. Srinivasan, S. Thomas, and E. Stefanakos, "Electrospun microfibers with embedded leuco dye-based thermochromic material for textile applications," *Journal of Industrial Textiles*, p. 1528083720987216, 2021.
- [248] A. Hakami, S. Srinivasan, H. Marildi, P. K. Biswas, S. L. Wallen, and E. K. Stefanakos, "Effects of multilayer thin film coatings on different thermochromic materials for thermal storage applications," in *Current Developments in Lens Design and Optical Engineering XXII*, 2021, vol. 11814: International Society for Optics and Photonics, p. 118140F.
- [249] S. Zheng, Y. Xu, Q. Shen, and H. Yang, "Preparation of thermochromic coatings and their energy saving analysis," *Solar Energy*, vol. 112, pp. 263-271, 2015.
- [250] A. A. Azemati, B. S. Hadavand, H. Hosseini, and A. S. Tajarrood, "Thermal modeling of mineral insulator in paints for energy saving," *Energy and Buildings*, vol. 56, pp. 109-114, 2013.
- [251] S. Özkayalar, E. Adıgüzel, S. A. Aksoy, and C. Alkan, "Reversible color-changing and thermal-energy storing nanocapsules of three-component thermochromic dyes," *Materials Chemistry and Physics*, vol. 252, p. 123162, 2020.
- [252] C. Alkan, A. Sarı, and A. Karaipekli, "Preparation, thermal properties and thermal reliability of microencapsulated n-eicosane as novel phase change material for thermal energy storage," *Energy Conversion and Management*, vol. 52, no. 1, pp. 687-692, 2011.

- [253] A. Dimoudi, S. Zoras, A. Kantzioura, X. Stogiannou, P. Kosmopoulos, and C. Pallas, "Use of cool materials and other bioclimatic interventions in outdoor places in order to mitigate the urban heat island in a medium size city in Greece," *Sustainable Cities and Society*, vol. 13, pp. 89-96, 2014.
- [254] A. J. Arnfield, "Two decades of urban climate research: a review of turbulence, exchanges of energy and water, and the urban heat island," *International Journal of Climatology: a Journal of the Royal Meteorological Society*, vol. 23, no. 1, pp. 1-26, 2003.
- [255] M. Santamouris, "Using cool pavements as a mitigation strategy to fight urban heat island—A review of the actual developments," *Renewable and Sustainable Energy Reviews*, vol. 26, pp. 224-240, 2013.
- [256] N. L. Alchapar, E. N. Correa, and M. A. Cantón, "Classification of building materials used in the urban envelopes according to their capacity for mitigation of the urban heat island in semiarid zones," *Energy and Buildings*, vol. 69, pp. 22-32, 2014.
- [257] R. Baetens, B. P. Jelle, and A. Gustavsen, "Properties, requirements and possibilities of smart windows for dynamic daylight and solar energy control in buildings: A state-of-the-art review," *Solar energy materials and solar cells*, vol. 94, no. 2, pp. 87-105, 2010.
- [258] M. Kolokotroni, B. Gowreesunker, and R. Giridharan, "Cool roof technology in London: An experimental and modelling study," *Energy and Buildings*, vol. 67, pp. 658-667, 2013.
- [259] G. M. Revel *et al.*, "Cool products for building envelope—Part II: Experimental and numerical evaluation of thermal performances," *Solar energy*, vol. 105, pp. 780-791, 2014.
- [260] A. Seeboth, R. Ruhmann, and O. Mühlhling, "Thermotropic and thermochromic polymer based materials for adaptive solar control," *Materials*, vol. 3, no. 12, pp. 5143-5168, 2010.
- [261] M. I. Khan, K. Azizli, S. Sufian, and Z. Man, "Sodium silicate-free geopolymers as coating materials: Effects of Na/Al and water/solid ratios on adhesion strength," *Ceramics International*, vol. 41, no. 2, pp. 2794-2805, 2015.

## Appendix A: Permissions, Copyright, and Acceptance Letter

The permission below is for the use of figure 1.



### PARTIES:

1. **Cambridge University Press** [CompanyNumber] (Licensor); and
2. **University of South Florida** (Licensee).

Thank you for your recent permission request. Some permission requests for use of material published by the Licensor, such as this one, are now being facilitated by PLSclear.

Set out in this licence cover sheet (the **Licence Cover Sheet**) are the principal terms under which Licensor has agreed to license certain Licensed Material (as defined below) to Licensee. The terms in this Licence Cover Sheet are subject to the attached General Terms and Conditions, which together with this Licence Cover Sheet constitute the licence agreement (the **Licence**) between Licensor and Licensee as regards the Licensed Material. The terms set out in this Licence Cover Sheet take precedence over any conflicting provision in the General Terms and Conditions.

### Free Of Charge Licence Terms

Licence Date: 23/09/2021  
PLSclear Ref No: 56085

### The Licensor

Company name: Cambridge University Press  
Address: University Printing House  
Shaftesbury Road  
Cambridge  
CB2 8BS  
GB

### The Licensee

Licensee Contact Name:  
Licensee Organisation Name:  
Licensee Address:

publisher: Cambridge University Press  
Are you requesting permission to reuse the cover of the publication? Yes

### For Use In Licensee's Publication(s)

usage type Book, Journal, Magazine or Academic Paper-Thesis / Dissertation  
Will your dissertation be placed in an online repository? No  
Author ABDULLATIF HAKAMI  
Estimated publication date 2022  
Language English  
Title of dissertation/thesis Microencapsulation of Thermochromic Materials for Thermal Storage and Energy Efficiency of Buildings  
University or institution University of South Florida  
Unlimited circulation? No

### Rights Granted

Exclusivity: Non-Exclusive  
Format: Thesis / Dissertation  
Language: English  
Territory: USA  
Duration: Lifetime of Licensee's Edition  
Maximum Circulation: 1

The permission below is for the use of figure 2.



This is a License Agreement between Abdullatif Hakami ("User") and Copyright Clearance Center, Inc. ("CCC") on behalf of the Rightsholder identified in the order details below. The license consists of the order details, the CCC Terms and Conditions below, and any Rightsholder Terms and Conditions which are included below.

All payments must be made in full to CCC in accordance with the CCC Terms and Conditions below.

Order Date	21-Sep-2021	Type of Use	Republish in a thesis/dissertation
Order License ID	1149192-1	Publisher	JOHN/WILEY & SONS, INC.
ISSN	0001-1541	Portion	Image/photo/illustration

#### LICENSED CONTENT

Publication Title	AIChE Journal	Rightsholder	John Wiley & Sons - Books
Article Title	First-principles modeling for optimal design, operation, and integration of energy conversion and storage systems	Publication Type	Journal
Author/Editor	AMERICAN INSTITUTE OF CHEMICAL ENGINEERS	Issue	7
Date	01/01/1955	Volume	65
Language	English	URL	<a href="http://onlinelibrary.wiley.com/journal/10...">http://onlinelibrary.wiley.com/journal/10...</a>
Country	United States of America		

#### REQUEST DETAILS

Portion Type	Image/photo/illustration	Distribution	United States
Number of images / photos / illustrations	5	Translation	Original language of publication
Format (select all that apply)	Electronic	Copies for the disabled?	No
Who will republish the content?	Academic institution	Minor editing privileges?	No
Duration of Use	Life of current and all future editions	Incidental promotional use?	No
Lifetime Unit Quantity	More than 2,000,000	Currency	USD
Rights Requested	Main product		

#### NEW WORK DETAILS

Title	Microencapsulation of Thermochromic Materials for Thermal Storage and Energy Efficiency of Buildings	Institution name	University of South Florida
Instructor name	Lee Stefanakos	Expected presentation date	2021-10-07

#### ADDITIONAL DETAILS

The requesting person / organization to appear on the license	Abdullatif Hakami
---	-------------------

The permission below is for the use of main product and figures 4,9,10,13,14 and 16.



This is a License Agreement between Abdullatif Hakami ("User") and Copyright Clearance Center, Inc. ("CCC") on behalf of the Rightsholder identified in the order details below. The license consists of the order details, the CCC Terms and Conditions below, and any Rightsholder Terms and Conditions which are included below.  
All payments must be made in full to CCC in accordance with the CCC Terms and Conditions below.

Order Date	03-Sep-2021	Type of Use	Republish in a thesis/dissertation
Order License ID	1145462-1	Publisher	Trans Tech Publications
ISSN	1662-9795	Portion	Chapter/article

#### LICENSED CONTENT

Publication Title	Key engineering materials	Publication Type	e-Journal
Article Title	Microencapsulation of Thermochromic Material by Silicon Oxide Nanoparticles	Start Page	41
		End Page	48
Date	01/01/1982	Volume	878
Language	English	URL	<a href="http://www.scientific.net/1013-9826/">http://www.scientific.net/1013-9826/</a>
Country	Switzerland		
Rightsholder	Trans Tech Publications, Ltd		

#### REQUEST DETAILS

Portion Type	Chapter/article	Rights Requested	Main product
Page range(s)	41 - 48	Distribution	United States
Total number of pages	8	Translation	Original language of publication
Format (select all that apply)	Electronic	Copies for the disabled?	No
Who will republish the content?	Academic institution	Minor editing privileges?	No
Duration of Use	Life of current and all future editions	Incidental promotional use?	No
Lifetime Unit Quantity	More than 2,000,000	Currency	USD

#### NEW WORK DETAILS

Title	Microencapsulation of Thermochromic Material by Silicon Oxide Nanoparticles	Institution name	University of South Florida
Instructor name	Elias Stefanakos	Expected presentation date	2021-10-11

#### ADDITIONAL DETAILS

Order reference number	N/A	The requesting person / organization to appear on the license	Abdullatif Hakami
------------------------	-----	---	-------------------

#### REUSE CONTENT DETAILS

Title, description or numeric reference of the portion(s)	Microencapsulation of Thermochromic Material by Silicon Oxide Nanoparticles	Title of the article/chapter the portion is from	Microencapsulation of Thermochromic Material by Silicon Oxide Nanoparticles
Editor of portion(s)	Hakami, Abdullatif; Indrakar, Sharan; Krishnegowda, Ashwini; Huang, Ming Yang; Sahebkar, Keon; Biswas, Prasanta Kumar; Stefanakos, Elias; Srinivasan, Sessa	Author of portion(s)	Hakami, Abdullatif; Indrakar, Sharan; Krishnegowda, Ashwini; Huang, Ming Yang; Sahebkar, Keon; Biswas, Prasanta Kumar; Stefanakos, Elias; Srinivasan, Sessa
Volume of serial or monograph	878	Issue, if republishing an article from a serial	N/A
Page or page range of portion	41-48	Publication date of portion	2021-03-01

The permission below is for the use of figure 20.



This is a License Agreement between Abdullatif Hakami /University of South Florida ("User") and Copyright Clearance Center, Inc. ("CCC") on behalf of the Rightsholder identified in the order details below. The license consists of the order details, the CCC Terms and Conditions below, and any Rightsholder Terms and Conditions which are included below. All payments must be made in full to CCC in accordance with the CCC Terms and Conditions below.

Order Date	09-Oct-2021	Type of Use	Republish in a thesis/dissertation
Order License ID	1153274-1	Publisher	ELSEVIER S.A.
ISSN	0378-7788	Portion	Image/photo/illustration

#### LICENSED CONTENT

Publication Title	Energy and buildings	Rightsholder	Elsevier Science & Technology Journals
Article Title	Adaptive thermochromic roof system: assessment of performance under different climates	Publication Type	Journal
Date	01/01/1977	Start Page	1
Language	English	End Page	14
Country	Switzerland	Volume	192

#### REQUEST DETAILS

Portion Type	Image/photo/illustration	Distribution	United States
Number of images / photos / illustrations	1	Translation	Original language of publication
Format (select all that apply)	Electronic	Copies for the disabled?	No
Who will republish the content?	Academic institution	Minor editing privileges?	No
Duration of Use	Life of current edition	Incidental promotional use?	No
Lifetime Unit Quantity	More than 2,000,000	Currency	USD
Rights Requested	Main product		

#### NEW WORK DETAILS

Title	Microencapsulation of Thermochromic Materials for Thermal Storage and Energy Efficiency of Buildings	Institution name	University of South Florida
Instructor name	Elias K. Stefanakos	Expected presentation date	2021-10-29

#### ADDITIONAL DETAILS

Order reference number	Fig.3	The requesting person / organization to appear on the license	Abdullatif Hakami /University of South Florida
------------------------	-------	---	--

#### REUSE CONTENT DETAILS

Title, description or numeric reference of the portion(s)	Microencapsulation of Thermochromic Materials for Thermal Storage and Energy Efficiency of Buildings	Title of the article/chapter the portion is from	Adaptive thermochromic roof system: assessment of performance under different climates
Editor of portion(s)	Yu, Xiong Bill; Hu, Jianying	Author of portion(s)	Yu, Xiong Bill; Hu, Jianying
Volume of serial or monograph	192	Issue, if republishing an article from a serial	N/A
Page or page range of portion	1-14	Publication date of portion	2019-06-01

The permission below is for the use of figure 22.



This is a License Agreement between Abdullatif Hakami / University of South Florida ("User") and Copyright Clearance Center, Inc. ("CCC") on behalf of the Rightsholder identified in the order details below. The license consists of the order details, the CCC Terms and Conditions below, and any Rightsholder Terms and Conditions which are included below. All payments must be made in full to CCC in accordance with the CCC Terms and Conditions below.

Order Date	09-Oct-2021	Type of Use	Republish in a thesis/dissertation
Order License ID	1153273-1	Publisher	ELSEVIER BV
ISSN	0950-0618	Portion	Image/photo/illustration

#### LICENSED CONTENT

Publication Title	Construction & building materials	Rightsholder	Elsevier Science & Technology Journals
Article Title	Adaptive building roof by coupling thermochromic material and phase change material: Energy performance under different climate conditions	Publication Type	Journal
		Start Page	120481
		Volume	262
Date	01/01/1987		
Language	English		
Country	Netherlands		

#### REQUEST DETAILS

Portion Type	Image/photo/illustration	Distribution	United States
Number of images / photos / illustrations	1	Translation	Original language of publication
Format (select all that apply)	Electronic	Copies for the disabled?	No
Who will republish the content?	Academic institution	Minor editing privileges?	No
Duration of Use	Life of current edition	Incidental promotional use?	No
Lifetime Unit Quantity	More than 2,000,000	Currency	USD
Rights Requested	Main product		

#### NEW WORK DETAILS

Title	Microencapsulation of Thermochromic Materials for Thermal Storage and Energy Efficiency of Buildings	Institution name	University of South Florida
Instructor name	Elias K. Stefanakos	Expected presentation date	2021-10-29

#### ADDITIONAL DETAILS

Order reference number	fig.4	The requesting person / organization to appear on the license	Abdullatif Hakami / University of South Florida
------------------------	-------	---	---

#### REUSE CONTENT DETAILS

Title, description or numeric reference of the portion(s)	Microencapsulation of Thermochromic Materials for Thermal Storage and Energy Efficiency of Buildings	Title of the article/chapter the portion is from	Adaptive building roof by coupling thermochromic material and phase change material: Energy performance under different climate conditions
Editor of portion(s)	Yu, Xiong (Bill); Hu, Jianying	Author of portion(s)	Yu, Xiong (Bill); Hu, Jianying
Volume of serial or monograph	262	Issue, if republishing an article from a serial	N/A
Page or page range of portion	120481	Publication date of portion	2020-11-30

The accepted letter below is for (Review on Thermo-chromic Materials: Development, Characterization and Applications) in chapter 2 and right now moved on to production.

**Date:** 22 Sep 2021  
**To:** "Elias Stefanakos" estefana@usf.edu  
**cc:** jctreditor@mlnichols.org  
**From:** "Journal of Coatings Technology and Research (JCTR)" hrogers@paint.org  
**Subject:** Decision on your manuscript JCTR-D-21-00165R2

---

Dear Dr. Stefanakos,

We are pleased to inform you that your manuscript, "Review on Thermo-chromic Materials: Development, Characterization and Applications", has been accepted for publication in

Journal of Coatings Technology and Research. You will be contacted by Springer Author Services in due course with a link to complete the grant of rights. Please note that you will receive your proofs after the publishing agreement has been received through the online system. Please remember to quote the manuscript number, JCTR-D-21-00165R2, whenever inquiring about your manuscript.

With best regards,

Mark Nichols, Ph.D.

Editor-in-Chief

Please note that this journal is a Transformative Journal (TJ). Authors may publish their research with us through the traditional subscription access route or make their paper immediately open access through payment of an article-processing charge (APC). Authors will not be required to make a final decision about access to their article until it has been accepted.

**Authors may need to take specific actions to achieve compliance with funder and institutional open access mandates.** If your research is supported by a funder that requires immediate open access (e.g. according to Plan S principles) then you should select the gold OA route, and we will direct you to the compliant route where possible. For authors selecting the subscription publication route our standard licensing terms will need to be accepted, including our self-archiving policies. Those standard licensing terms will supersede any other terms that the author or any third party may assert apply to any version of the manuscript.

The confirm letter below is for (Elsa – Elsevier as chapter of book) in chapter 3.

## Fw: 'Multifunctional Phase Change Materials. Fundamentals, Properties and Applications' Elsevier book



Faculty of Materials Science and Ceramics  
AGH University of Science and Technology  
Al. Mickiewicza 30, 30-059 Krakow, Poland  
tel. 48-12-6172239, e-mail: kingapie@agh.edu.pl

W dniu 2021-07-21 00:59, Sesa Srinivasan napisał(a):

Dear Professor Kinga Pielichowska,

We have signed to contribute for Chapter 5, Thermochromic and color switching phase change materials PCMs.

Can you please provide an idea how many pages is recommended for a book chapter? Does chapter should be comprehensive review or the current research results can be publishable. If you have any model template, please share it with me. I have received the Manuscript Writing Guidelines PDF file from Joshua Mearns.

Thank you very much.  
Sesa Srinivasan

**From:** Kinga Pielichowska <kingapie@agh.edu.pl>

**Sent:** Tuesday, October 5, 2021 4:22 AM

**To:** Sesa Srinivasan <ssrinivasan@floridapoly.edu>

**Subject:** Re: 'Multifunctional Phase Change Materials. Fundamentals, Properties and Applications' Elsevier book

Dear Dr. Srinivasan,  
thank you for submitting the chapter.  
Kind regards,  
Kinga Pielichowska

W dniu 2021-07-21 15:58, Sesa Srinivasan napisał(a):

Thank you so very much.

Best,

The permission below is for the use of the published paper entitled (Effects of Multilayer Thin Film Coatings on Different Thermochromic Materials for Thermal Storage Applications) in chapter 4 of this dissertation.

**USF Outlook** Search Meet Now

New message Delete Archive Junk Sweep Move to Categorize Snooze Ur

**Inbox** Filter

- Joseph Butts (ORG00995 : ... Tue 12:34 PM  
A Quick Overview of the ETD Process The...
- Constructible  
August Construction Report... Tue 7:33 AM  
What's slowing down & what's holding st...
- This week
- no-reply@copyright.com  
Your Request to Trans Tech ... Mon 3:58 PM  
Dear Mrs. Abdullatif Hakami, Thank you f...
- enginform\_gr@mailman.rc.usf.edu  
Spring Internship with PIRG Mon 3:38 PM  
Remote Internship Opportunities with Flo...
- Katie Sinclair  
> Reprint and Re-Use Perm... Mon 2:43 PM  
Dear Abdullatif Hakami, Thank you for se...

**Reprint and Re-Use Permission**

AH  
Mon 8/30/2021 11:21 AM  
To: reprint\_permission@spie.org

Hi, Would you please let me know if I can get copyright permission for my work to use in my dissertation?

**Title and author:**  
Effects of multilayer thin film coatings on different thermochromic materials for thermal storage applications

**Volume, issue, and page numbers**  
Proceedings Volume 11814, Current Developments in Lens Design and Optical Engineering XXII; 118140F (2021)

**What you would like to reproduce**  
The manuscript for my dissertation

**Where you will republish the requested material.**  
University of South Florida

**USF Outlook** Search Meet Now

New message Delete Archive Junk Sweep Move to Categorize Snooze Ur

**Inbox** Filter

- Joseph Butts (ORG00995 : ... Tue 12:34 PM  
A Quick Overview of the ETD Process The...
- Constructible  
August Construction Report... Tue 7:33 AM  
What's slowing down & what's holding st...
- This week
- no-reply@copyright.com  
Your Request to Trans Tech ... Mon 3:58 PM  
Dear Mrs. Abdullatif Hakami, Thank you f...
- enginform\_gr@mailman.rc.usf.edu  
Spring Internship with PIRG Mon 3:38 PM  
Remote Internship Opportunities with Flo...
- Katie Sinclair  
> Reprint and Re-Use Perm... Mon 2:43 PM  
Dear Abdullatif Hakami, Thank you for se...
- Clare Dennison  
> TEM Imaging Mon 1:41 PM  
Hi, thanks for your email! Can I ask what ...
- Science Exchange  
Welcome to Science Exchan... Mon 1:32 PM  
Welcome to Science Exchange! Connect. ...

**Reprint and Re-Use Permission**

University of South Florida

Thank you,  
Abdullatif Hakami

KS  
Mon 8/30/2021 2:43 PM  
To: Abdullatif Hakami

Dear Abdullatif Hakami,

Thank you for seeking permission from SPIE to reprint material from our publications. SPIE shares the copyright with you, so as author you retain the right to reproduce your paper in part or in whole.

Publisher's permission is hereby granted under the following conditions:  
(1) the material to be used has appeared in our publication without credit or acknowledgment to another source; and  
(2) you credit the original SPIE publication. Include the authors' names, title of paper, volume title, SPIE volume number, and year of publication in your credit statement.

Best wishes on your dissertation. Please let me know if I may be of any further assistance.

Best,  
Katie Sinclair  
Editorial Assistant, Publications  
SPIE – the international society for optics and photonics

### **About the Author**

M.S. of Science in Electrical Engineering (2018) from University of South Florida Tampa, FL, USA | Bachelor of Science in Electrical Engineering (2013-2016) from Gannon University Erie, PA, USA, bachelor's in business administration (2006-2009) from King Abdulaziz University, Jeddah, Saudi Arabia with Diploma in Saudi Electricity Company (2004-2005) from Saudi Electricity Company Training Institute. He worked in Saudi Electricity Company as gas turbine operation and control at Jizan City Gas power plant operation for five years. Has Research Areas are Distributed and large-scale optimization algorithms, Control theory, Power systems, thermochromic materials, and Simulations. He is currently pursuing a Ph.D degree in Electrical Engineering at the Clean Energy Research Center, University of South Florida, Tampa, Florida, USA, on Thermochromic materials, his advisor Dr. Elias Stefanakos.